Dynamical processes in the evolution of Cut Off Lows over South Africa

By

Khuthadzo Khangale

16014648

A Dissertation submitted to the Department of Earth Science in the Faculty of Science Engineering and Agriculture for fulfilment of a Master's of Earth Sciences degree in Hydrology and Water Resources

UNIVERSITY OF VENDA

Supervisor: Dr FI Mathivha (SAEON)

Co-supervisors: Prof T Ndarana (University of Pretoria)

Prof H Chikoore (University of Limopo)

July 2023

Declaration

I, Khuthadzo Khangale (16014648), hereby declare that this dissertation submitted for the fulfilment of a Master of Earth Sciences in Hydrology and Water Resources under the Department of Earth Sciences at the University of Venda has not been submitted previously for a degree at this or any other university. This is my own work in design and execution and all reference materials contained therein have been fully acknowledged.

Signature: __*Khangale.k*_____ Date: _*20/02/2023*_____

Table of contents

Abstract

This study presented deviations in the evolution of Cut-off lows (COLs) through four COLs events over the South African domain from a case study point of view. Furthermore, this study demonstrated COLs as cold-cored low-pressure systems estranged from westerly wind belts above . COLs are hazardous as they are mostly associated with unbearable precipitations and winds. The main aim of this study is to develop an understanding of dynamical processes during COLs. ERA5 data sets were used throughout the study to achieve objectives. Mean seal level pressure surfaces along with the 250 hPa geopotential heights were used to link the existence of COLs with ridging highs, the results shows that COLs that develop north of the subdivided study region (C and D) are mostly associated with Type-N ridging highs, whereas those that develop south (A and B) are associated with Type-S ridging highs. COLs were identified using 500 hPa geopotential height and the 330K potential vorticity. The results showed that high negative pool of potential vorticity is one of the principal factors during COL genesis. The small-scale jet associated with COLs tends to disappear as the COL dissipates. Some COLs extend to 850 hPa and further towards the surface and while others may not. COLs that extend towards the surface are associated with deeper PV intrusions. Cold cores of COLs are usually found at 500 hPa and uplifting of air during COLs occur further east from its centre which is filled with cold air mass. COLs tend to propagate east as soon as they are formed, but the speed (distance/time) is different from one COL to the next. The mechanism involved in COL development was investigated in detail using the eddy kinetic energy (EKE) budget applied to data from ERA5 reanalysis. This approach considers the most important processes involved such as the Ageostrophic flux convergence (AFC), Baroclinic convergence (BRC) and the Barotropic convergence (BRT). The results showed that the AFC together with the BRC are important for the EKE growth. Furthermore, AFC is responsible for the COL genesis, BRC is necessary for system maintenance and the BRT affects COLs negatively. The operational forecasting of these weather systems across the nation can be enhanced by the application of the knowledge about the evolution in the characteristics of COL events from this study.

Keywords: Cut-Off Lows, extreme events, Case studies, dynamical processes

Acknowledgements

Firstly, I would like to thank the Almighty God for granting me the opportunity to be able to finish my research and helping me overcome the challenges that it came with. I want to express my sincere gratitude to Prof T Ndarana who have helped so much in shaping this research and my other supervisors who were working effortlessly for this project to be what it is today. Prof H Chikoore, Dr MJ Bopape and Dr FI Mathivha, I thank you for everything you have done for me and hopefully you will continue to do so in the future. I would also like to thank Donald Nkabinde for helping with MATLAB basics through my research.

Special thanks to NRF-Access project for funding this research project throughout and the European Centre for Medium-Range Weather Forecasts ERA5 data sets which were used to analyse the evolution of Cut-off lows. Lastly, I would like to thank my family for their unlimited support and for allowing me to pursue my passion.

List of Figures

List of Acronyms

AFC	Ageostrophic fluxes convergence
BRC	Baroclinic convergence
BRT	Barotropic convergence
COL	Cut-Off Low
CORDEX	Coordinated Regional Climate Downscaling Experiment
ECMWF	European Centre for Medium-Range Weather forecasts
EKE	Eddy kinetic energy
ENSO	El Niño Southern Oscillation
ERA5	ECMWF Re-Analysis
Gph	Geopotential height
GRADS	Grid Analysis and Display System
MATLAB	Matrix Laboratory
MCRV	Minima of Cyclonic Relative Vorticity
MKE	Mean Kinetic Energy
OLR	Out-going long wave radiation
Pe	Available potential energy
PV	Potential Vorticity
RWB	Rossby wave breaking
SAO	Semi-Annual Oscillation
SAWS	South African Weather Service
SST	Sea Surface Temperature
SWIO	Southwestern Indian Ocean
TC	Tropical cyclone
TTTs	Tropical-Temperate Troughs

Chapter 1: Introduction

1.1 Background

South Africa situated south of the African continent, is a semi-arid region with most areas experiencing summer rainfall other than the Western Cape area which experiences winter rainfall (Mediterranean climate) (Reason and Rouault, 2002; Stella *et al*, 2013). Cloud bands in tropical-temperate troughs (TTTs), cold fronts, cut-off lows (COLs), tropical continental lows, mesoscale convective systems, and landfalling tropical cyclones from the South-Western Indian Ocean are among the main precipitation-producing weather systems over South Africa (SWIO) (Muofhe *et al*, 2020). South Africa is also known for extreme temperatures, whilst the temperatures of the adjacent tropical and subtropical oceans modulate winds as warmer oceans are associated with low atmospheric pressure and rainfall (Ummmenhofer *et al*, 2009; Iyakaremnye *et al*, 2021).

Cut-off lows (COLs) can be described as low-pressure systems that are closed, cold-cored and have been cut off from the dominant westerlies aloft. (Ndarana and Waugh, 2010). However, most of these rain-bearing systems have strong seasonality but South African COL are observed to occur all year round (Taljaard, 1985; Singleton and Reason, 2007; Muofhe *et al*, 2020). It is also found that these systems occur frequently between 20°S and 50°S (mid-latitudes) and they are more common in March-May season which adds more numbers in comparison to the other seasons with about 11 COLs that occurs yearly in the mid-latitudes (Singleton and Reason, 2007; Barnes *et al*, 2021a). However, these systems are baroclinic and their development is associated with cold fronts and therefore cold air advection at the surface (Ndarana and Waugh, 2010).

There are studies which demonstrates that COL rainy days significantly contribute to precipitation in South Africa, particularly along the south and east coasts as well as inland, over the transition zone between the summer and winter rainfall domains, where they contribute between 25% and more than 35% of annual accumulation (Favre *et al*, 2012; Abba Omar. and Abiodun, 2020). For example, a cut-off low over southwestern South Africa caused more than 500 mm of rain to fall over Port Elizabeth in 24 hours in September 1968, and a COL over central South Africa prompted a similar amount of rain to fall over East London in August 1970 (Singleton and Reason 2007).

In terms of occurrence, some COLs are preceded by downstream baroclinic wave development which is characterised by two energy centres (eddy kinetic energy), one located downstream (subtropics) and the other upstream (mid-latitudes) associated with mid-latitude jets (Ndarana *et al*, 2021). In addition to this, jet streaks play a significant part in development

and propagation of COLs over the Southern Hemisphere (Ndarana *et al*, 2020; Barnes *et al*, 2021a).

COLs are either associated with Rossby wave breaking (RWB) events (89%) or potential vorticity (PV) intrusions (11%), where high PV air is advected from the north to the south (Ndarana *et al*, 2021; Barnes *et al*, 2021b; Muofhe et al, 2020; Ndarana and Waugh, 2010). From the above studies, RWB is described as a sudden and permanent modification of the contours of PV material that enables the meridional PV gradient to change, while PV is described as an absolute circulation of an air parcel that is enclosed between two isentropic surfaces ((Ndarana and Waugh, 2010; Barnes *et al*,2021b).

Barnes *et al* (2021b) found that there is an opening in the upper troposphere that permits the exchange of moist air between the stratosphere and the troposphere when events force high potential vorticity air there. Also, Ndarana and Waugh, (2010) concluded that RWB plays a crucial part in creating the split flow associated with COLs, which occurs as the Rossby wave breaks. The value of PV is said to be lower at the troposphere but, it is expected to increase from the troposphere to the stratosphere due to significant change of static stability (Ndarana and Waugh, 2010).

Some RWB events do not produce COLs but, most of them do, whereas some COLs extend to the surface, and some does not extend to the surface, but about 60% of COLs that occurs over the Southern Hemisphere is reported to extend to the surface (Barnes *et al*, 2021a; Ndarana and Waugh, 2010). It was found that COLs are capable of cold conditions(snowfalls) and floods which makes about 20% of all floods experienced in South Africa (Barnes *et al,* 2021; Muofhe *et al*, 2020; Ndarana and Waugh, 2010; Singleton and Reason, 2007).

Most studies of COLs in the South African region focuses mostly on the climatology of COLs but not the deviations in dynamical processes during the formation and propagation of these systems. Furthermore, whether the frequency, seasonality, duration, and size of these systems will change positively or negatively in the future remain unknown. Hence, this study will use case studies to look at deviations and other changes (similarities) in these systems to better understand the evolution of these systems using four selected extreme COLs events that occurred in the South African region in the past.

1.2 Problem statement and motivation

There is limited knowledge on the evolution of COLs due to fewer studies that consider how terrain and mid-latitude storms affect COLs over the study (Muofhe *et al*, 2020; Abba Omar and Abiodun, 2021). This limited knowledge capacity hinders the forecast of COLs over the country. However, it is necessary to have accurate forecasts of weather systems to provide

early warning systems as well as to prevent loss of lives. Most studies conducted in the South African domain focuses mostly on the climatological behaviour of the weather system but not its behaviour from a case study point of view (Barnes *et al,* 2021a; Muofhe et al, 2020; Ndarana and Waugh, 2010; Singleton and Reason, 2007). Hence, case studies provide a broad overview of weather systems as well as their impacts on the environment, people, and the economy.

COLs are one of the worst weather systems that occurs in the SH which are mostly associated with cold conditions/heavy rainfall leading to snowfalls/floods (Muofhe *et al*, 2020). Moreover, floods can result in disruption of natural habitats and other natural beauties such as the Mpumalanga three roundavels in South Africa (Milly *et al*, 2002). Snowfalls may destroy buildings and car windows, and it might cause injuries to humans in the process, and as such floods/snowfalls poses threats to the environment and to the people living in it (Eisenberg and Warner, 2005). However, from another point of view, COLs occur all year round and may be responsible for winter rainfall in some parts of the country (Barnes *et al,* 2021a). Heavy rainfall may be of importance to the environment as to fill dried up dams, rivers and irrigate crops in the process. Hence, weather systems are needed to prevent semi-arid regions from turning into deserts (Modarres and da Silva, 2007).

Some COLs may extend to the surface, and some may not extend to the surface, and this is evident by a surface cyclone that often accompany these systems (deep COLs) that extended to the surface (Barnes *et al,* 2021a). However, this study seeks to find out why there is a variation in COLs that extends to the surface and those that do not extend to the surface from a case study point of view. Some COLs are preceded by downstream developments of baroclinic waves (Ndarana *et al*, 2021). Thus, this study seeks to find out why and how these events are preceded by downstream developments from a case study point of view.

Some RWB events produces COLs, and some do not produce COLs (Ndarana and Waugh, 2010). Furthermore, wave breaking events tends to disappear as COLs dissipates, and as such, this study seeks to find out why it happens that way. The overturning of PV has not been studied from the case study point of view. Hence, this study will showcase its evolution and the behaviour of certain standard variables such as winds as the PV overturns. Furthermore, this study will also look at other changes of PV in terms of isentropic transport of air.

1.3 Research questions

- How does the evolution of COLs look like from case studies point of view using PV diagnostics?

- What is the vertical structure of COLs during their development, intensification, maturity and dissipation phases?
- What is the vertical structure of COLs energetics?

1.4 Aim and objectives

1.4.1 General objective

To develop an understanding of dynamical processes during COLs over the South African domain

1.4.2 Specific objectives

- To investigate the evolution of COLs case studies using PV diagnostics.
- To investigate the vertical structure of COLs during their development, intensification, maturity and dissipation phases.
- To investigate the vertical structure of COLs energetics.

1.5 Organisation of the mini dissertation

The research project comprises of six chapters and the descripts of what is contained in each chapter is summarised below:

Chapter 1 provided a background on cut-off lows and associated dynamical processes for the evolution. This chapter also describes the study area (South Africa) and presented the aim and objectives of the study.

Chapter 2 includes an overview of numerous works that were relevant to this investigation and assisted in understanding how cut-off lows evolved and what impacts they generated over the study. Additionally, it offers various approaches, models, and data from related earlier work.

Chapter 3 describes the data sets used in this study (case studies), data sources (ECMWF ERA5), programming language (MATLAB), and methods adopted and applied to investigate dynamical processes in the evolution of Cut-off lows over South Africa.

Chapter 4 presents the climatological part of results obtained in this study. In this chapter, the evolution of four cut-off lows was mapped using their climatological characteristics. Also, the deviations within this cut-off lows from their climatological behaviours were discussed.

Chapter 5 provides the energetics part of the results obtained in this study. In this chapter, the evolution of four cut-off lows was mapped using energetics (eddy kinetic energy balance). Also, the deviations within this cut-off lows from the energy balances were discussed.

Chapter 6 In this chapter, discussion of findings and broad conclusions have been drawn. This chapter also offers suggestions for future research projects on how to better analyse and comprehend the evolution of dynamical processes during cut-off lows over South Africa.

Chapter 2: Literature review

2.1 **Introduction**

A literature review looks at books, academic articles, and any other sources pertinent to a certain topic, field of study, or theory and uses that information to describe, summarise, and critically evaluate those works in connection to the research subject being looked at (Fink, 2014). This study is focused on Investigating deviations in the evolution of dynamical processes during cut-off Lows (COLs) from their climatological behaviour. Very few studies in the Southern Hemisphere produces results to achieve their objectives from a case study approach (Singleton and Reason, 2007; Muofhe *et al*, 2020). There has been a great deal of research into whether the characteristics of COLs have changed or would change in a warming climate, and if so, how, frequently with contradictory results. The aim of this chapter is to study the behaviour of COLs that occurred in the past for better understanding of their evolution and characteristics.

2.2 **Rainfall producing systems over South Africa**

The Inter-tropical Convergence Zone (ITCZ) is the primary rain distributor over southern Africa (Liu *et al*, 2020) and its location and seasonal variation determines the climate of the region. The ITCZ is a zone of low pressure in the tropics characterized by trade winds convergence from either hemisphere. Southeast trade winds from the south Indian Ocean converge with cross equatorial winds from the Northern Hemisphere in the monsoon trough. The temperature of the adjacent tropical and subtropical oceans also modulates winds as warmer oceans are generally associated with low atmospheric pressure and rainfall (Felicísimo *et al*, 2008). Violent weather systems with extreme winds such as tropical cyclones generally form over the warm tropical oceans (Washington and Preston, 2006).

Cloud bands in tropical-temperate troughs (TTTs), cold fronts, cut-off lows (COLs), tropical continental lows, mesoscale convective systems, and landfalling tropical cyclones from the South-Western Indian Ocean are among the main precipitation-producing weather systems over South Africa (SWIO) (Muofhe *et al*, 2020). In addition to this, northwest to southeast oriented cloud bands is associated with a significant amount of summer rainfall caused by the convergence of tropical disturbances over northern Namibia and southern Angola with upper-level westerly waves over South Africa (Ndarana *et al*, 2022).

Cloud bands define tropical-extratropical interactions, also known as TTTs locally but a universal occurrence. They provide more than 30% of the climatological rainfall from October to March despite only being found in the Southern Hemisphere on the continents of South

America and Australia, with the largest contribution (40%) occurring in the middle of the wet season (Ndarana *et al*, 2022). The patterns of outgoing long wave radiation (OLR) anomalies that characterize these cloud bands' structure can be used to identify both the clouds and the accompanying precipitation (Fauchereau *et al*, 2009; Hart *et al*, 2013). Additionally, these dominant OLR anomaly patterns are negative (positive) across South Africa (Madagascar), respectively, which denotes enhanced (suppressed) convection over these areas (Ndarana *et al*., 2022).

The Angola low, which under suitable conditions may migrate southward as a tropical continental low and can generate significant rainfall over the South African domain, as well as random air mass thunderstorms may all contribute to South African summer rainfall (Ndarana *et al*, 2022). The deadliest and feared weather systems on Earth are tropical cyclones (TC), sometimes known as tropical storms (Change, 2006) . They are strong air vortices that form over warm tropical oceans. Severe TCs frequently result in devastating winds, high surges, torrential rain, and catastrophic floods, which can lead to considerable property damage and fatalities (Wang *et al*, 2004; Stull, 2016). Although in some circumstances the heavy rains brought on by a TC might temporarily alleviate drought conditions, this also helps the local population and agricultural industry. A TC's track and intensity must be accurately predicted to prevent calamities that could be brought on by it (Wang *et al*, 2004). A tropical cyclone generates winds that exceed 119 km (74 miles) per hour. In extreme cases winds may exceed 240 km (150 miles) per hour, and gusts may surpass 320 km (200 miles) per hour.

Hurricanes or tropical storms are mostly influenced by the strength and direction of upper-level winds (Stull, 2016). Coastal regions are mostly vulnerable to the impact of tropical storms than inland areas because of their primary energy driving the storm (warm ocean). However, tropical storms produce winds stronger and faster than any normal wind. Hence, they are destructive and life threatening. Tropical storms increase the speed and energy of winds needed for them to survive longer.

In addition to summer rainfall experienced in South Africa, COLs contribute rainfall in the domain throughout the year because they occur all year round, although they are more frequent during the March-May season (Muofhe *et al*, 2020). COLs can be described as low-pressure systems that are closed, cold-cored and have been detached from the main westerlies aloft (Ndarana and Waugh, 2010).

2.3 **Cut-Off Lows detection**

Previous studies detected COLs differently but mostly using the 500 hPa geopotential height and 300 hPa relative vorticity (Pinheiro *et al*, 2017; Barnes *et al*, 2020). The 500 hPa

geopotential height COL detection is based on recognition of closed geopotential contours at 500 hPa, and for a contour to be regarded as closed, its starting and ending longitudes and latitudes must be identical (Ndarana *et al*, 2020; Ndarana *et al*, 2021). Ndarana *et al*, (2021) further demonstrated that, the centre of each closed contour should be the middle most grid point and these points are saved as potential COL points. In terms of other lows that develop across the Southern Hemisphere, the tropical, subpolar, and polar lows should be excluded as potential COLs by requiring that the latitude and longitudes centres of the closed contours be confined between 15°S and 50°S latitude ring, following (Singleton and Reason, 2007; Ndarana and Waugh, 2010). However, the above-mentioned steps identify potential closed circulations but do not distinguish between high and low-pressure system (Singleton and Reason, 2007; Ndarana *et al*, 2020).

Ndarana *et al*, (2021) argued that, to distinguish between high and low pressure system, the COL centre should be assumed to be the location in the closed contour within the lowest geopotential value. The zonal component of flow south of the potential COL point should also be negative (Ndarana *et al*, 2020). As in Ndarana and Waugh (2010), COLs are argued to be a cold-cored system. It was further argued that the 850-500 hPa thickness fields be used to separate potential COL locations that fit the cold core condition from those that do not (Ndarana *et al*, 2021). For a COL point to be associated with a cold core of the close cyclonic circulation, its thickness value must be lower than that of at least five surrounding grid points (Ndarana *et al*, 2020). However, all COL locations that do not meet this requirement should be excluded from being COL locations (Ndarana *et al*, 2020).

The concentrated closed contours are believed to represent a single COL pressure system, and COL centres within a distance of 1000 km between two successive time steps should be taken to be part of the same COL (Ndarana *et al*, 2020; Ndarana *et al*, 2021). COLs last longer than 24 hours and those that do not are disregarded (Muofhe *et al*, 2020; Ndarana *et al*, 2021). Ndarana *et al*, (2020) further demonstrated that COLs have missing time steps in between and this is mostly dominant when six-hourly data is used for a study and not on three-hourly data.

The tracking of the 300 hPa relative vorticity COL is more dependent on well-known physical characteristics of the COL in question (Pinheiro *et al*, 2017). This tracking method requires the tracking of all vorticity centres. This method is different from the preceding one in that it does not differentiate between closed circulations and troughs in the raised levels (Pinheiro *et al*, 2017). This method's subsequent steps consider the following physical criteria: Following are the steps: tracking the Minima of Cyclonic Relative Vorticity (MCRV), temperature filtering, potential vorticity filtering, recognizing easterly flow south of the MCRV, and vorticity filtering

(Pinheiro et al, 2017). However, the 300 hPa isobaric level should be used to apply each of the requirements. To exclude tracks with conspicuously short life cycles, statistical analysis prioritizes COLs that last at least 24 hours as in the other method mentioned above (Pinheiro *et al*, 2017; Ndarana *et al*, 2020).

2.4 **Characteristics of Cut-Off Lows**

In this study, frequency of COLs refers to how often the COL system occurs. The extended duration of COLs observed is guaranteed by the vorticity approach for detecting COLs, although this has no impact on the overall frequency (Pinheiro *et al*, 2017). Moreover, Previous research shows that summer is the season with the highest incidence of COL detections (Singleton and Reason, 2007; Pinheiro *et al*, 2017). As in Singleton and Reason, (2007), it is found that about 11 COLs occur a year in the midlatitudes, and they prefer the March-May season. COLs last longer than 24 hours and sometimes more than two days in case of deep COLs. However, the cumulus convection's latent heat release and the technique used to locate the COLs core tend to minimize the horizontal temperature difference across the system, which reduces the frequency and/or duration of COLs (Pinheiro *et al*, 2017).

In general, COLs were less frequent in the Southern Hemisphere between the periods 1979 and 1999 respectively, but they increased from the early 2000s (10%) and reach the maxima indicating an increase in trends of COLs as time goes on (Pinheiro *et al*, 2017). The midlatitudes between 20°S and 50°S are where COLs typically occur, though, and they are either connected to RWB occurrences or PV where there is a north-south advection of high PV air (Ndarana and Waugh, 2010). As demonstrated in Pinheiro *et al*, (2017), when the same domain and time-period were considered, there were some variations in seasonality, i.e., in descending order of frequency: summer, autumn, winter, and spring, even though the variations among the seasons are not that significant. In general, it is the pressure level utilized, not the technique used to identify the COLs, that differs between COLs at 500 hPa and 300 hPa. This suggests that, at a given pressure level, the seasonality appears to depend more on the dataset than on the technique used to find the COLs.

Through seasonal changes in jet stream configuration, it has been hypothesized that the latitudinal temperature gradients and temperature differences between continental and oceanic regions may be to account for the seasonal cycle in the numbers and placements of COLs (Nieto *et al*, 2008). However, COLs contribute more than 30% of the climatological rainfall between October and March, increasing to about 40% during wet seasons over the South African mainland. As in Singleton and Reason, (2007), the weakening of the SAO and a change in zonal wave number three, which also had an impact on the preferred location of

these systems from southwest subtropical southern Africa to the northeast of the region, triggered a shift in the preferred season for cut-off lows from March to May and June to August in the 1980s.

2.5 **Cut-Off Lows and their extensions to the surface**

There are very few studies in the Southern Hemisphere that concentrate on COL depth, their extensions to the surface, as well as their link to surface cyclones that frequently accompany these systems (Barnes *et al*, 2021a). In addition, deep COLs that extends to the surface prefers March to May season of COLs, high latitudes, are more mobile, and last longer than those that do not extend to the surface. However, high PV driven by RWB events eventual push tropospheric air towards the tropopause where the depth of intrusions is more critical and is proven to be critical to the development of COLs extensions (Barnes *et al*, 2021a). In the mid-latitudes, deeper incursion is linked to deep COLs.

Moreover, warm potential temperature anomalies collocated with upper-level features plays a critical role in cyclogenesis which in turn can inhibit surface ward extensions and result in shallow COLs when out of space with coupled upper tropospheric processes (surface features logging behind upper-level processes) (Barnes *et al*, 2021a). For example, the south-western Cape of South Africa was hit by an intense surface low pressure system and related cut-off low on June 6 and 7, 2017, and it was known as the "Cape storm" because it was accompanied by extremely large waves, strong winds, and heavy rains, which led to fatalities and damage to infrastructure (Barnes *et al*, 2021b). More recently, during the 2019 Easter weekend (22-24 April), a COL devastated KwaZulu- Natal in South Africa which caused damage to health facilities, including flash flooding, water pipe damage, washed-away walls, uprooted electric poles, and damage to water pipelines (Muofhe *et al*, 2020). In addition, a surface cyclone followed just after the COL (Cyclone Kenneth) (Cambaza *et al*, 2019).

2.6 **Dynamical processes during Cut-Off Lows**

Two energy centres, one upstream in the midlatitudes and the other downstream in the subtropics, have evolved to make up downstream development (Ndarana *et al*, 2021). However, the difference between upstream and downstream eddy kinetic energy is that the upstream (downstream) develops and maximises before (during) the formation of close COL cyclonic circulation (Ndarana *et al*, 2021). Moreover, Midlatitudes jets are linked to the upstream eddy kinetic energy. The baroclinic (BRC) and barotropic (BRT) conversions, and the ageostrophic flux convergence (AFC) are of consideration looking at midlatitude disturbances also known to researchers as Downstream development (Ndarana *et al*, 2021; Pinheiro *et al*, 2022).

Additionally, the downstream energy centre expands by absorbing energy via AFC, which transports eddy kinetic energy from the upstream centre in a north-easterly direction. The upstream eddy kinetic energy accumulates its energy by BRC conversion from eddy available potential energy to eddy kinetic energy (Ndarana *et al*, 2021). AFC and BRC conversion contribute to EKE growth for COLs which characterizes the downstream baroclinic development (Pinheiro *et al*, 2022). Moreover, the processes connected to Rossby wave breaking (RWB) on the midlatitude dynamical tropopause are what necessarily lead to these ageostrophic geopotential fluxes, which is how the downstream energy transfer links South African COLs to midlatitude processes (Ndarana *et al*, 2021).

The BRC conversion is essential for system maintenance, but the AFC is crucial for the COLs' genesis and intensification phases, according to Pinheiro *et al*, (2021). Friction and other mechanisms like dispersive fluxes (ageostrophic flux divergence) that are not accounted for in the EKE equation thus contribute to the dissipation of the COLs. The BRT conversion also contributes negatively on COL development by transferring EKE to the zonal flow kinetic energy which is enough to hinder COL intensification (Pinheiro *et al*, 2021).

2.7 **Jet streaks and their roles in Cut-Off Lows evolution**

A jet streak can be defined as an area where winds are stronger than the surrounding area (jet stream). However, strong jets are usually found in regions of large tropopause pressure gradients (Kunz *et al*, 2009). In addition, Strong gradients are combined by PV advection through poleward heat fluxes close to the jet zones (Edouard *et al*, 1997). The midlatitude jet which is found upstream between the eddy kinetic centres is assumed to impact the closed circulation of COLs (Ndarana *et al*, 2021). Additionally, the transfer of EKE from the upstream midlatitude jet to the downstream EKE centre is caused by the anticyclonic barotropic shear (Pinheiro *et al*, 2021).

Jets plays an important role in COLs during their development, maturity and the dissipation stage. For example, midlatitude jets supply energy via baroclinic conversion which is transferred to the rear side of the COL which in turn use the energy for intensification (Pinheiro *et a*l, 2021). Jet streaks forms and propagates eastward during COLs due to the advection of zonal momentum by the zonal flow (Ndarana *et al,* 2021). Moreover, the air within the COL continues to be colder than the air around it, irrespective of the fact that the jet stream represents the boundary between two separate air masses (Nieto *et al*, 2008). The major belt of COL activity changes approximately 5° towards the equator from summer to winter in the Southern Hemisphere due to jet streams (polar and the subtropical), as shown in Pinheiro *et*

al, (2019) and Ndarana *et al*, (2021). In addition, Jets affects the seasonality of COLs (Pinheiro *et al*, 2019).

2.8 Potential Vorticity and Rossby Wave Breaking events

RWB is the quick, irreversible distortion of PV contours that flip back on themselves, reversing the PV's meridional gradient. PV is the absolute circulation of an enclosed air parcel between two isentropic surfaces. Most Southern Hemisphere research use PV anomalies to depict RWB events and to meet their objectives in respect to RWB events. (Singleton and Reason 2007; Ndarana and Waugh, 2010; Barnes *et al,* 2020; Ndarana *et al*, 2021). Moreover, COLs are either associated with RWB events or potential vorticity. According to Pinheiro *et al,* (2017), several studies that looked at COLs from the perspective of PV have shown that the formation of COLs is caused by the separation of a single PV anomaly from its stratospheric air reservoir..

High PV intrusions enable air interchange between the lower stratosphere and upper troposphere, which influences the ozone concentration in the lower troposphere and makes PV a useful metric for tracking COLs (Pinheiro *et al*, 2017; Ndarana *et al*, 2021). Yet, the emergence of COLs is caused by the separation of a single PV anomaly from its supply of stratospheric air. A resurgence in interest in PV on isentropic surfaces has resulted in the transformation of this technology into a valuable diagnostic tool for researchers and even for the interpretation of daily weather maps (Edouard *et al*, 1997). Furthermore, COLs are caused by high PV anomalies caused by Rossby wave breaking (RWB) events that carry stratospheric air in an isentropic direction toward the equator (Ndarana *et al*, 2021).

The frequency of COLs that occurs in response to RWB events in the southern Hemisphere is better compared to COLs without the link to RWB events, which indicates that PV anomalies are an important factor that affect the seasonality of COLs (Pinheiro *et al*, 2017). In addition, it is reasonable to believe that the seasonal variability of the jet stream influences the seasonality of COLs since the PV anomalies are considered to be the result of RWB events, which are connected to split jet flow. (Pinheiro *et al*, 2019). However, previous studies concluded that the cut-off phenomena from COL genesis is a result of distinct RWB process (Pinheiro *et al*, 2021; Ndarana and Waugh, 2010). Hence, COLs are preceded by RWB scenarios (events) (Ndarana *et al*, 2021).

2.9 **Review of research techniques used in similar studies**

2.9.1 **Case study approach**

An overview or comprehensive grasp of a difficult topic in its actual context can be produced using the research technique known as the case study. In the realms of business, law, policy, and scientific research, the significance of the case study technique is widely acknowledged. (Crowe *et al*, 2011). Different researchers have used this method when conducting their studies such as Muofhe *et al*, (2020) for a case study of Forecasting intense Cut-Off Lows in South Africa Using 4.4 km Unified Model; Chapman *et al*, (2017) for a case study of the urban heat island of London quantified using Netatmo weather stations; Singleton and Reason, (2007) for a case study of Variability in the characteristics of cut-off low pressure systems over subtropical southern Africa; Kaminski *et al*, (2002) for a case study of a seasonal cycle in assimilating atmospheric data into a terrestrial biosphere model; Chameides *et al*, (1999) for a case study of the effects of atmospheric aerosols and regional haze on agriculture: an opportunity to enhance crop yields in China through emission controls;. However, the case study approach showed positive results in achieving objectives mentioned on each of the studies mentioned above.

We can never be sure if a case study investigated is representative of the larger body of similar instances, and the conclusion drawn from a particular case may not be transferable. Case studies tend to allow a researcher to investigate a topic in far more detail than might be possible if they were trying to deal with many research participants (nomothetic approach) with the aim of averaging (McLeod, 2019). Case studies are one of the best ways to stimulate research because if the findings are valuable when completed, they can lead to new and advanced research in the field, but it is very possible for the author or research to be biased when carrying out the research. Furthermore, as it is usual for people to be vulnerable to prejudice, this bias could be for the person, the method of data collection, or the interpretation of the data..

2.9.2 **Correlation studies**

Correlation analysis is a measure of a relationship between two variables, and it is widely used to prevent incorrect analysis (Mwafulirwa, 1999). Different researchers have used correlation carrying out their experiments and research such as Tinsley *et al*, (1993); Uhlik *et al*, (1993); Nakajima *et al*, (2001); Elliot *et al*, (2008) for their studies in atmospheric sciences. Correlation studies have been used before and it has been confirmed to be effective in determining the relationship between two variables (Mwafulirwa, 1999). Furthermore, the studies mentioned

above together with variables correlated showed positive results in achieving the objectives mentioned in the studies.

Most techniques used in scientific studies have both strengths and their limitations. Hence, correlation studies allow researchers to collect more data than experiments provide but it is also known that correlation studies only uncover relationships between the variables that may not been previously discovered, hence, it does not offer a convincing explanation for why there is a connection in the first place (Louis, 2020). Moreover, the limitation will be that correlation studies cannot provide information regarding which variable is responsible for influencing the other, so it is then assumed. However, a correlation study can help researchers determine the direction and strength of each relationship, making it possible to narrow the findings in future studies as needed to determine causation experimentally as needed (Louis, 2020).

2.9.3 **Composite analysis**

Composite analysis is a useful technique to determine structural basic characteristics of a climatological phenomenon that are not simple to observe or that occurred over time. Furthermore, it can be simplified to be a sampling technique based on the conditional probability of a certain event occurring (El Nino or La Nina). For a climate composite, one might composite the weather over a large area over a period of many years by an ENSO index to study how precipitation or temperature is influenced by the phenomenon. Composite analysis basically entails the collection of large numbers of cases of a given meteorological phenomenon, then these cases are composited together as a collection, perhaps with different types of stratification using one or more covariates that are suspected to have an influence on the phenomenon (Ren *et al*, 2020).

Different researchers in climate sciences have used composite analysis in the past such as Feldstein, (1998); Huijun, (2000); Hopsch *et al*, (2012); Ndarana *et al*, (2020) and Barnes *et al,* (2021b) when conducting their experiments/research. Composite analysis been declared effective method in compositing a large group of different variables with the support of different studies such as those mentioned above showing positive results in achieving the objectives of each study. Composite indicators provide easy information for the public which is readable but with the limitation that the researcher can hide a lot of work in data collection. However, composite analysis allows comparison of complex dimensions by users, hence, it may be misused.

2.10 **Summary**

The above-reviewed literature explained the characteristics of COLs such as that the COL system prefers wet seasons (increased frequency), different methods of COLs detection used in the past, COLs and their extensions to the surface. COLs are preceded by downstream developments of baroclinic waves (Ndarana *et al*, 2021). Jet streaks (jet stream) is an important factor considering the genesis of COLs as well as the propagation and dissipation stage of COLs. Previous studies indicated the usefulness of PV anomalies to represent RWB events to achieve objectives. It was also concluded that not all RWB events produces COLs. The impacts of COLs over the vulnerable regions were discussed such as cold conditions (snow), strong winds, heavy rainfall (floods), runaway fires, storm surge and extremely large waves which threatens lives and the environment as a host. Previous method used to discuss or to achieve objectives were discussed in this chapter such as composite analysis, correlations, and case study. This study adopted case study method to better understand COLs that occurs over the South African domain and to achieve study objectives.

Chapter 3: Methodology

3.1 **Introduction**

The aim of this chapter is to describe and present data that was used in this study. This chapter also described methods that were used to analyse data to achieve specific objectives outlined in Chapter one. It was found that these systems (Cut-Off Lows) occur frequently between 20°S and 50°S (mid-latitudes) and they are more common in March and May season which adds more numbers in comparison to the other seasons on about 11 Cut-Off Lows (COLs) that occurs yearly in the mid-latitudes (Barnes *et al*, 2021a; Singleton and Reason, 2007). Dynamical processes in the evolution of COLs over South Africa were analysed using case studies.

3.2 **Study area**

South Africa is located south of the African continent. Southern Africa is a relatively dry region of the African continent, which generally experiences summer rainfall except the Western Cape province which experiences Winter rainfall (Mediterranean climate) (Reason and Rouault, 2002). The South African topography is characterized by an elevated plateau over the eastern side, with the highest being 2.5 km above mean sea level (Taljaard,1999; Muofhe *et al*, 2020). The steep escarpment of the region runs from the Soutpansberg area in Limpopo Province, becoming Drakensberg over KwaZulu-Natal Province, and the northern parts of the Eastern Cape Province.

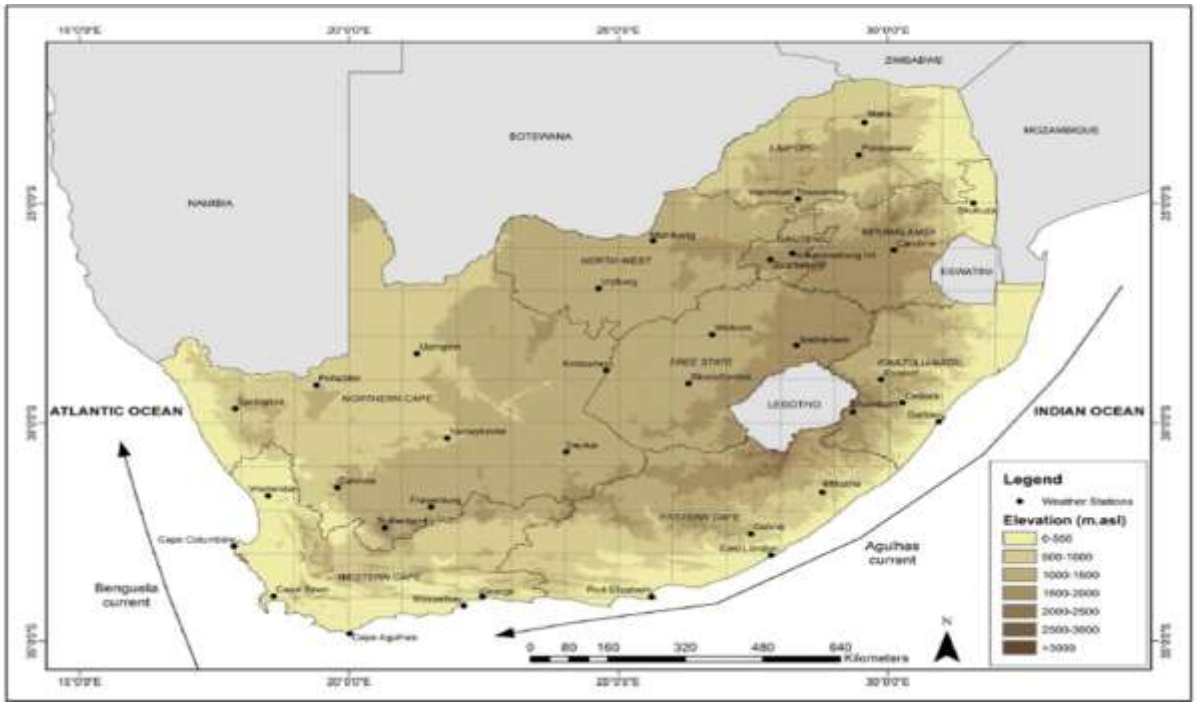

Figure 3.1 South African map covered with weather stations and elevations starting from > 500 m to 3000 m above mean sea level (Source: Van der Walt and Fitchett, 2020).

3.3 **Description of datasets and Cut-Off Low influenced map**

This study relied on ERA5 Reanalysis datasets to achieve its objectives. ERA5 is the fifth generation European Centre for Medium-Range Weather Forecasts (ECMWF) atmospheric reanalysis of the global climate covering the period from January 1940 to present. ERA5 provides hourly estimates of many atmospheric, land and oceanic climate variables. This study used reanalysis data sets at 21 mandatory levels (1000 hPa, 925 hPa, 850 hPa, 700 hPa, 500 hPa, 400 hPa, 300 hPa, 250 hPa, 200 hPa, 150 hPa, 100 hPa, 70 hPa, 50 hPa, 30 hPa, 20 hPa, 10 hPa, 7 hPa, 5 hPa, 3 hPa, 2 hPa, 1 hPa). Reanalysis data sets that were used are Zonal Wind (U), Meridional wind (V), Potential Vorticity (PV), Air Temperature, Geopotential height (z), vertical velocity (w), and alpha (α). The map attached below (Figure 3.2) was used to classify COLs events according to where they originate, intensify and where they impacted. For this study, four severe COLs events were chosen for the purpose of the study, to investigate deviations within these COLs during their evolutions. The COLs are selected based on where they developed and matured as they evolved. Event one (April 22-24, 2019) occurred at region A , event two (Oct 10-11, 2017) occurred at region B, event three (May 13-15, 2016) occurred at region C and event four (Nov 15-17, 2017) occurred at region D respectively (Singleton and Reason, 2007).

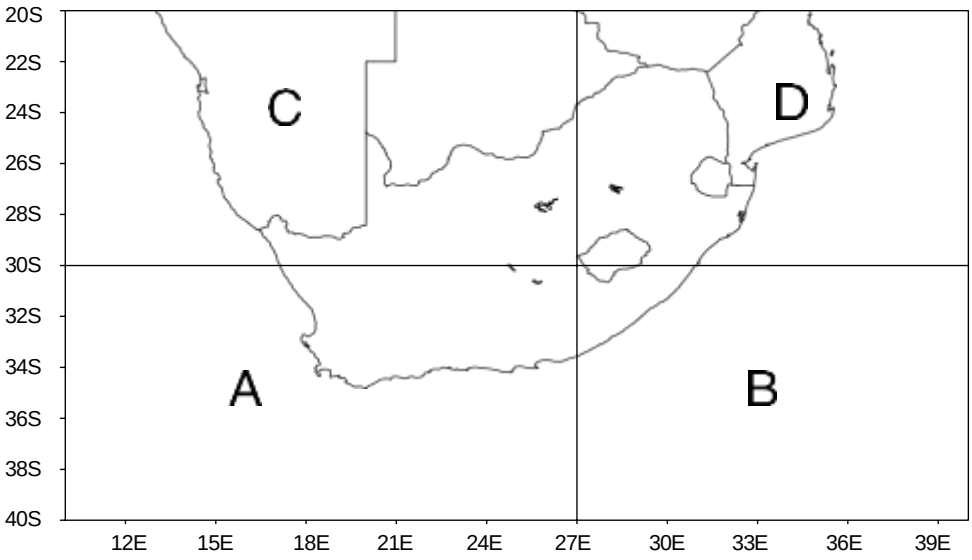

Figure 3.2 Map of the domain covered by the cut-off low climatology divided into regions A, B, C and D over subtropical southern Africa (Singleton and Reason, 2007)

3.3.1 **Reanalysis data**

3.3.1.1 ***Three Components of the Wind (Zonal, Meridional and Vertical)***

Zonal wind (U) is the component of a wind along a particular parallel of latitude. The u-component of the wind was collected six hourly from ERA5 reanalysis data sets at mandatory levels as mentioned above. To this study, Zonal wind datasets were collected for both results chapters (four and five). For chapter four, this data sets were collected to showcase the location and the evolution of jets streaks during COLs. Most studies such as Singleton and Reason, (2006) and Ndarana *et al*, (2021) also used the zonal wind component to look at the jets. However, this study adopted a method used in Ndarana *et al,* (2020), assuming a basic state flow of zonal wind defined by the 31-day time mean centred on the day of the COL events and the perturbations which are the deviations from that time mean, in order to generate the local energetics fields (chapter 5) that evolve in space and time. Additionally, the results of the energy budget study are not considerably affected by low frequency fundamental state flow (Lackmann *et al*, 1999). MATLAB was employed to calculate the basic state, perturbations and to visualise analysis mentioned above.

Meridional wind (V) can be described as the v-component of the wind where the flow follows the north-south or south-north pattern along the longitude's lines. The v-component of the wind was collected six hourly from ERA5 reanalysis data sets at mandatory levels as mentioned above. For the purpose of this study, meridional velocity was obtained mainly for chapter 5 to compute the eddy kinetic energy budget. A basic state flow of meridional wind defined by the 31-day time mean centred on the day of the COL events was assumed and the perturbations are the deviations from that time mean (Ndarana *et al*, 2020). MATLAB was also employed in this case for calculations and visualisation.

Vertical velocity is the speed of air motion in the upward or downward direction. The ECMWF ERA5 uses a pressure based vertical co-ordinate system and pressure decreases with height. Furthermore, positive values represent downward motion while negative values represent upward motion also known as omega (ω). vertical velocity data sets were collected six hourly from ERA5 reanalysis data sets at mandatory levels as mentioned above. Most studies such as (Ndarana *et al*, 2021; Pinheiro *et al*,2017) also used the vertical component to look at areas where there is an uplift of air to achieve their study objectives. For the purpose of this study, vertical velocity datasets were collected for both results chapters (four and five). For chapter four, this data sets were collected to showcase the location and the strength of the upward motion for the four COLs events. Whilst, for chapter 5, it was used to calculate a basic state defined by the 31- day time mean centred on the day of the COLs events and perturbations

which are basically the deviations from that time mean (Ndarana *et al*, 2020). MATLAB was also employed here for computations and data display.

3.3.1.2 ***Mean Sea level pressure***

Mean sea level pressure (MSLP) can be defined as the average atmospheric pressure at mean sea level. Meteorologist commonly uses MSLP to identify weather systems at the surface (Ndarana *et al*, 2021; Barnes *et al*, 2021; Ndarana *et al*, 2018). For this study, MSLP was used to investigate the link between COLs and ridging highs that occurs in the Southern Hemisphere. MSLP data sets were obtained at mandatory levels mentioned above six hourly from ECMWF ERA5 to help identify whether the COL event in question is associated with either Type-N or Type-S ridging high. MATLAB was employed to visualise the results.

3.3.1.3 ***Potential Vorticity***

PV can be described as an absolute circulation of an air parcel that is enclosed between two isentropic surfaces (Ndarana and Waugh, 2010; Ndarana and Waugh, 2011). This study adopted the method of using PV to represents RWB events from Ndarana and Waugh, (2010). Hence, PV datasets were extracted from ERA5 reanalysis datasets six hourly at mandatory levels mentioned above to highlight the development, intensity, and propagation of COLs systems over the study. The basic state (31-days mean) and perturbations were also calculated to provide anomalies and for the energetics part (Chapter five). Moreover, this study adopted Edouard *et al*, (1997) method to interpolate PV fields linearly from pressure levels into 330 K, 340 K and 350 K isentropic surfaces, respectively. MATLAB was also employed on this occasion to calculate and visualise the results.

$$\text{Pv} = \text{g}\left[f + \frac{1}{\alpha\cos\emptyset}\frac{\partial v}{\partial\lambda} - \frac{1}{\alpha\cos\emptyset}\frac{\partial(u\cos\emptyset)}{\partial\emptyset}\right]\left(-\frac{\partial\theta}{\partial\text{p}}\right), \quad (1)$$

Where Pv is the potential velocity, u and v are the zonal and meridional velocity fields, respectively, θ is the potential temperature, f is the Coriolis parameter, g is the gravitational acceleration and α is the radius of the earth .

3.3.1.4 ***Air Temperature***

Air temperature can be described as the measurements of how hot or cold the air is. Air temperature data was extracted from ERA5 reanalysis six hourly at mandatory levels mentioned above for the duration (days) of the COLs that occurred over the study. furthermore, the above-mentioned air temperature data was used to calculate potential temperatures, which was used to display isentropic surfaces for the purpose of this study.

Hence, other authors such as Singleton and Reason, (2006) also used the same method to display isentropic surfaces. MATLAB was employed to calculate and display the isentropic surfaces.

Mathematical expression:

$$\theta = T\left(\frac{1000}{P}\right)^{\frac{R_d}{C_p}} \quad (2)$$

Where the potential temperature is denoted by θ , air temperature is denoted by T, atmospheric pressure level is denoted by P, Specific gas constant for air is denoted by Rd = 287 (J/kg·K) and Specific heat of dry air at constant pressure is denoted by CP = 1004 (J/kg·K)

3.3.1.5 ***Geopotential Height***

Geopotential height estimates the actual height of a pressure surface above mean sea-level (Remsberg *et al*, 2003). It stands for the highest point on the pressure surface, where the observation was made. Because freezing air masses are denser than warm ones, their pressure surfaces are often lower in the former and higher in the latter. Height therefore decreases in cold air masses and increases in warm air masses. For this study, Geopotential height data was extracted three hourly and six hourly from ERA5 reanalysis datasets to calculate anomalies for Chapter four and energetics (Chapter five). Furthermore, Geopotential height dataset were used to showcase the propagation of COLs from west to east in the Southern Hemisphere. However, MATLAB was employed to calculate the basic state and perturbations and to produce/display the plots. Most studies (Barnes *et al*, 2021a; Muofhe *et al*, 2020; Singleton and Reason, 2006; Ndarana and Waugh, 2010) that focus on COLs in the Southern Hemisphere also used Geopotential height datasets to detect the COLs and to check if the COL extends to the surface or not.

3.3.1.6 ***Eddy kinetic energy***

Eddy kinetic energy (EKE) is commonly defined as the kinetic energy of the time-varying component of the velocity field. Datasets such as the three components of the wind (U, V, ω), MSLP, PV, air temperature and z were extracted at mandatory levels as mentioned above from ERA5 reanalysis to compute the EKE budget. This strategy considers the key elements that characterize the evolution of midlatitude disturbances, such as ageostrophic flux convergence (AFC), barotropic flux convergence (BRT), and baroclinic and barotropic conversions (Pinheiro *et al*, 2021). However, this study adopted the methods used in Ndarana

et al, (2020) to compute the EKE budget to highlight deviations of energy balances within the four COLs events. MATLAB was employed for EKE budget computations and to produce plots.

The local energetics fields that evolve in space and time, centred on the day of the COL events, were thought to be produced by a fundamental state flow defined by a 31-day mean, and the perturbations are the deviations from that temporal mean (Danielson *et al*, 2006; Ndarana *et al*, 2020). Simpler equations are produced when the 31-day time mean basic state flow is used, and the findings of the energy budget analysis are not always influenced by low frequency basic state flow. The final breakdown of the total variables is as follows.:

$$U = U_m + u \quad (3)$$

$$V = V_m + v \quad (4)$$

$$\Phi = \Phi_m + \phi \quad (5)$$

$$\Theta = \Theta_m + \theta \quad (6)$$

where the capital letters/Greek symbols with (without) subscript m represents the time mean (total) variables, respectively. The lowercase symbols represent the perturbation fields and U = Ui + Vj + ωk is the three-dimensional velocity flow and V = Ui + Vj is the horizontal flow on isobaric surfaces. The symbols Φ and Θ are the geopotential and potential temperature, respectively. The form of eddy kinetic energy (Ke) used in this study is.

$$K_e = \frac{1}{2} v.v \quad (7)$$

Here the zonal and meridional momentum correlation, the vertical flux divergence of the rate of work by aerodynamic stress and the curvature terms are all incorporated in the residual term, to obtain.

$$\partial_t K_e = -\nabla_p \cdot (VK_e) - \partial_{p(}\omega K_e) - v \cdot \nabla_p \phi + [v \cdot (u \cdot \nabla) V_m] + \text{Residual} \quad (8)$$

which is the Ke equation. As in Ndarana *et al*, (2020), Ke generation term $-v \cdot \nabla_p \phi$ was decomposed as follows.

$$-v \cdot \nabla_p \phi = -\omega\alpha - \nabla_p \cdot (v\phi)_\alpha - \partial p(\omega\phi) \quad (9)$$

Then we assumed a variable f so that

$$(v\phi)_\alpha = v\phi - k \times \nabla (\phi^2 / 2f(y) \quad (10)$$

It also represents the ageostrophic geopotential flux (Ndarana *et al*, 2020). Hence it follows that Ke is produced by two processes: (a) baroclinic conversion, which is brought on by vertical eddy heat fluxes and is represented by the first component in Eq. (9); and (b) ageostrophic flux convergence, which is represented by the second term in Eq. (9). This system of energy equations adopted from Ndarana *et al*, (2020) and Pinheiro *et al*, 2022 was used to describe downstream development, involving two energy centres, one upstream and the other downstream, during which Ke is moved by means of energy fluxes ($\nabla p \cdot (VKe)$), whilst the upstream centre radiates energy downstream into the centre to the east of it by means of the ageostrophic geopotential fluxes in Eq. (10).

3.4 **Methods of analysis**

3.4.1 **Case Study Approach**

Case study is a research technique that is used to generate an overview or a multi-faceted understanding of a complex issue in its real-life context. For this study, case studies were used to understand the climatology and the evolution of COLs over South Africa. Furthermore, four case studies of COLs were selected from the study area map above (Figure 3.2) to look at COLs from different views and to understand their deviations/patterns in terms of formation, size, seasonality and their propagations. However, case studies are the main approach of this study to validate the information we already have on the evolution of COLs from a climatological point of view. Most scientists/researchers rely on case studies to achieve their objectives (Muofhe *et al*, 2020; Singleton and Reason, 2006).

3.5 **Summary**

This chapter described datasets and data sources that was used in the study together with method of analysis such as case study approach. ERA5 reanalysis datasets was used to map various circulating parameters like Geopotential heights and the three components of the wind. MATLAB was a useful tool for computations and visualisation in investigating deviations in dynamical processes during COLs formation from their climatological behaviour. However, ERA5 reanalysis datasets also gave a detail overview on changes in energy balances that occurs during COLs.

Chapter 4: Synoptic analysis evolution of Cut-Off Lows

4.1 Introduction

In this chapter, we present the life cycles of Cut-Off Lows (COLs) that are selected for the study in 3D point of view (zonal, meridional and the vertical point of view). For instance, the climatology of Potential Vorticity (PV) representing the dynamic tropopause in the atmosphere, the isentropic surfaces representing the potential temperature, the zonal wind representing the jets in the atmosphere were presented to highlight the development, maturity, propagation, and the decay stage of the COLs selected for the study. Breaking events occurs before the formation of COLs (Ndarana and Waugh, 2010). Therefore, the climatology of four case studies of COLs that occurred previously in the study area was presented below.

4.2 Evolution of Cut-Off Lows

4.2.1 Mean Sea level pressure evolution of COLs

We first consider the horizontal evolution of COLs over the study using mean sea level pressure surfaces and geopotential heights (250 hPa) and their link to ridging high processes. Figure 4.1 (a-f) below shows the climatological evolution of COLs with associated ridging highs. Figure 4.1 (a-b) highlights the behaviour of the geopotential heights and mean sea level pressures before the formation of the COLs events, as the COLs events tend to develop at t = 0 hours (Figure 4.1 c). Type-N (Type-S) ridging highs are observed to show a more (less) zonal structure of mean sea level pressure surfaces and they are expected to extend/move across (south of) the mainland as they evolve over time (Ndarana *et al*, 2018).

Figure 4.1 showed a meridional (north-south movement) structure of mean sea level before the formation of the COL, and it extended further south as the COL event started forming up until its decay stages (Figure 4.1 a-f). Although it breaks off as soon as it extended far south from the mainland, it leaves behind a stronger ridging high component which is clearly visible starting from Figure 4.1 (d-f). The highest-pressure level was spotted more comfortable at about 40°S from t = 12 hours up until t = 36 hours. In addition, COLs associated with ridging highs that extends south as they evolve are mostly linked to Type-S ridging high (Ndarana *et al*, 2021).

The 250 hPa geopotential did not show any sign of folding 24 hours prior to the formation of the COL but it only started to fold 12 hours prior the formation of the COL event (Figure 4.1 a-b). whilst intense folding of geopotential contours in this case represents the life cycle of the COL, through its development up until it decays. The COL is clearly visible starting from Figure

4.1 (c-f) where there was intense folding which showed consistency as the COL event propagates eastward from where it developed up until the final stage (36 hours).

a) t = -24 hours

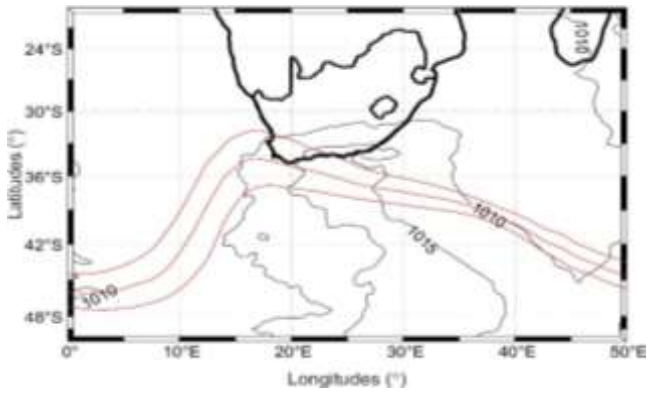

d) t = 12 hours

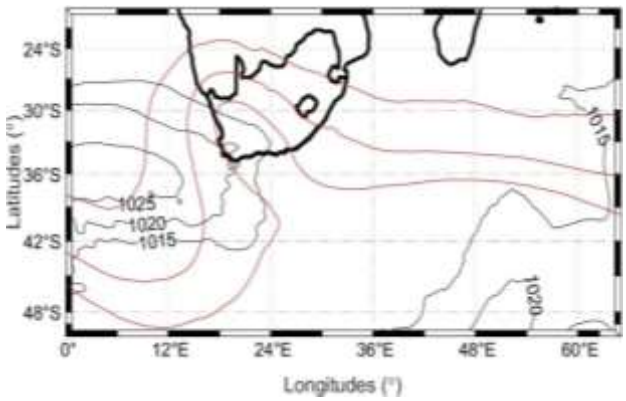

b) t = -12 hours

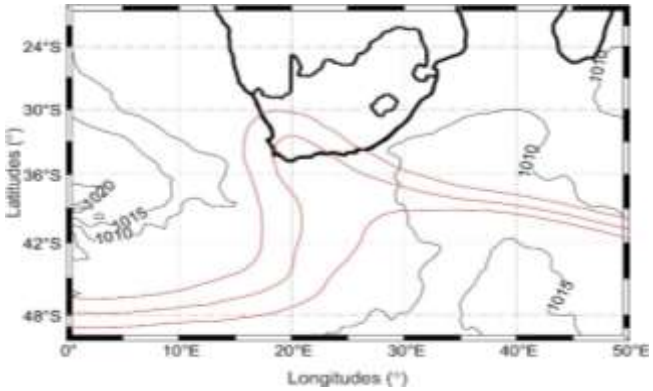

e) t = 24 hours

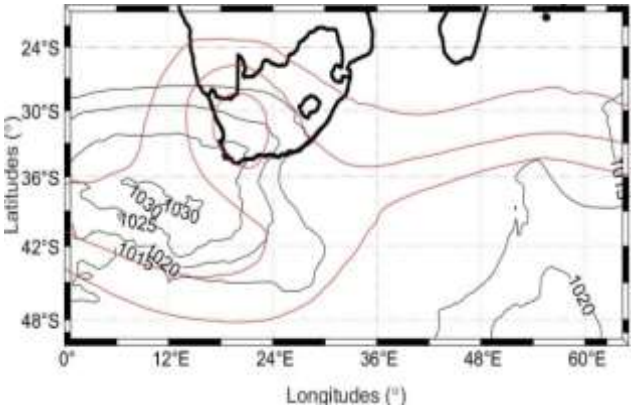

c) t = 0 hours

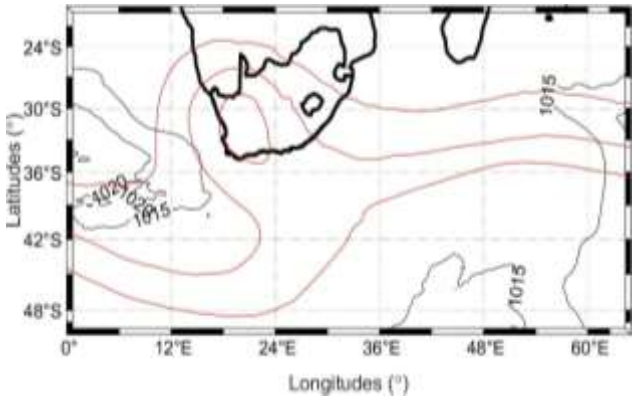

f) t = 36 hours

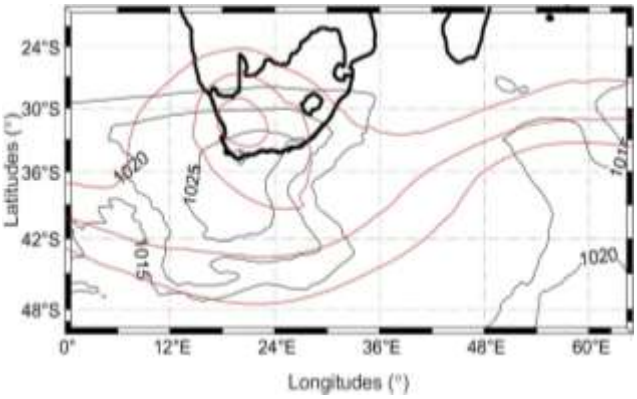

Figure 4.1: Time-lagged evolution of mean sea level pressure (thin contours) and geopotential heights (solid red) demonstrating impacts of diverse types of ridging highs on cut-off lows for **event 1** over South Africa.

Figure 4.2 also showed a meridional (north-south movement) structure of mean sea level before the formation of the COL (Figure 4.2 a-b), but as soon as the COL forms, the mean

sea level pressure extended further south as the col event started forming up until its decay stages (Figure 4.2 c-f). just like event one, the break off left a behind a stronger ridging high component which is clearly visible starting from Figure 4.2 (d-f). The highest-pressure level was spotted more comfortable at about 36°S from t = 12 hours up until t = 36 hours. Moreover, Event 2 can be linked to Type-S ridging highs through its evolution (Ndarana *et al*, 2021).

The 250 hPa geopotential show some signs of folding 24 hours prior to the formation of the COL, but it only became more intense at the day of COL formation (Figure 4.2 c). Folding of the geopotential contours represents the closed circulation of COL and the location where it developed over the study. Although 24 hours (Figure 4.2 e-f) after the development of the COL, the geopotential contours began to change shape from folding contours to be more like flat contours to represent the decay stages of the COL event. Unlike event one, event two shows signs of weakness (decay) as soon as the COL was fully developed according to the geopotential contours (Figure 4.2 d) indicating that the event was weaker than the event one in terms of the closed-circulation associated with COL events represented by the 250 hPa geopotential heights in this case.

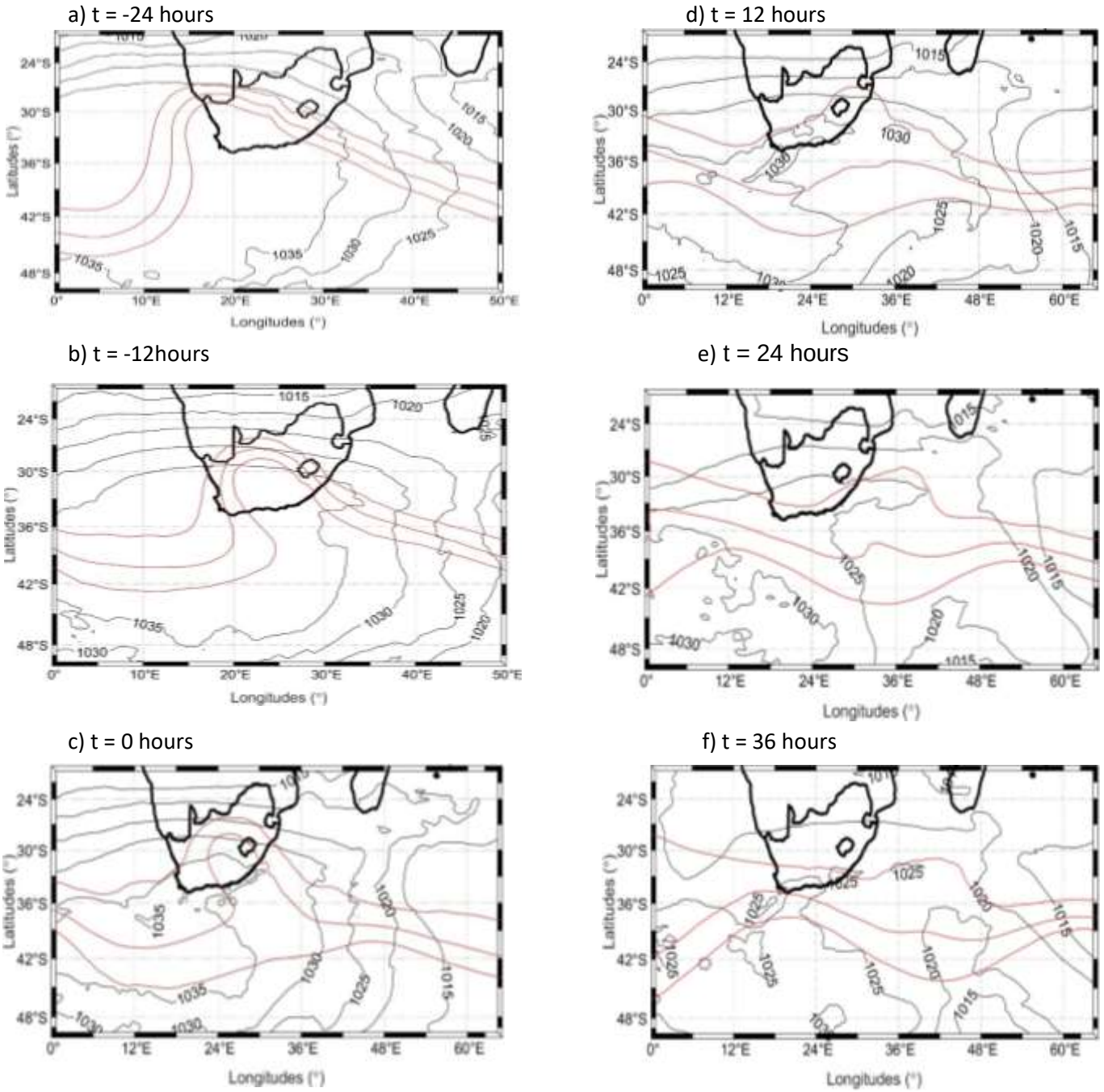

Figure 4.2: Time-lagged evolution of mean sea level pressure (thin contours) and geopotential heights (solid red) demonstrating impacts of diverse types of ridging highs on cut-off lows for **event 2** over South Africa.

Event three shows a more zonal structure of mean sea level pressure 24 hours prior to the COL development (Figure 4.3 a-b), which in this case extends/moves across the mainland as the COL event evolves overtime. The ridging high associated with the above-mentioned characteristics breaks off from the parent south Atlantic Ocean, leaving behind a weaker ridging component resulting in a stronger south Atlantic high (Ndarana *et al*, 2021). The highest pressure was clearly visible at latitudes lower than 30°S, which allowed the movement

across the mainland. Unlike event one and two, event three according to the associated characteristics of ridging highs is linked to Type-N ridging high.

The 250 hPa geopotential contours indicated folding from Figure 4.3 (a-b) up until the COL closed-circulation developed and started propagating east from Figure 4.3 (c-e). Figure 4.3 (f) shows that the geopotential contours became flatter as soon as the COL circulation starts to dissipate. Unlike event one and two, event three indicated signs of dissipation after 36 hours of formation, which in terms of geopotential contours indicates that event three was weaker than event one but stronger than event two.

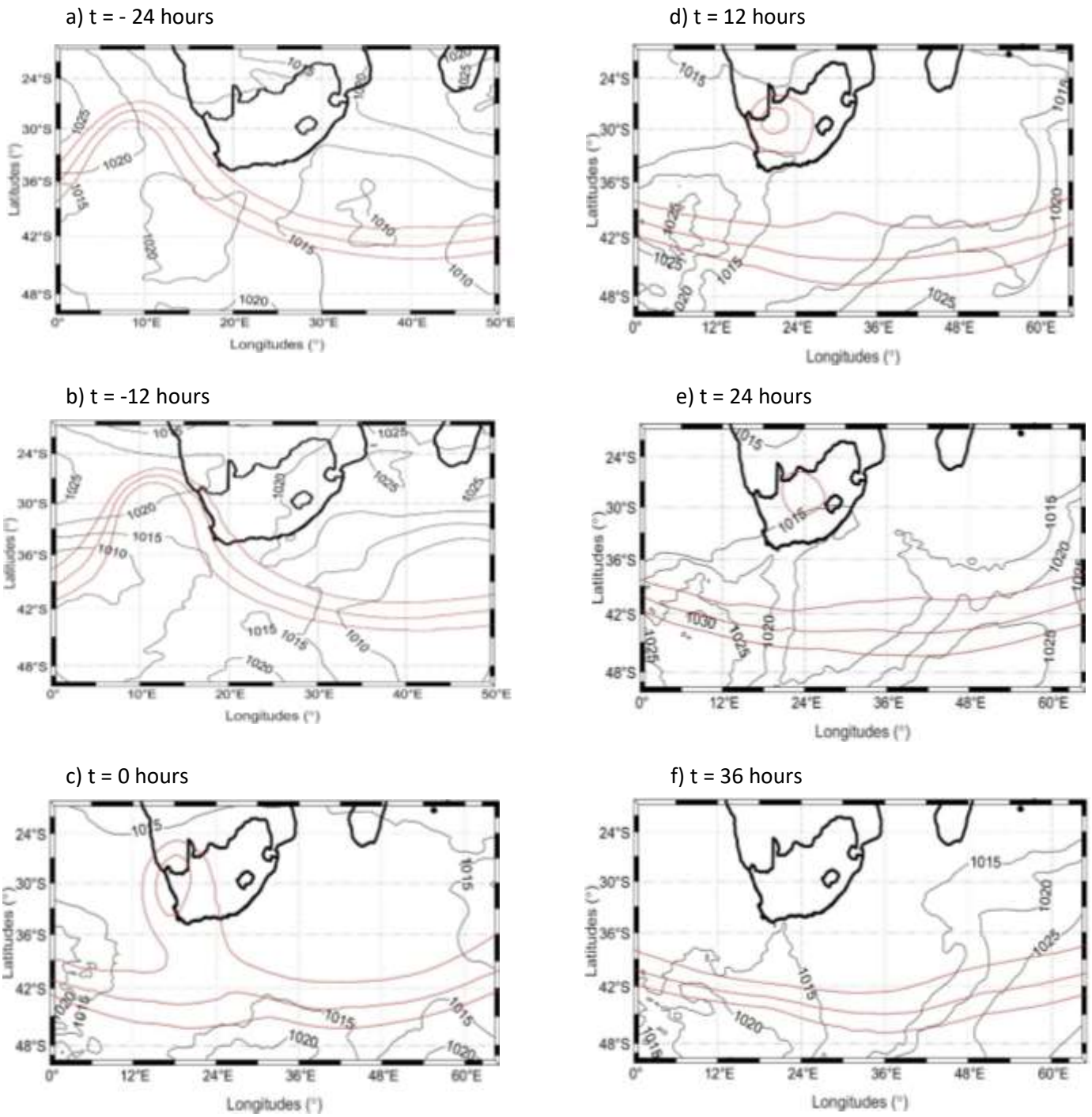

Figure 4.3: Time-lagged evolution of mean sea level pressure (thin contours) and geopotential heights (solid red) demonstrating impacts of diverse types of ridging highs on cut-off lows for **event 3** over South Africa.

Event four also shows a more zonal structure of mean sea level pressure, which in this case extends/moves across the mainland as the COL event evolves overtime (Figure 4.4 a-f). The ridging high associated with the above-mentioned characteristics breaks off from the parent south Atlantic Ocean, leaving behind a weaker ridging component resulting in a stronger south Atlantic high (Ndarana *et al*, 2021). The highest pressure was clearly visible at latitudes lower

than 40°S 24 hours and 12 hours prior to the formation of the COL. But as soon as the COL event forms, the highest-pressure surface was located far north at about 26°S. In conclusion, event four according to the associated characteristics of ridging highs is possible linked to Type-N ridging high.

The 250 hPa showed signs of folding 24 hours prior to the formation of the COL event (Figure 4.4 a-b), but a complete fold was clearly visible indicating closed-circulation from the day the COL formed (Figure 4.4 c). The geopotential contours started to weaken as the COL propagated east 12 hours after the formation (Figure 4.4 d-f). Like event one, the 250 hPa geopotential contours remained even after 36 hours of formation which indicates that the COL event was stronger than both event two and event three in terms of COL closed-circulation represented by geopotential heights.

a) t = -24 hours

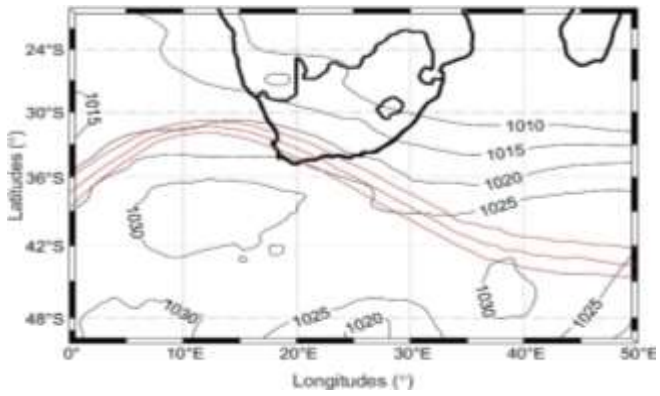

d) t =12 hours

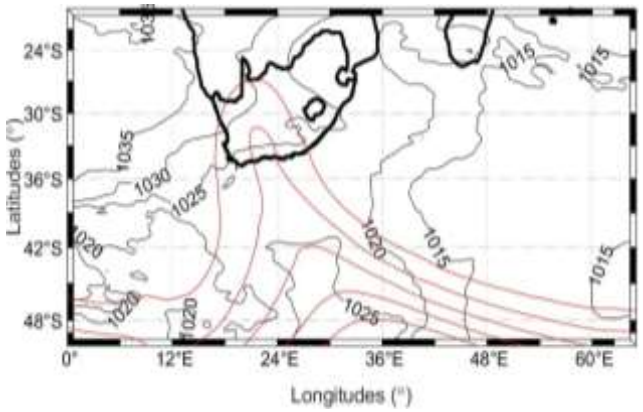

b) t = -12 hours

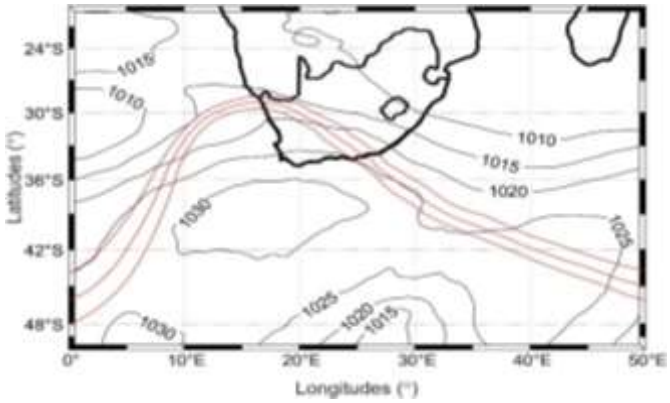

e) t = 24 hours

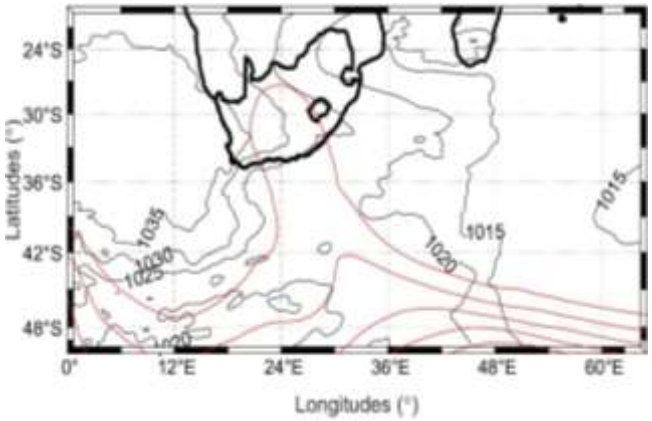

c) t = 0 hours

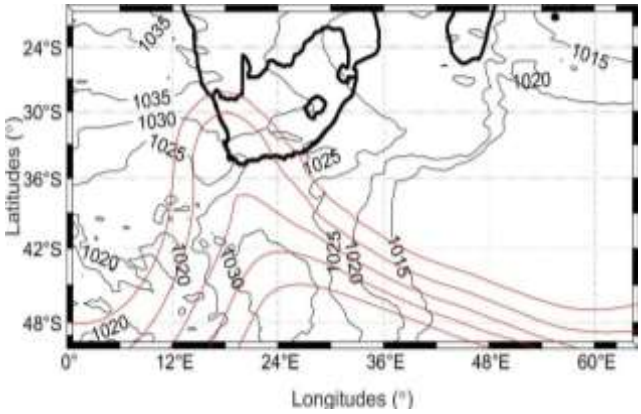

f) t = 36 hours

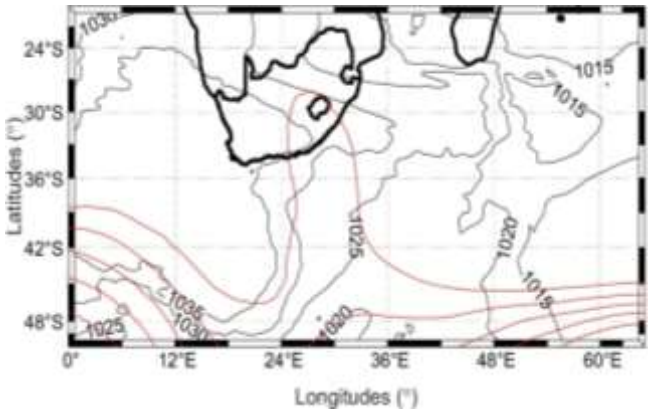

Figure 4.4: Time-lagged evolution of mean sea level pressure (thin contours) and geopotential heights (solid red) demonstrating impacts of diverse types of ridging highs on cut-off lows for **event 4** over South Africa.

4.2.2 **Geopotential height and Potential Vorticity identification of COLs**

In this study, high negative pool of PV (shaded) in geopotential contours' circulation represents the intensity of the COL event. The 500 hPa geopotential contour represents the closed circulation of the COL and it is also used to identify where the circulation was in terms of regions above (Figure 3.3). The vertical structures of PV presented below show how the definition of COL works, and that is, that a COL occurs when the circulation has been detached from the mid latitude flow (Figure 4.5 a-f, Figure 4.6 a-f, Figure 4.7 a-f and Figure 4.8 a-f). Positive (negative) pool of PV represents low (high) intensity of the COL event.

24 hours prior to the formation of the COL event one, there was high negative pool of PV coming from the south Atlantic Ocean, although there was no/less circulation during this period over the study indicating that the COL event is not yet formed (Figure 4.5 a). However, 12 hours prior to the formation of the COL event one, the geopotential contours start to show signs of folding indicating that a closed circulation will be formed as time surpasses, but at this point and time, the high PV intensity was reduced compared to the previous time slot and it was located where there are signs of folding of the geopotential contours (Figure 4.5 b).

High level circulation of geopotential contours compared to the previous day was located at about 31°S 21°E on this day (Figure 4.5 c) indicating a strong closed circulation with high intensity of PV at the centre of the circulation (COL is formed). However, 12 hours after the formation of the COL event one, the intensity of PV starts to decrease indicating that the COL is getting weaker as time goes by, although the geopotential closed circulation contours remained consistent throughout this event life cycle (Figure 4.5 d-f).

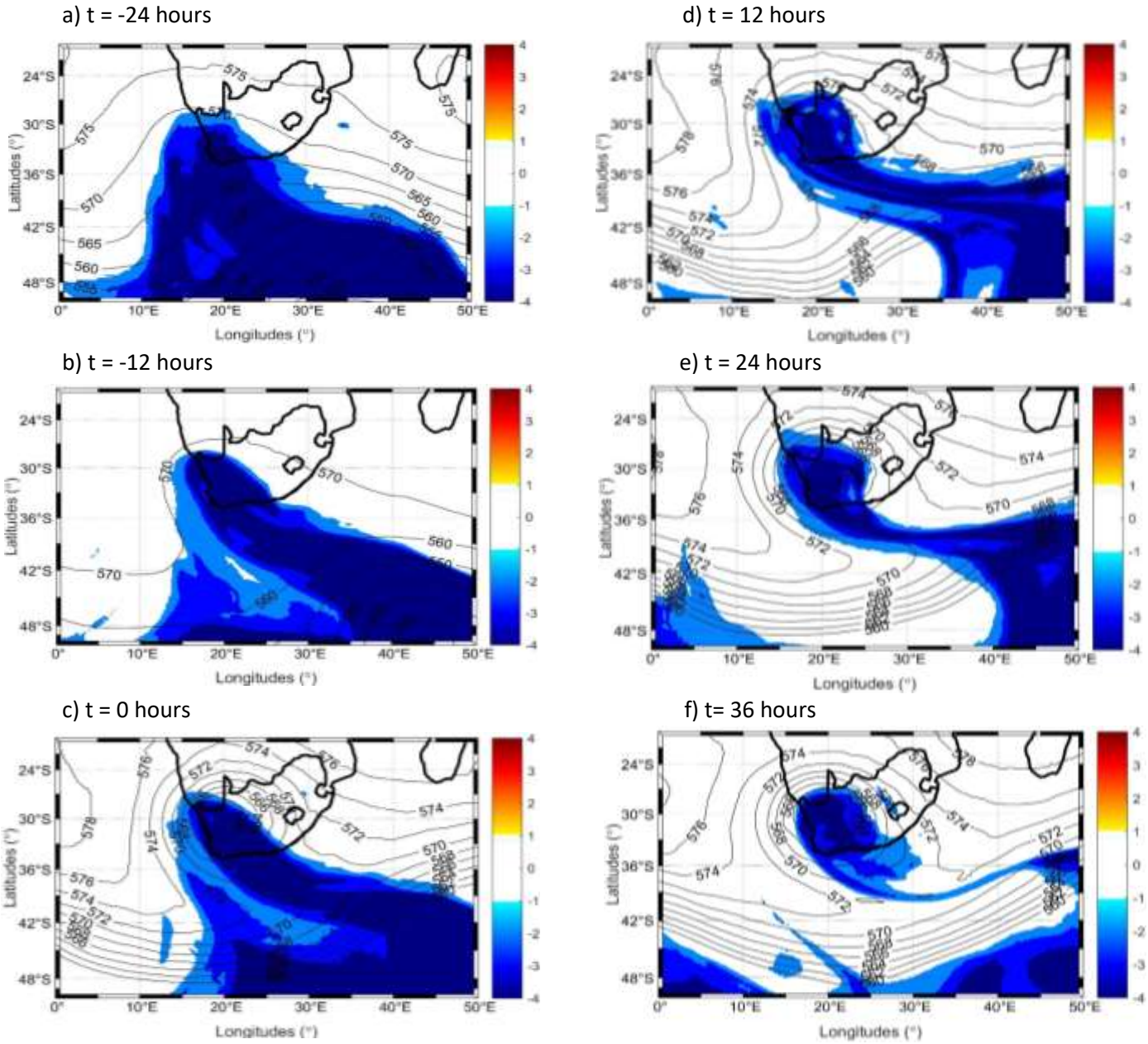

Figure 4.5: Time-lagged evolution of potential vorticity (shaded in blue) and geopotential heights (line contours) for **event 1**. Potential vorticity is plotted at 330 K and the geopotential height is plotted at 500 hPa.

Comparatively, 24 hours prior to the formation of the COL event two, there was high PV coming from the south Atlantic Ocean, although in this case, there was already signs of folding of geopotential contours indicating that there will be a closed circulation developing in the next day over the study, but the COL event is not yet formed at this stage (Figure 4.6 a). However, 12 hours prior to the formation of the COL event two, the geopotential contours showed visible signs of folding, but there were no signs of closed circulation at this stage. Although the high

PV intensity was reduced compared to the previous time slot, it was located where there are signs of folding of the geopotential contours as in event one (Figure 4.6 b).

High level circulation of geopotential contours compared to the previous day was located at about 30°S 29°E of the South African region at this day (Figure 4.6 c) indicating a strong closed circulation with high intensity of PV at the centre of the circulation (COL is formed). However, 12 hours after the formation of the COL event two, the intensity of PV starts to decrease indicating that the COL is getting weaker as time goes by, although in this case unlike event one, another wave of high PV intensity was coming into the region from the south Atlantic Ocean (Figure 4.6 d-f). The geopotential closed circulation contours indicated signs of inconsistency after the day of the formation representing the decay stages of the event two, unlike event one which was consistent throughout its life cycle and can only assume its decay stages by looking at the depth of PV wave (Figure 4.6 e-f).

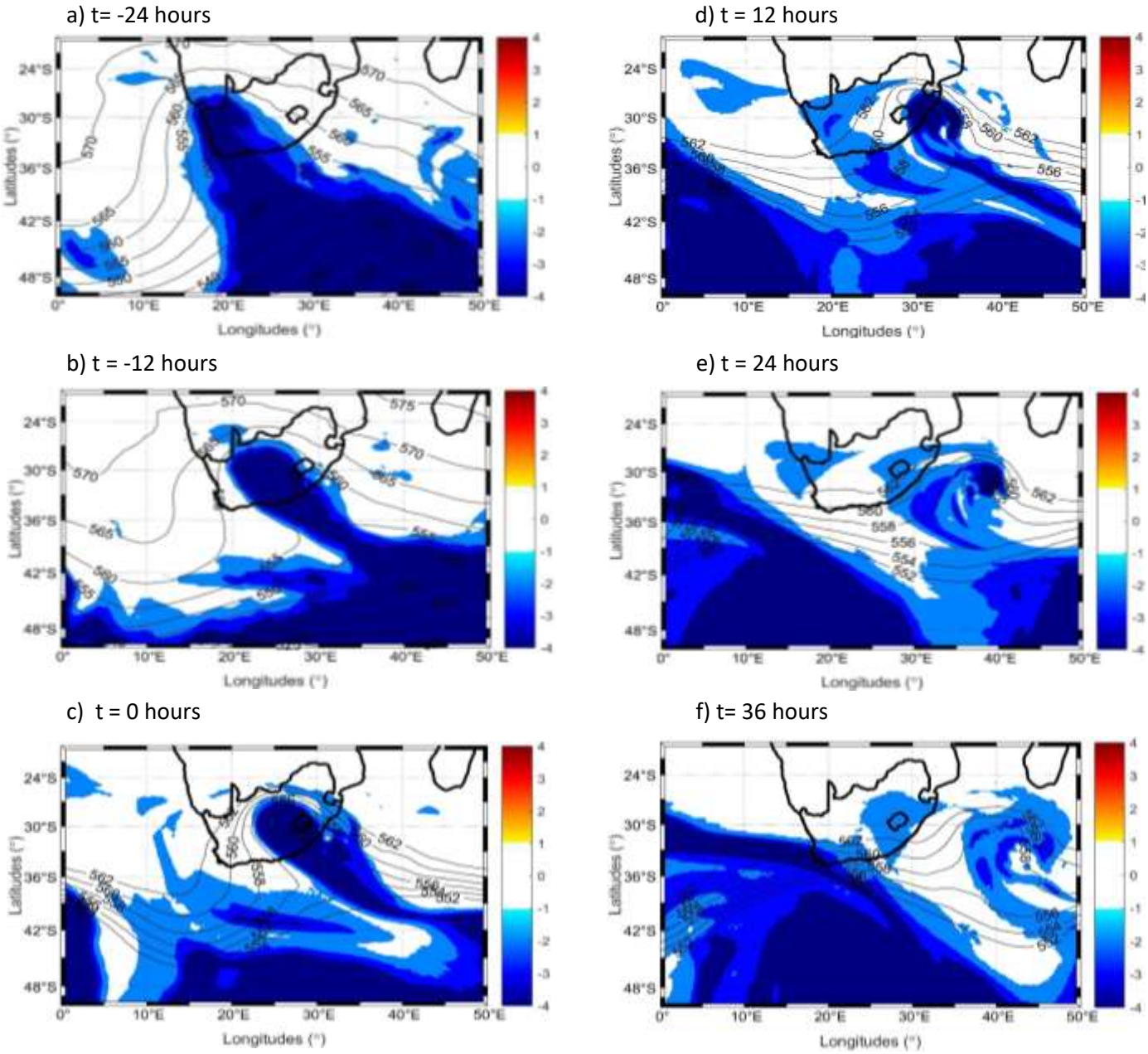

Figure 4.6: Time-lagged evolution of potential vorticity (shaded in blue) and geopotential heights (line contours) for **event 2**. Potential vorticity is plotted at 330 K and the geopotential height is plotted at 500 hPa.

There was a high negative pool of PV coming from the south Atlantic Ocean as in event two (24 hours prior to the formation of COL event three). Although in this case, there was already signs of closed circulation forming of geopotential contours indicating that there will be a closed system developing in the next day over the study (the close circulation of the geopotential contours was located west of the South African region) (Figure 4.7 a). However, 12 hours prior to the formation of the COL event three, the geopotential contours already show the folding stage of the geopotential contours, but there were no signs of closed circulation at

this stage, although the high PV intensity was reduced compared to the previous time slot, it was located where there are signs of folding of the geopotential contours as in event one and two (Figure 4.7 b).

High level circulation of geopotential contours compared to the previous day was located at about 29°S 18°E of the South African region at this day (Figure 4.7 c) indicating a strong centre of closed circulation with high intensity of PV at the centre of the circulation (COL is formed). However, 12 hours after the formation of the COL event three, the intensity of PV starts to decrease indicating that the COL is getting weaker as time goes by, although in this case unlike event one, another wave of high PV intensity was coming into the region from the south Atlantic Ocean as in event two (Figure 4.6 d-f). The geopotential closed circulation contours indicated signs of consistency after the day of the formation of the COL, where we can only assume the decay stage of the COL event by looking at the depth of the PV wave as in event one, whereas the decay stages of event three are also indicated by the geopotential contours (Figure 4.7 d-f).

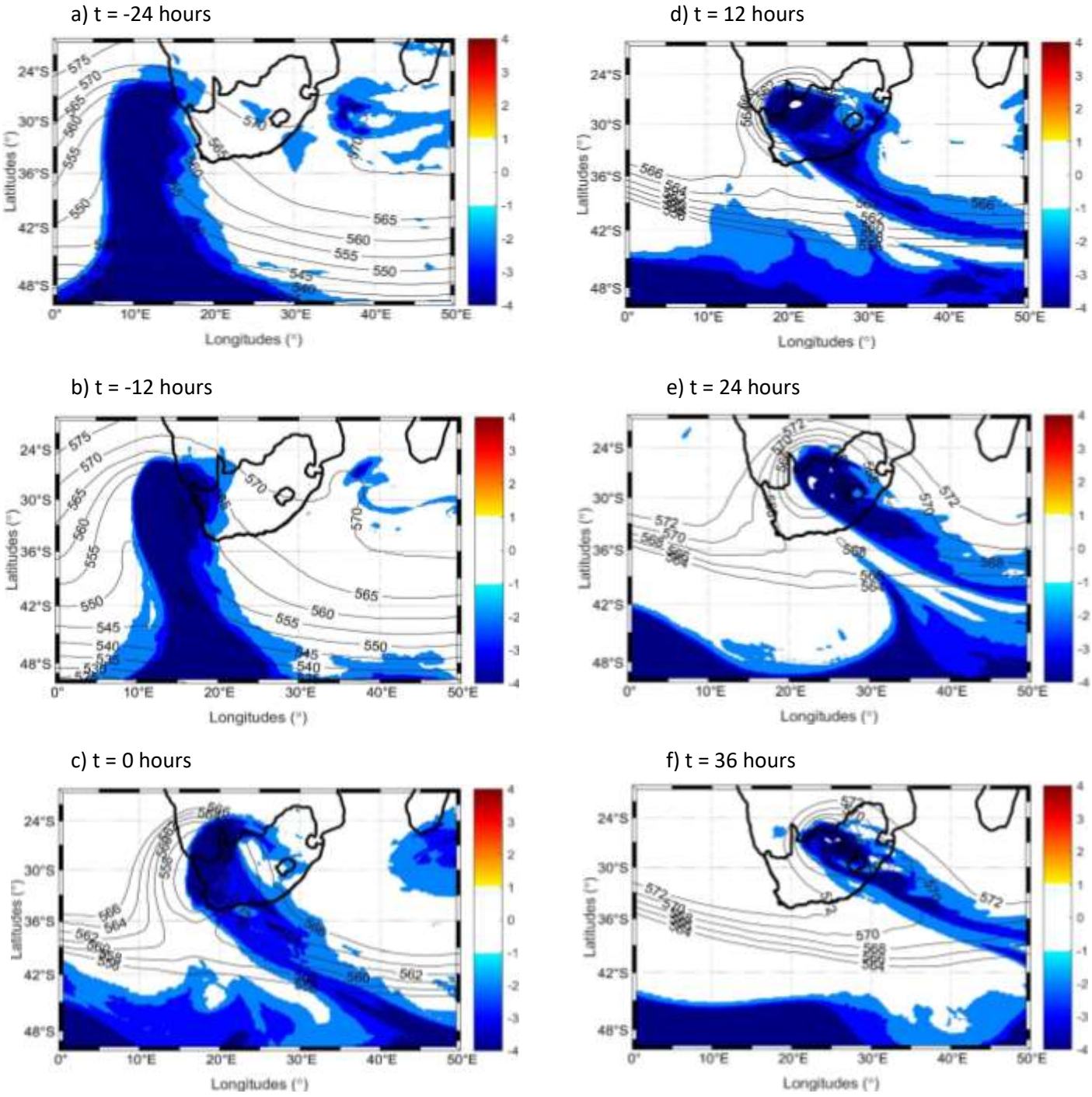

Figure 4.7: Time-lagged evolution of potential vorticity (shaded in blue) and geopotential heights (line contours) for **event 3**. Potential vorticity is plotted at 330 K and the geopotential height is plotted at 500 hPa.

In the same vein, 24 hours prior to the formation of the COL event four, there was high PV coming from the south Atlantic Ocean, although in this case, there was already signs of folding of geopotential contours indicating that there will be a closed circulation developing in the next day over the study, but the COL event is not yet formed at this stage (Figure 4.8 a). However,

12 hours prior to the formation of the COL event four, the geopotential contours already show the folding stage of the geopotential contours, but there were no signs of closed circulation at this stage, although the high PV intensity was reduced compared to the previous time slot (12 hours), it was located where there are signs of folding of the geopotential contours as in event three (Figure 4.8 b).

High level circulation of geopotential contours compared to the previous day was located at about 29°S 27°E of the South African region at this day representing a mature COL (Figure 4.8 d), a strong closed circulation with high intensity of PV at the centre of the circulation was also observed. However, 12 hours after the formation of the COL event four, the intensity of PV starts to decrease indicating that the COL is getting weaker as time goes by, although in this case like event one, there was less/no wave of high PV intensity moving into the region from the south Atlantic Ocean (Figure 4.8 d-f). The geopotential closed circulation contours indicated signs of consistency after the day of the formation representing a stronger decay stage of the COL compared to event two but like event one and three which were consistent throughout their life cycles and can only assume their decay stages by looking at the depth of PV wave (Figure 4.8 e-f).

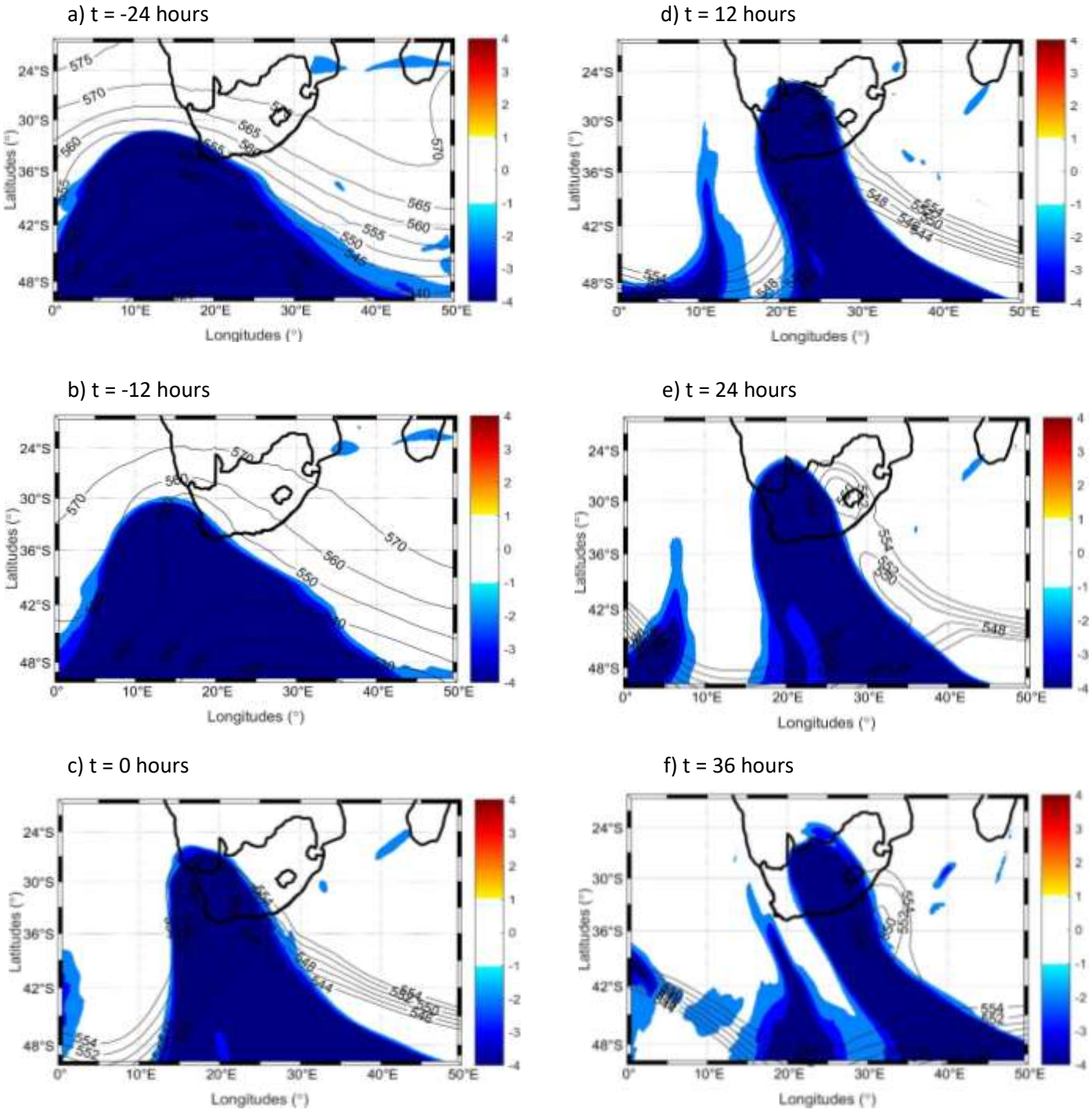

Figure 4.8: Time-lagged evolution of potential vorticity (shaded in blue) and geopotential heights (line contours) for **event 4**. Potential vorticity is plotted at 330 K and the geopotential height is plotted at 500 hPa.

4.3 **Potential Vorticity (PV) analysis of COLs (2D)**

4.3.1 **Zonal profiles of the COLs events**

In this case, the blue line contours from the figures (a-f) below represent the PV (-2.5, -2 and -1.5 PVU) indicating the position of the dynamical tropopause in the atmosphere. Nieto *et al*, (2008) and Ndarana *et al*, (2020) demonstrated that any opening in the dynamic tropopause will cause folding of the PV which result in the intrusion of stratospheric air into the upper troposphere. The folding of the PV will indicate various stages of the COL event life cycle in question. The grey labelled line contours from the figures (a-f) below represent the isentropic surfaces which in this case will indicate the cold cores of the COLs. The brownish shaded surfaces from the figures (a-f) below represent the zonal wind indicating the location of small-scale jet.

There were no signs of folding of the PV contours as this observation was supported by weaker jet just above it prior (24 hours) to the formation of the COL event one (Figure 4.9 a). Hence, 12 hours prior to the formation of the COL, there were less/little folds observed over the study but in this case, the jet increased in strength compared to the previous 12 hours (Figure 4.9 b). On the contrary, we observed the folding of the PV at t = 0, which indicates an opening in the dynamic tropopause allowing the intrusion of stratospheric air into the troposphere resulting in formation of the COL (Figure 4.9 c). following the centre of the COL (21°E), the jet is getting weaker as the COL is getting deeper as it evolves compared to the previous 12 hours during the formation and it also shows signs of extension to the surface as the COL extends towards the surface (Figure 4.9 d-f).

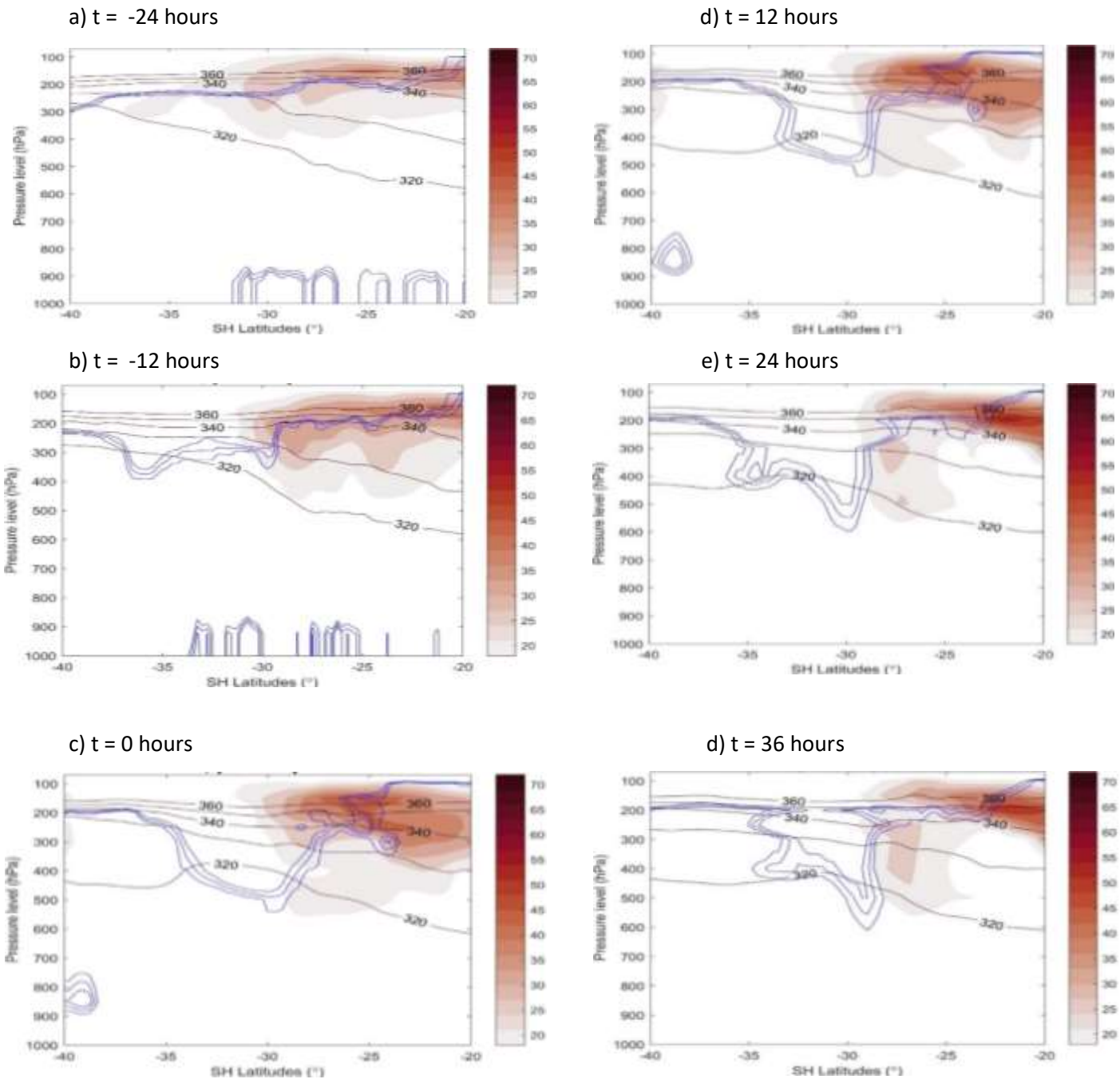

Figure 4.9: Time-lagged evolution of latitudinal profiles of potential vorticity (blue contours), potential temperature (grey contours) and zonal wind (shaded) for **event 1**. The potential vorticity is plotted at -2.5,-2 and -1.5 PVU and the zonal wind is plotted from 18 to 72 m/s throughout the time steps.

Compared to event one at this stage, there was signs of folding of the PV observed 24 hours prior to the formation of the COL event two, with strong jet just above it (Figure 4.10 a). Hence, the jet is also indicating signs of extensions to the surface even before the COL is formed (Figure 4.10 a-b). There were folds observed over the study at about 35°S to 25°S prior to the

formation of the COL (12 hours), but in this case, the jet increased in strength with reduced size compared to the previous 12 hours (Figure 4.10 b). on the contrary, we observed high folding of the PV at t = 0, which indicates an opening in the dynamic tropopause allowing the intrusion of stratospheric air into the troposphere resulting in formation of the COL (Figure 4.10 c). following the centre of the COL (27°E), the jet getting weaker compared to the day the COL was formed but is also extending to the surface as the COL is getting deeper and evolving over time (Figure 4.10 d-f). The decay stage of this COL (event two) is better than event one because it shows that the COL extended to the surface along with its jets (reached about 900 hPa) (Figure 4.10 f).

a) t = -24 hours

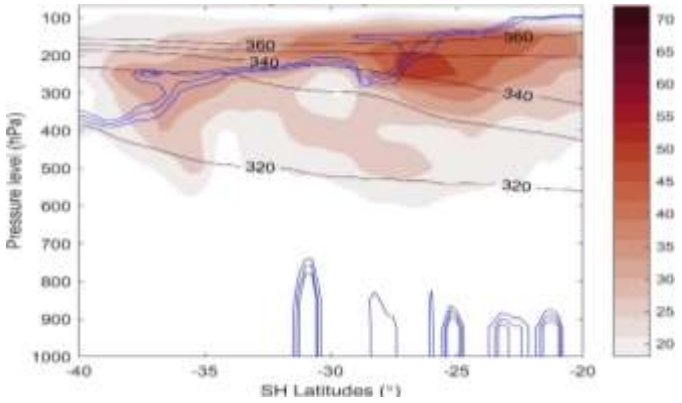

d) t = 12 hours

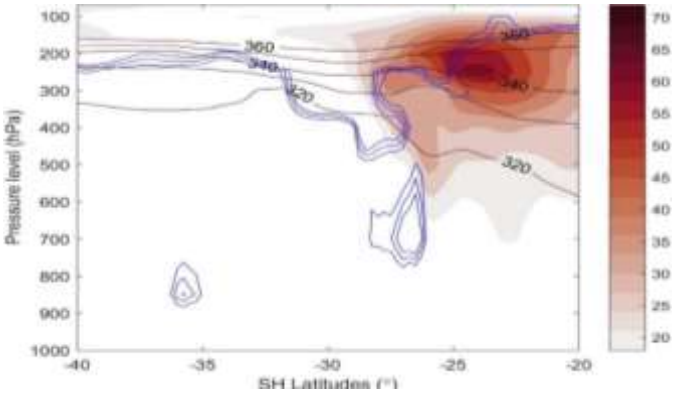

b) t = -12 hours

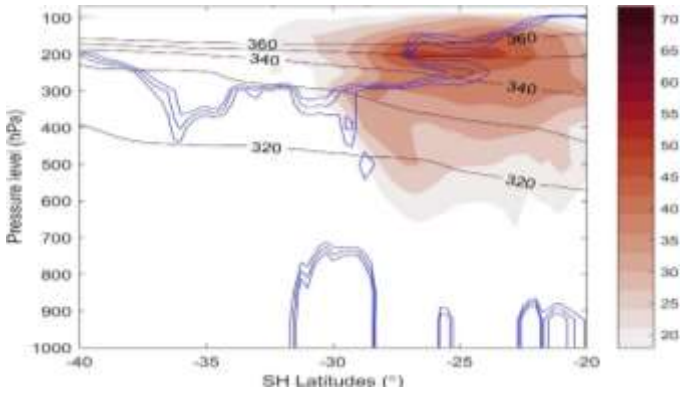

e) t = 24 hours

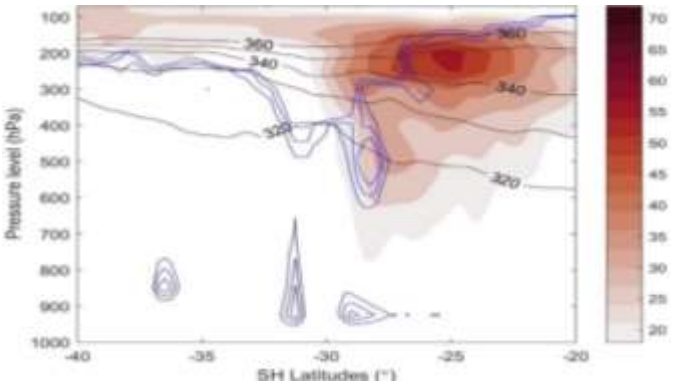

c) t = 0 hours

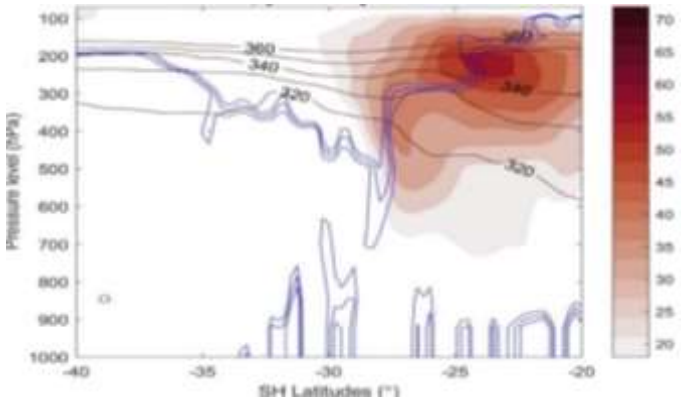

f) t = 36 hours

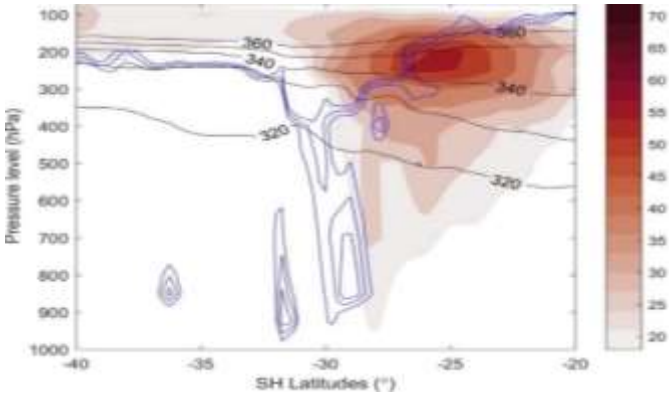

Figure 4.10: Time-lagged evolution of latitudinal profiles of potential vorticity (blue contours), potential temperature (grey contours) and zonal wind (shaded) for **event 2**. The potential vorticity is plotted at -2.5,-2 and -1.5 PVU and the zonal wind is plotted from 18 to 72 m/s throughout the time steps.

Similarly, event three figures (4.11 a-f) like event two indicated no/less signs of folding of the PV contours observed 24 hours prior to COL genesis, with stronger jet propagating east from the west. Unlike event two, the jet is not indicating signs of extensions to the surface even

before the COL is formed (Figure 4.11 a). There were signs of folding 12 hours prior to the formation of the COL observed over the study at about 25°S, with an increased jet strength compared to the previous 12 hours (Figure 4.11 b). On the contrary, we observed high folding of the PV at t = 0, which indicates an opening in the dynamic tropopause allowing the intrusion of stratospheric air into the troposphere resulting in formation of the COL (Figure 4.11 c). following the centre of the COL (27°E), the jet getting stronger compared to the day the COL was formed but is also extending to the surface as the COL is getting deeper and evolving over time (Figure 4.11 d-f). The decay stage of this COL (event three) is better than event one because the folding of the dynamic tropopause is deep, but the COL do not extend further than 500 hPa to the surface along with its jet (Figure 4.11 e-f).

a) t = -24 hours

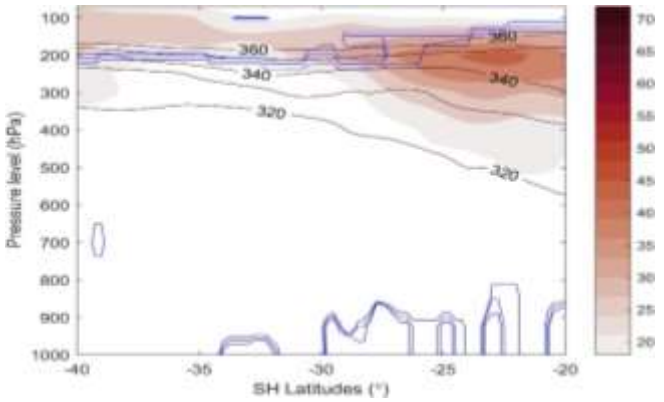

d) t = 12 hours

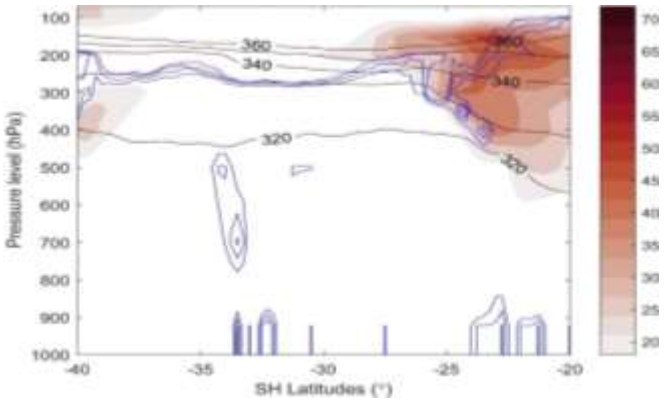

b) t = -12 hours

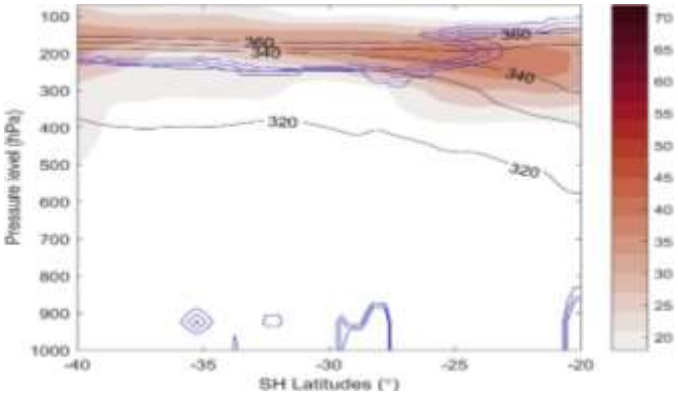

e) t = 24 hours

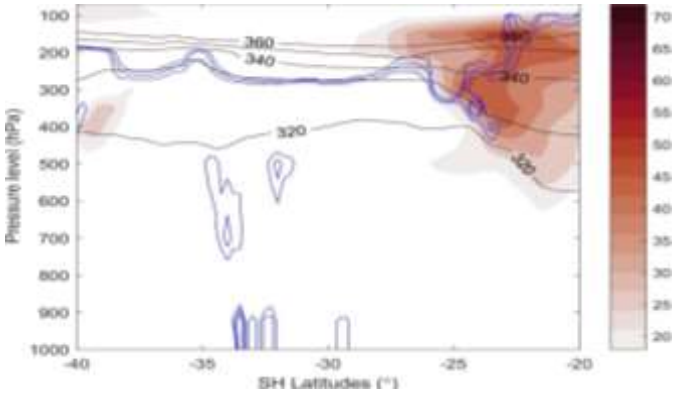

c) t = 0 hours

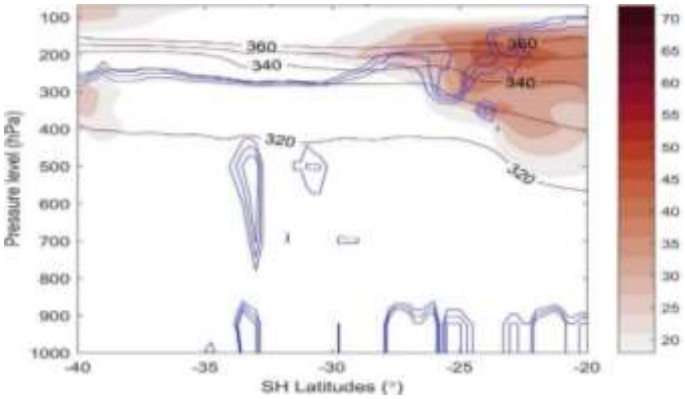

f) t = 36 hours

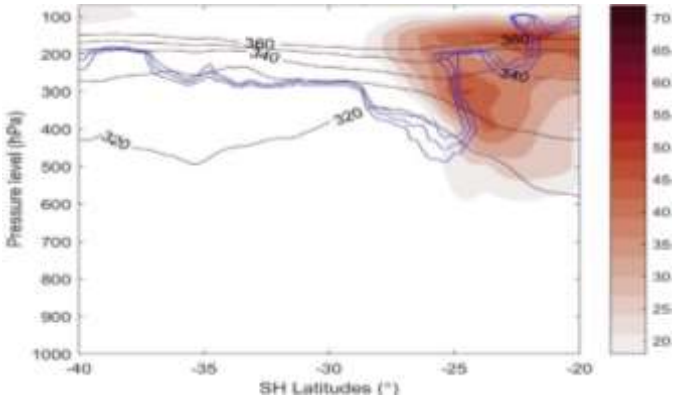

Figure 4.11: Time-lagged evolution of latitudinal profiles of potential vorticity (blue contours), potential temperature (grey contours) and zonal wind (shaded) for **event 3**. The potential vorticity is plotted at -2.5,-2 and -1.5 PVU and the zonal wind is plotted from 18 to 72 m/s throughout the time steps.

As in event three, there were no/less signs of folding of the PV contours observed with stronger jet propagating east from the west 24 hours prior to the formation of the COL event four (Figure 4.12 a). Like event three, the jet is not indicating signs of extensions to the surface even before

the COL is formed (Figure 4.12 a-b). There were signs of folding observed over the study at about 30°S to 25°S prior (12 hours) to the formation of the COL with strengthened jet compared to the previous 12 hours (Figure 4.12 b). on the contrary, we observed high folding of the PV at t = 0, which indicates an opening in the dynamic tropopause allowing the intrusion of stratospheric air into the troposphere resulting in formation of the COL (Figure 4.12 c). following the centre of the COL (18°E), the jet getting weaker compared to the day the COL was formed but is also extending to the surface as the COL is getting deeper and evolving over time (Figure 4.12 d-f). The decay stage of this COL (event four) is similar to event one because the folding of the dynamic tropopause is deep, but the COL do not extend further than 600hPa to the surface along with its jet (Figure 4.12 e-f).

a) t = -24 hours

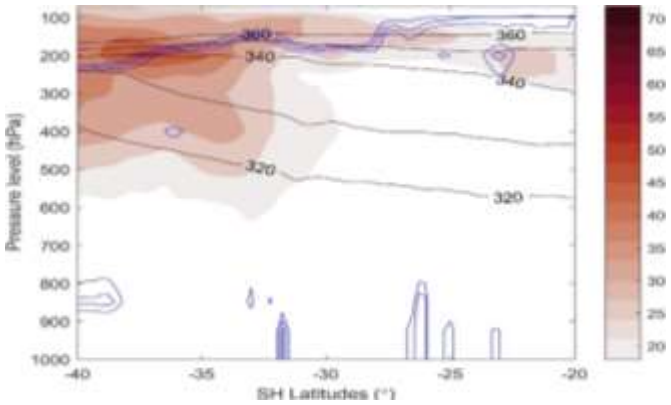

d) t = 12 hours

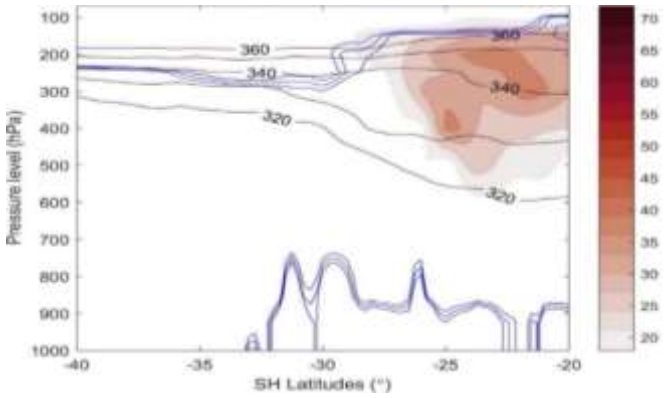

b) t = - 12 hours

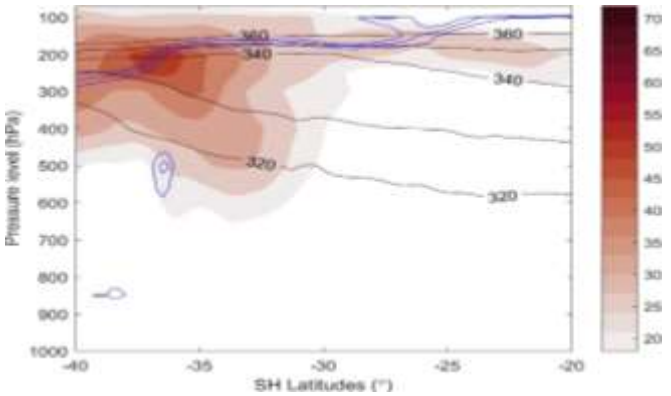

e) t = 24 hours

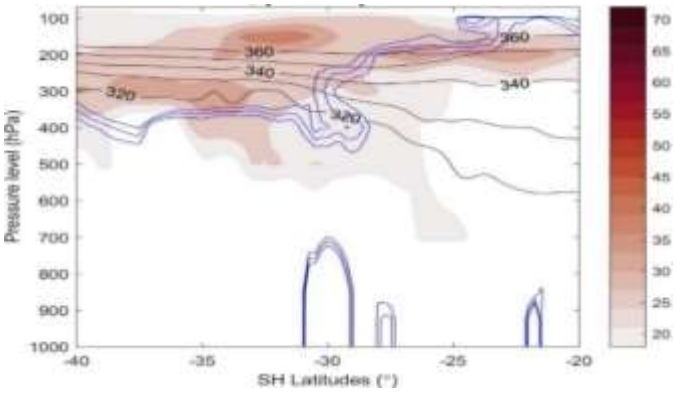

c) t = 0 hours

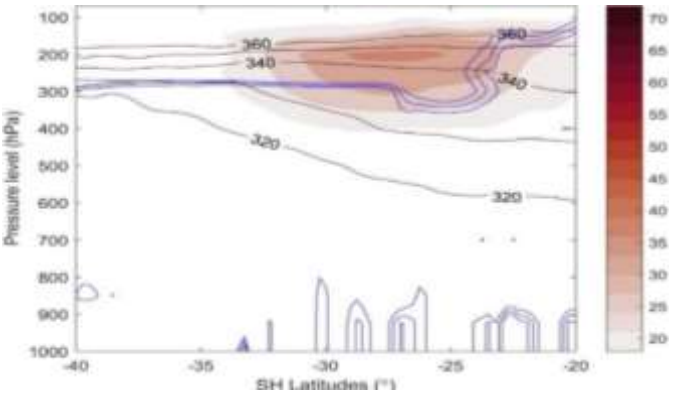

f) t = 36 hours

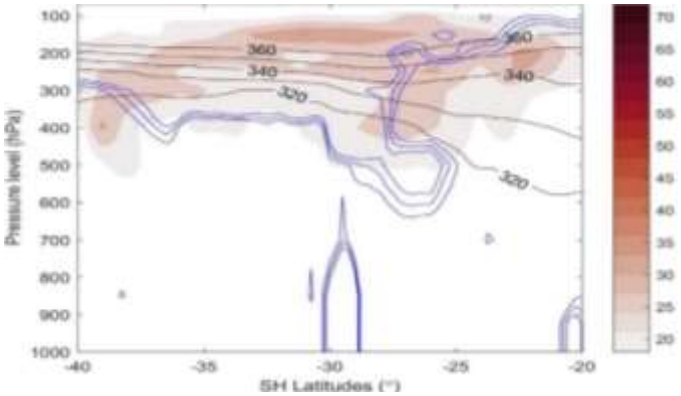

Figure 4.12: Time-lagged evolution of latitudinal profiles of potential vorticity (blue contours), potential temperature (grey contours) and zonal wind (shaded) for **event 4**. The potential vorticity is plotted at -2.5,-2 and -1.5 PVU and the zonal wind is plotted from 18 to 72 m/s throughout the time steps.

.

4.3.2 **Meridional profiles of COLs**

This section of the study presented the meridional view of COLs (Figure 4.13 - 4.16 a-f) using jet streak (brownish shaded) propagation to the east along with its intensity and the location of cold cores (grey line contours). In this case, the folding of the dynamical tropopause represented by the PV (blue line contours) will be observed with COL extensions towards the surface. The cold-cores of the COLs events are presented using the 330 K contour (grey).

The PV contours were more zonal and narrower with little/ no folding observed 24 hours prior to the day the COL event one formed with the jet developing just above it (Figure 4.13 a). Moreover, the cold core of the COL represented by the 330 K contour was not visible at this stage (Figure 4.13 a). There was a clear indication of folding at about 18°E before the COL forms, with the dynamical tropopause allowing the intrusion of stratospheric air into the upper troposphere (Figure 4.13 b). whilst the jet streak was getting stronger compared to the previous timeslot propagating east (Figure 4.13 b).

During the day the COL event one forms, the PV intrusions deepens compared to the previous timeslots along with its jet getting stronger and more stable just above it, whilst the cold core of the COL event was observed during this time at about 18°E (Figure 4.13 c). Hence, 12 hours after the COL event one formed, PV intrusions increases compared to the previous timeslot with its jet increasing in strength but still stable in movement located above the PV, whilst the cold core was more intense at this timeslot compared to the previous timeslots.

The decaying stages of the COL from this view was presented with the folding of the PV becoming weak/stable compared to the previous timeslots, along with its jet initialising movements towards the east with increasing strength compared to the previous timeslots(Figure 4.13 e-f). At this point, the cold core of the COL event was still observed but it was not intense as the day the COL event was formed. This indicates that this event (event one) was still stronger even during its decay stages in terms of the jet streak, PV, and its cold core (Figure 4.13 e-f).

a) t = -24 hours

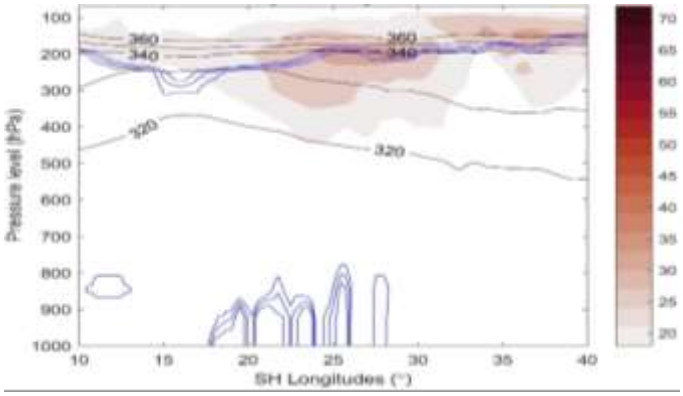

d) t = 12 hours

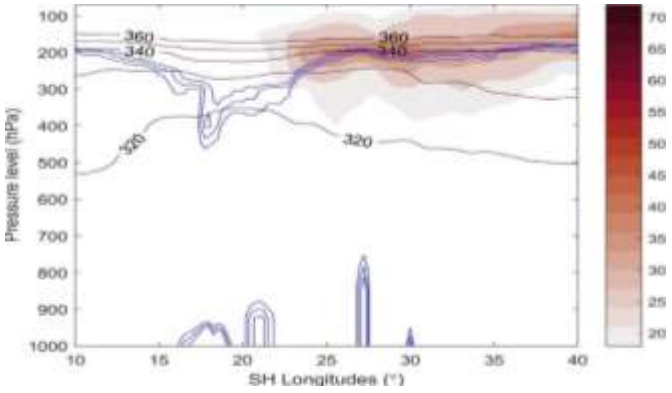

b) t = -12 hours

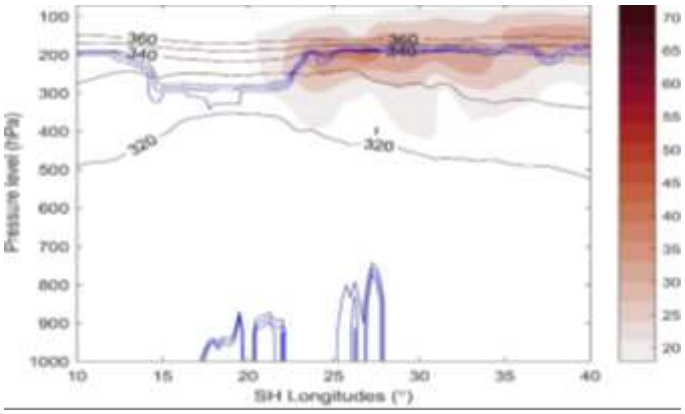

e) t = 24 hours

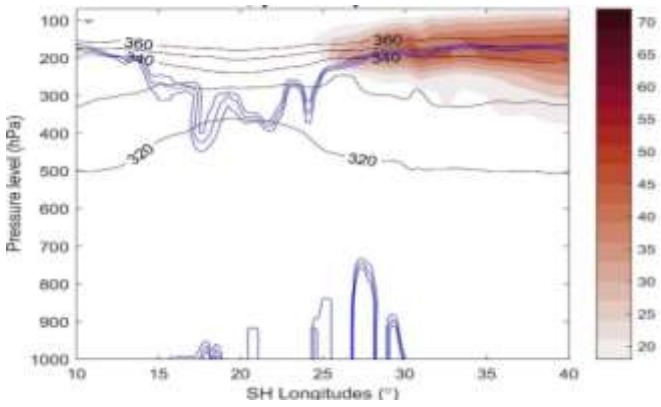

c) t = 0 hours

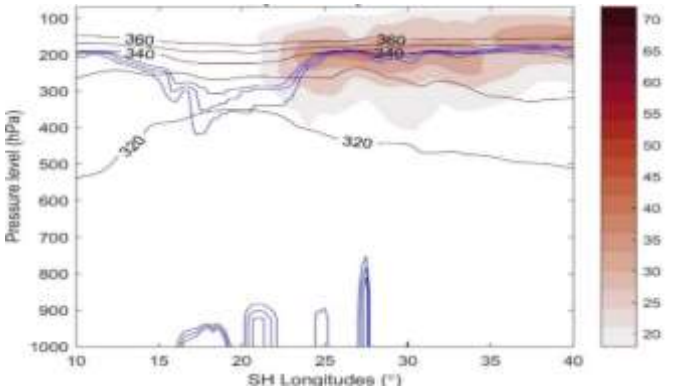

f) t = 36 hours

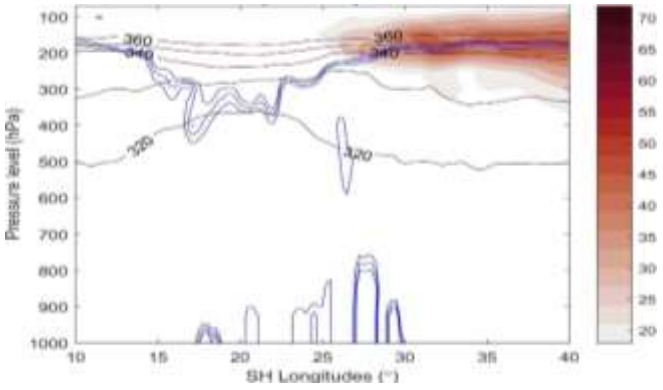

Figure 4.13 Time-lagged evolution of longitudinal profiles of potential vorticity (blue contours), potential temperature (grey contours) and zonal wind (shaded) for **event 1**. The potential vorticity is plotted at -2.5,-2 and -1.5 PVU and the zonal wind is plotted from 18 to 72 m/s throughout the time steps for **event**1.

The PV contours indicated signs of folds with deep intensity prior to the day the COL event two formed (Figure 4.14 a). A stronger jet compared to event one was observed developing at this stage just above the PV folds with the cold core of the COL represented by the 330 K

contour present at this stage (Figure 4.14 a). However, 12 hours before the COL forms, the folding of the PV increased at about 23°E with the dynamical tropopause allowing the intrusion of stratospheric air into the upper troposphere (Figure 4.14 b). Whilst the jet streak got stronger compared to the previous timeslot propagating east along with PV intrusions, the cold core of the COL was still developing at this stage (Figure 4.14 b).

During the day the COL event two forms, the PV intrusions deepens compared to the previous timeslots along with its jet getting stronger indicating signs of extensions to the surface as the PV deepens (Figure 4.14 c). The cold core of the COL event was observed completely developed during this time at about 27°E (Figure 4.14 c). Hence, 12 hours after the COL event two formed, PV intrusions increases compared to the previous timeslot with its jet increasing in strength and getting longer but still located above the PV (Figure 4.14 d). The cold core was less intense at this stage (Figure 4.14 d) compared to the previous timeslot (t = 0 hours).

The decaying stages of the COL event from this view was presented with the folding of the PV becoming stable and the COL extending towards the surface up to about 900 hPa compared to the previous timeslots, along with its jet continuing its movements towards the east with increasing strength compared to the previous timeslots (Figure 4.14 e-f). Like event one, the cold core of the COL event was still observed but it was not intense as the day the COL event was formed. This indicates that this event (event two) was still stronger during its decay stages in terms of the jet streak and cold core, but its PV was different in terms of extensions to the surface (Figure 4.14 e-f).

In conclusion, event two was stronger than event one in terms of developing stages in terms of the PV intrusions, stronger jet but similar during the mature stage where the cold core of the events was observed around the same time steps. Hence, the decay stages of the COL represent the stage where the COL is dissipating and the two events were different in terms of the jet getting stronger (weaker) and narrow (broad) on event two (one) as it propagates east, although the PV indicated signs of extensions to the surface on event two and not on event one, the cold cores were stable on both events (Figure 4.14 e-f).

a) t = -24 hours

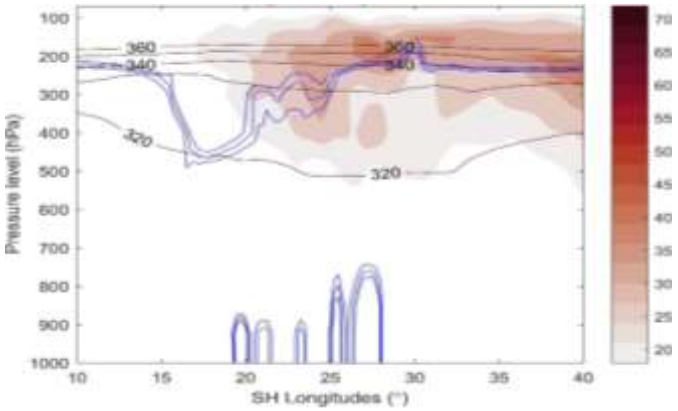

d) t = 12 hours

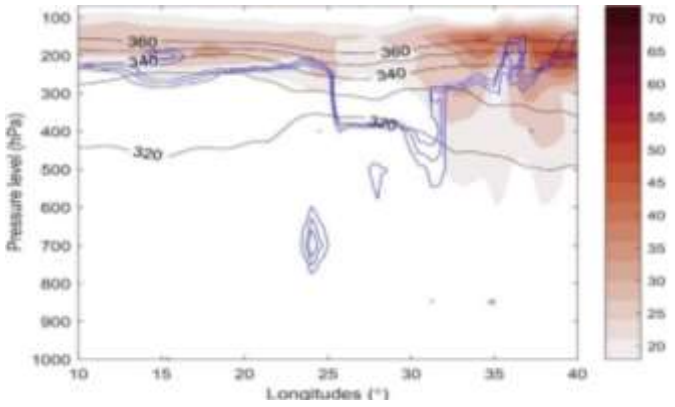

b) t = -12 hours

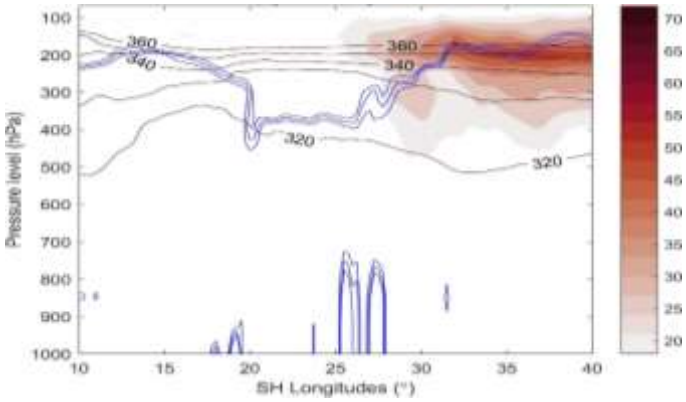

e) t = 24 hours

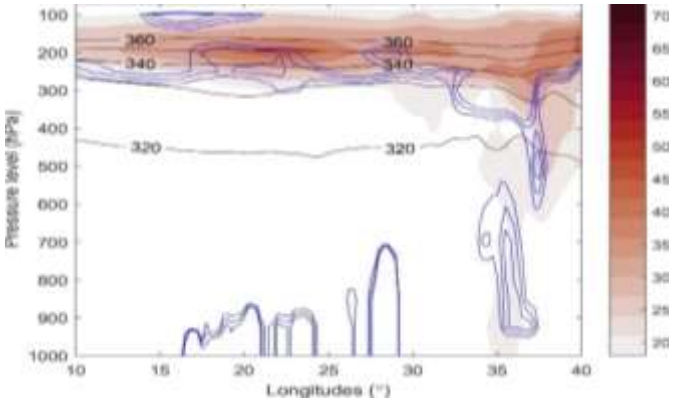

c) t = 0 hours

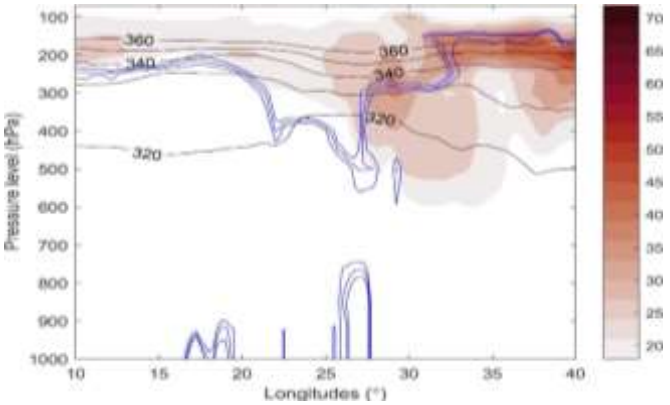

f) t = 36 hours

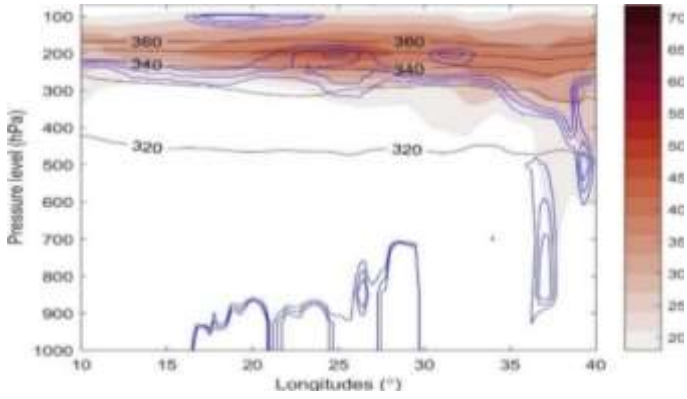

Figure 4.14 Time-lagged evolution of longitudinal profiles of potential vorticity (blue contours), potential temperature (grey contours) and zonal wind (shaded) for **event 2**. The potential vorticity is plotted at -2.5,-2 and -1.5 PVU and the zonal wind is plotted from 18 to 72 m/s throughout the time steps for **event 2**.

Like event one, 24 hours prior to the day the COL event three forms, the PV contours were more zonal and narrower with little/ no folding observed at this time with the jet developing just above it. Moreover, the cold core of the COL represented by the 330 K contour was not visible

at this stage (Figure 4.15 a). However, 12 hours before the COL forms, there was little/less indication of folding at about 10°E to 20°E where the dynamical tropopause allow the intrusion of stratospheric air into the upper troposphere, whilst the jet streak is getting stronger compared to the previous timeslot and is also propagating east (Figure 4.15 b).

During the day the COL event three forms, the PV intrusions deepens compared to the previous timeslots along with its jet getting stronger and propagating east just above it, whilst the cold core of the COL event was observed during this time at about 20°E (Figure 4.15 c). Hence, 12 hours after the COL event three formed, PV intrusions decreases compared to the previous timeslot with its jet increasing in strength but becoming narrower located above the PV, whilst the cold core was more intense at this timeslot compared to the previous timeslots (Figure 4.15 d). The cut off stage was also observed at this time step for this COL event (Figure 4.15 d)

The decaying stages of the COL event from this view was presented with the folding of the PV (PV intrusions) becoming weak/stable compared to the previous timeslots, along with its jet propagations to the east with increasing strength compared to the previous timeslots (Figure 4.15 e-f). At this point, the cold core of the COL event was still observed but it was not intense as the day the COL event was formed. This indicates that this event (event three) was still stronger even during its decay stages in terms of the jet streak, PV, and its cold core.

On the contrary, the development stages of COL event three were different compared to event two in terms of the folding of the PV for stratospheric air intrusions but similar with event one with little/less folding during this time steps. However, events one and three are similar in terms of the strength and narrower shape of the jet streak developing just above it, whereas the jet streak of event two is broad during its development stages. The cold cores of this events were observed intensively at about the same timesteps where the COL formed and matured. Hence, the decay stages of the COL represent the stage where the COL is dissipating, and the strengthening of the jet compared to its maturity stages on event three. The jet got stronger (weaker) and narrow (broad) on event two (one) as it propagates east. Although the PV indicated signs of extensions to the surface on event two and three not on event one, the cold cores were stable here on (Figure 4.15 e-f).

a) t = -24 hours

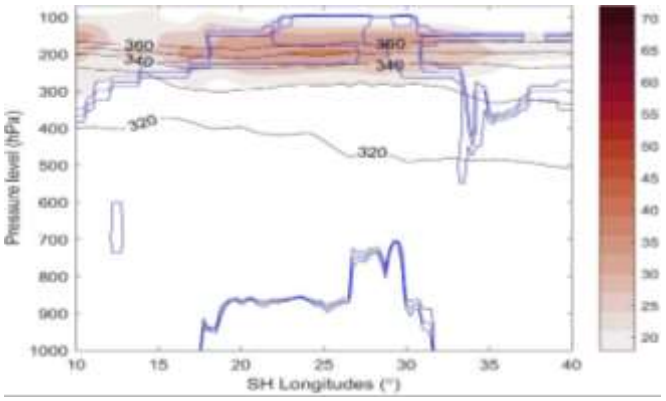

d) t = 12 hours

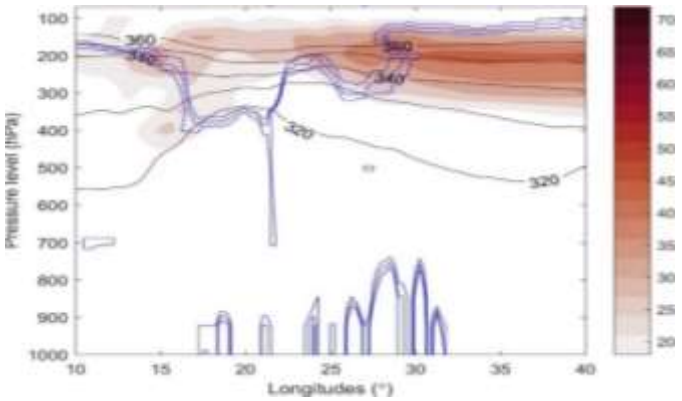

b) t = -12 hours

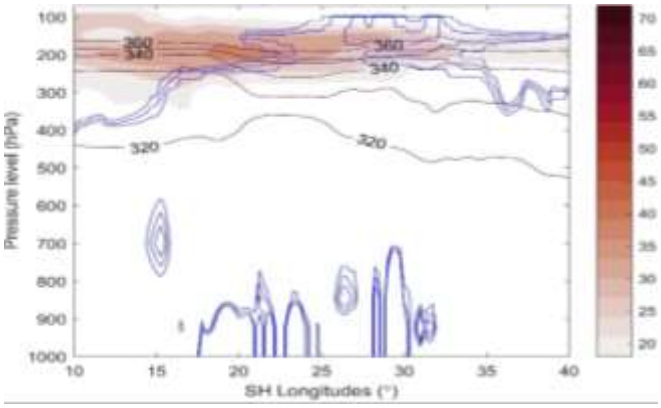

e) t = 24 hours

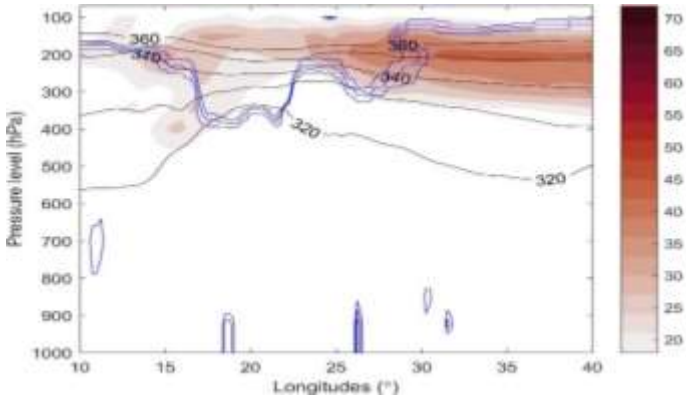

c) t = 0 hours

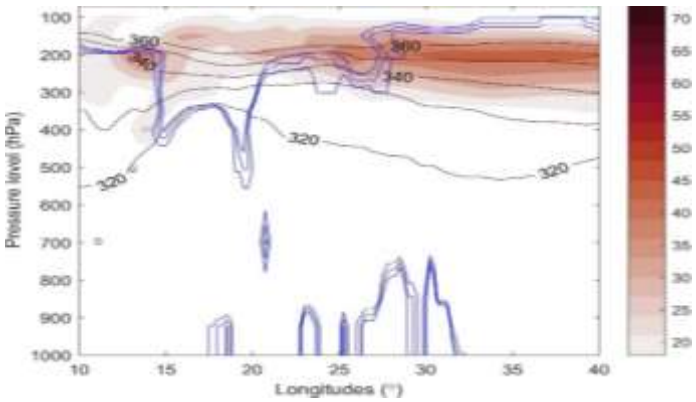

f) t = 36 hours

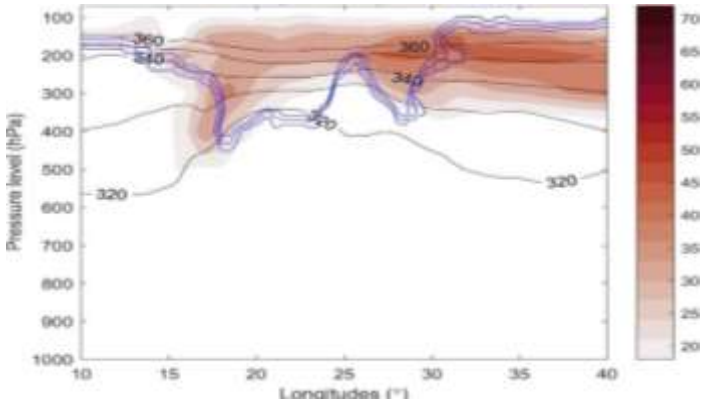

Figure 4.15 Time-lagged evolution of longitudinal profiles of potential vorticity (blue contours), potential temperature (grey contours) and zonal wind (shaded) for **event 3**. The potential vorticity is plotted at -2.5,-2 and -1.5 PVU and the zonal wind is plotted from 18 to 72 m/s throughout the time steps for **event 3**.

Unlike event two, 24 hours prior to the day the COL event four forms, the PV contours were more zonal and narrower with little/ no folding observed at this time with the jet developing just above it (Figure 4.16 a). as in event one and three, the cold core of the COL represented by the 330 K contour was not visible at this stage (Figure 4.16 a). However, 12 hours before the

COL forms, there was no clear indication of folding of the dynamical tropopause allowing the intrusion of stratospheric air into the upper troposphere, whilst the jet streak is getting stronger compared to the previous timeslot and is also propagating east with extensions to the towards the surface up to about 600 hPa (Figure 4.16 b).

During the day the COL event four forms, the PV intrusions deepens compared to the previous timeslots along with its jet getting stronger and more stable further east compared to the initial position just above it (Figure 4.16 c) . The cold core of the COL event was observed developing during this time at about 32°E (Figure 4.16 c). Hence, 12 hours after the COL event four formed, PV intrusions decreased compared to the previous timeslot with its jet also decreasing in strength but still stable in movement located above the PV, although the cold core was less intense at this timeslot compared to the previous timeslots (Figure 4.16 d).

The decaying stages of the COL event from this view was presented with the folding of the PV becoming stronger 24 hours after the COL was formed compared to the previous timeslots, along with its jet getting stronger again located where there are high PV intrusions (Figure 4.16 e-f). At this point, the cold core of the COL event was observed, and it was more intense compared to the day the COL event was formed. This indicates that this event (event four) was still stronger even during its decay stages in terms of the jet streak, PV and its cold core.

The development stages of this COL event was different to event two in terms of the folding of the PV for stratospheric air intrusions but similar with event one and three with little/less folding during this time steps (Figure 4.13 and Figure 4.15 a-b). However, events two and four are similar in terms of the strength and broad shape of the jet streak developing just above it, whereas the jet streak of events one and three are narrower during their development stages. The cold cores of this event were observed intensively at about the stages of dissipation unlike on event one to three (Figure 4.16 e-f). Consequently , the decay stages of the COL represent the stage where the COL is dissipating and the jet was still intense and broad compared to its maturity stages on event four, whereas the jet getting stronger (weaker) and narrow (broad) on event two (one) as it propagates east. Although the PV indicated signs of extensions to the surface on event two, three, four and not on event one and cold cores were stable at this point on (Figure 4.16 e-f).

a) t = -24 hours

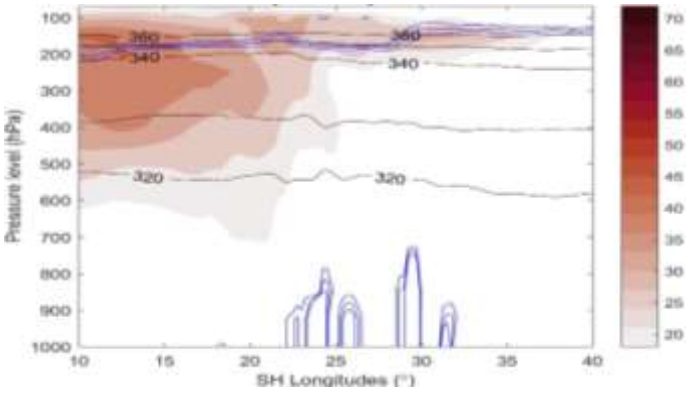

d) t = 12 hours

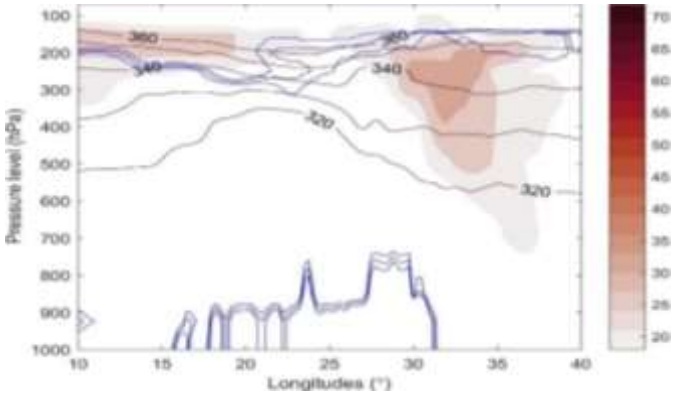

b) t = -12 hours

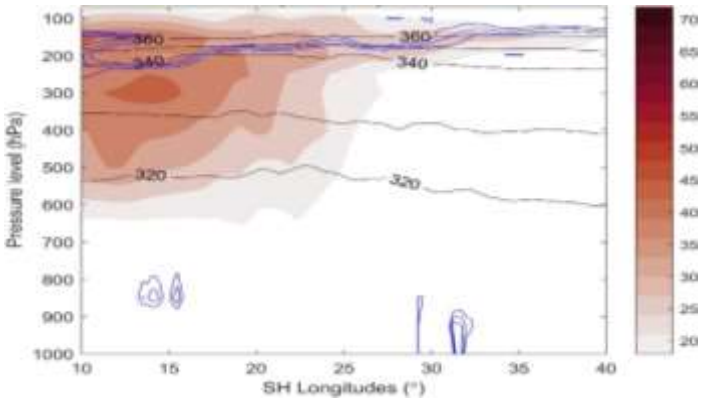

e) t = 24 hours

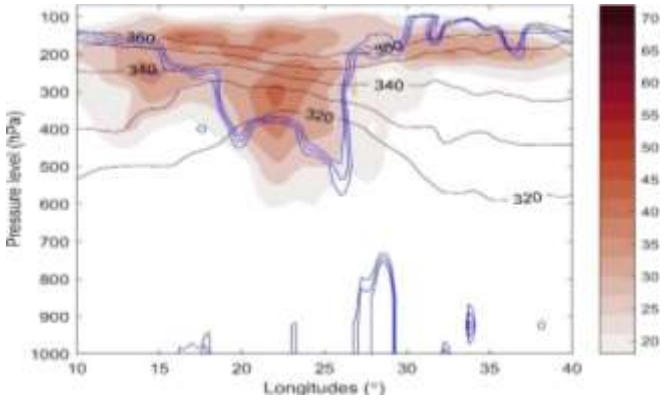

c) t = 0 hours

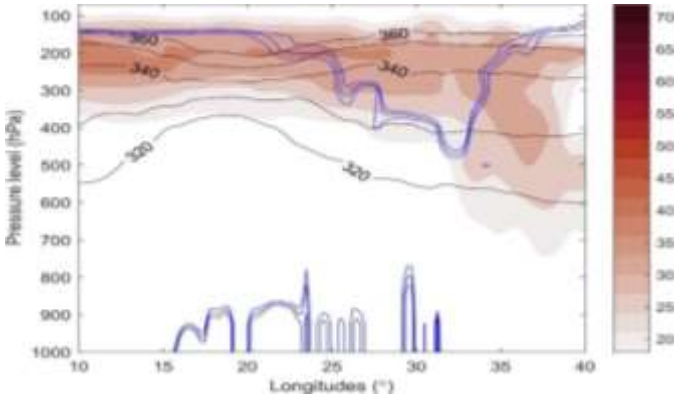

f) t = 36 hours

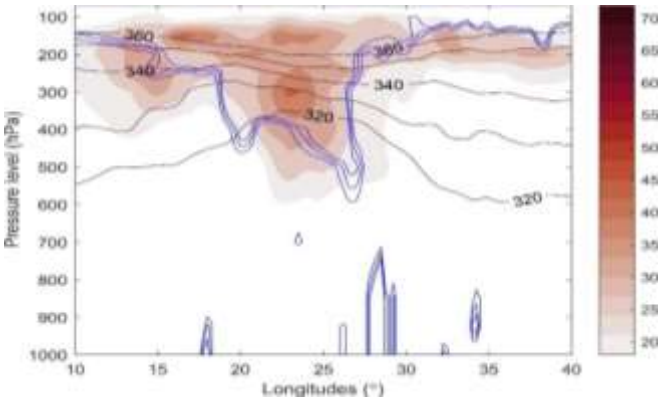

Figure 4.16 Time-lagged evolution of longitudinal profiles of potential vorticity (blue contours), potential temperature (grey contours) and zonal wind (shaded) for **event 4**. The potential vorticity is plotted at -2.5,-2 and -1.5 PVU and the zonal wind is plotted from 18 to 72 m/s throughout the time steps for **event 4**.

4.4 **Vertical analysis of COLs**

4.4.1 **Vertical motion associated with COLs events**

Vertical velocity (omega) is associated with downward (upward) motion with value of vertical velocity (omega) being positive (negative) in the Southern Hemisphere (Muofhe *et al*, 2020). Nevertheless, in terms of analysis in this study, the blueish shaded contours represent areas where there is an uplift, and the green-yellowish shaded contours represent areas where there is a downward motion (Figure 4.17 a-f). Although, in terms of COLs events, we expect to see upward motion of air further east where the COL developed and downward motion just behind the COL (Ndarana *et al*, 2020; Muofhe *et al*, 2020). Omega is lowest closer to the surface and reaches maximum at about 500 hPa which is concluded to be a level of non-divergence, as informed by the continuity equation in isobaric coordinates (O'Brien, 1970; Bazarov *et al*, 2019).

There were indications of upliftment at about 34°E of the study prior to the formation of the COL event one (Figure 4.17 a), although it was little/less compared to the downward motion on the far left at about 12°E (Figure 4.17 a). At this stage, the centre of the COL was expected to be located within these coordinates (12°E to 34°E). The next 12 hours showed an increase in terms of omega over the study and a decrease in vertical motion compared to the previous time slot which was now located at about 30°E instead of 34°E, whilst the shaded omega contour increases up to about 700 hPa (Figure 4.17 b).

During the day the COL was formed, the centre of the COL event one was located at about 31°S, 21°E, between the upward and downward motion location according to Figure (4.17 c). However, the vertical velocity was at about 0 m/s during this day to indicate the formation of COL event one which is characterised by upward motion located far east from the centre of the COL (Figure 4.17 c). Omega (upward motion) increased up to about 600 hPa at this stage. 12 hours after the COL formed, omega (upward motion) continued to increase up to about 500 hPa to indicate rising air which sorely represent convergence at the surface and is associated with clouds formation and rainfall (Figure 4.17 d).

The decay stages of the COL event in this section of the study were presented with another area of high vertical velocity development and a decrease in omega as the COL evolved over the study (Figure 4.17 e-f). Although there was still a bit of uplift as the COL is about to dissipate, but it was not intense as the day the COL formed. Vertical velocity was now located closer to omega than before to indicate balance in the atmosphere representing the decay stage of the COL event one (Figure 4.17 e-f).

a) t = -24 hours

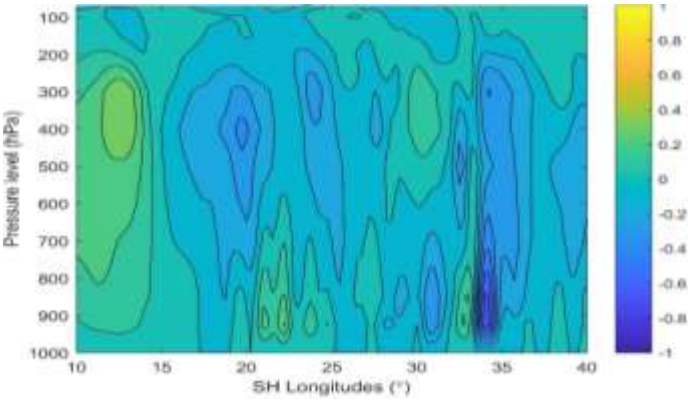

b) t = -12 hours

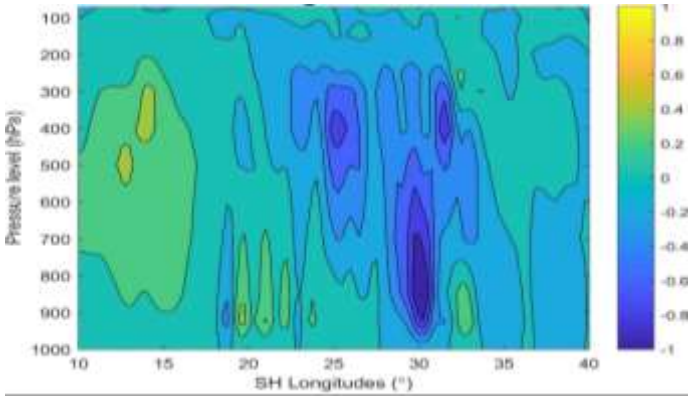

c) t = 0 hours

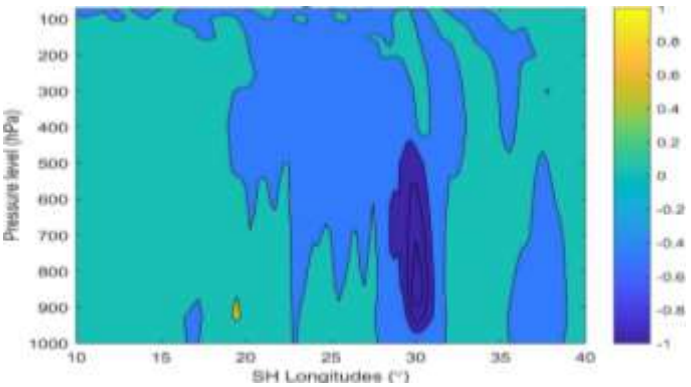

d) t = 12 hours

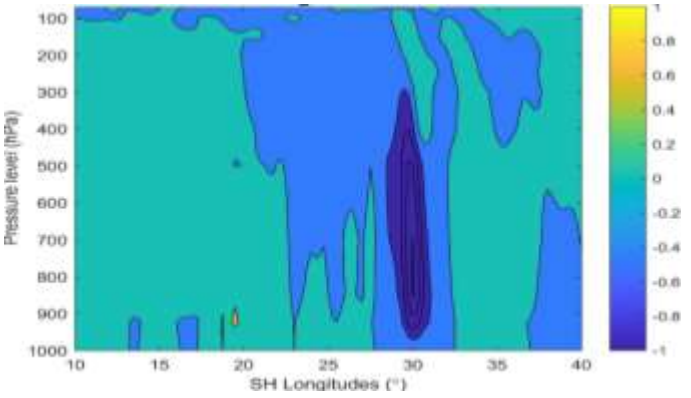

e) t = 24 hours

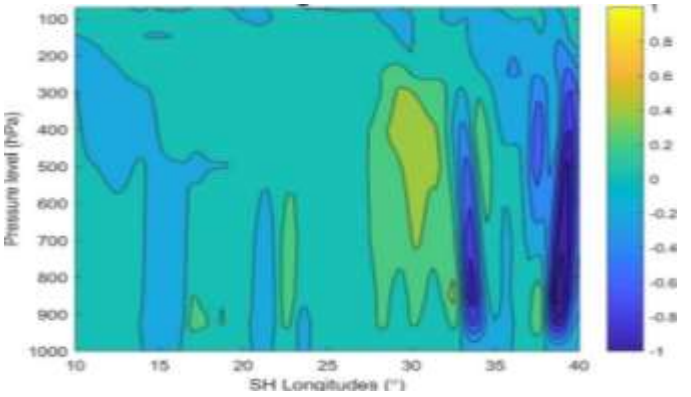

f) t = 36 hours

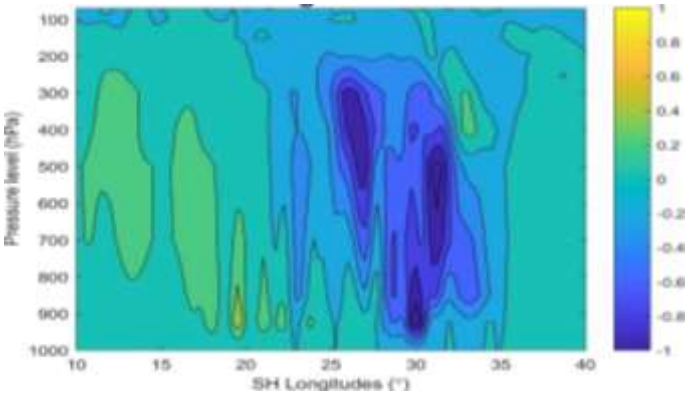

Figure 4.17: Time-lagged vertical profiles of vertical velocity evolution for **event 1**. Positive (negative) values represent vertical velocity(omega). Positive (negative)values are represented by green, yellow (blue) colours.

There were little/no indication of uplift over the study prior to the formation of the COL event two (Figure 4.18 a). Although the study also had no/little downward motion indication as expected indirectly representing balance in the atmosphere (Figure 4.18 a). The next 12 hours showed little/no changes compared to the previous time slot due to calmness and balance in

the atmosphere represented by little/less vertical velocity and omega (Figure 4.18 b) . Hence, omega is expected to increase during the day the COL event forms because COLs are associated with upward motions.

During the day the COL was formed, the centre of the COL event one was located at about 31°S, 29°E and its omega was located at about 30°E, not so far east of the centre of the COL event according to Figure (4.18 c). On contrary, the vertical velocity was at about 0 m/s during this day to indicate the formation of COL event one which is characterised by upward motion located east from the centre of the COL (Figure 4.18 c). Omega (upward motion) increased up to about 700 hPa at this stage (Figure 4.18 d). Vertical velocity (downward motion) dominated with an increase down to about 900 hPa (from 400 hPa) 12 hours after the COL formed (Figure 4.18 d). These motion in the atmosphere indicate sinking air which sorely represent divergence at the surface associated with clear skies and no rainfall (Figure 4.18 d).

The decay stages of the COL event in this section of the study were presented with another area of high omega development and a decrease in vertical velocity compared to the previous time slot as the COL evolved over the study (Figure 4.18 e). Although downward motion was still observed at this stage as the COL is about to dissipate, it was not intense as the previous time slot (Figure 4.18 e-f). Vertical velocity was at its lowest point during this period with an increasing omega to represent a stronger dissipation stage of the COL (Figure 4.18 e-f).

In comparison to event one, the development stage of event two in terms of the vertical velocity and omega was different because there were already signs of upward motion (downward motion) on event one prior to the formation of the COL (Figure 4.17 a-b and Figure 4.18 a-b). Event two was mostly dominated by calmness at this stage (Figure 4.18 a-b). Furthermore, during the day COL events formed, the study was mostly dominated with omega (upward motion) east of the centre of the COL, but unlike event one, event two only increased up to about 700 hPa at this stage (Figure 4.18 c) . The decay stages of events one and two are completely different as one is characterised by increasing vertical velocity (event one) and the other with increasing omega (event two) at this stage (Figure 4.17 e-f and Figure 4.18 e-f).

a) t = -24 hours

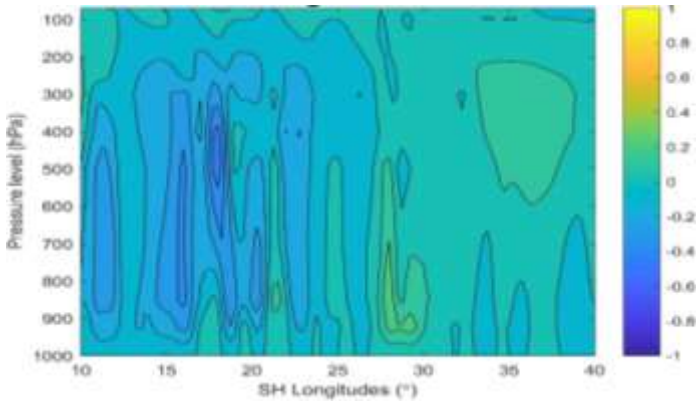

d) t = 12 hours

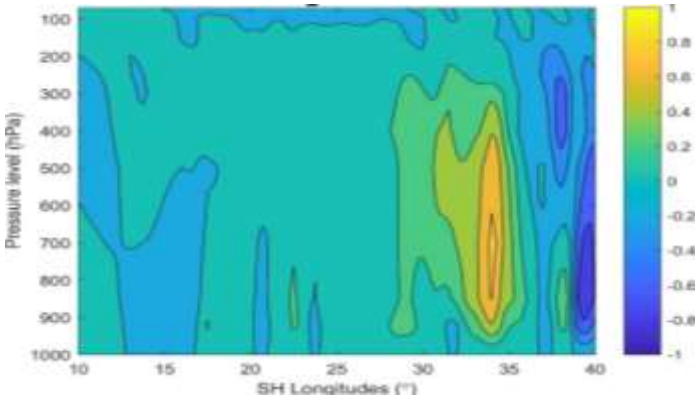

b) t = -12 hours

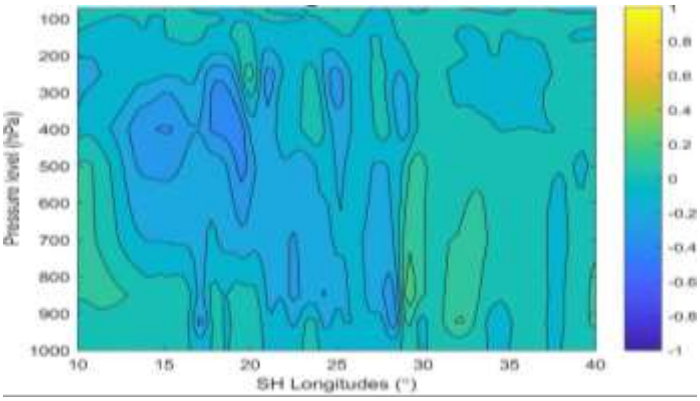

e) t = 24 hours

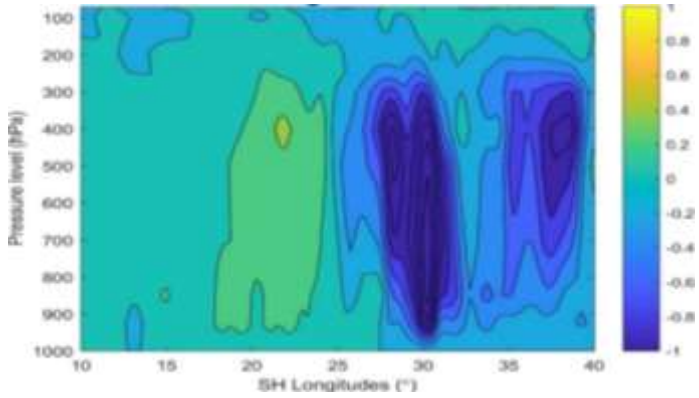

c) t = 0 hours

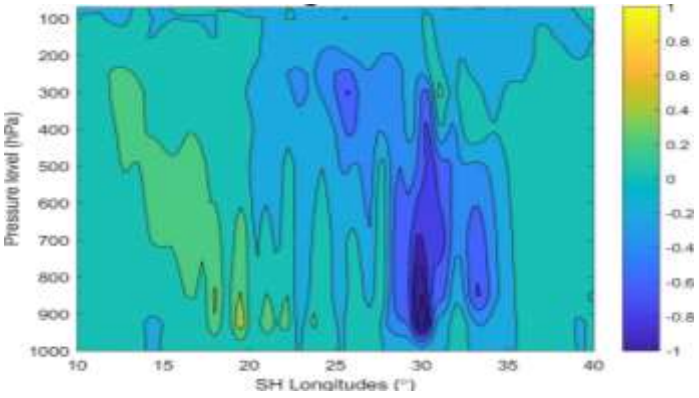

f) t =36 hours

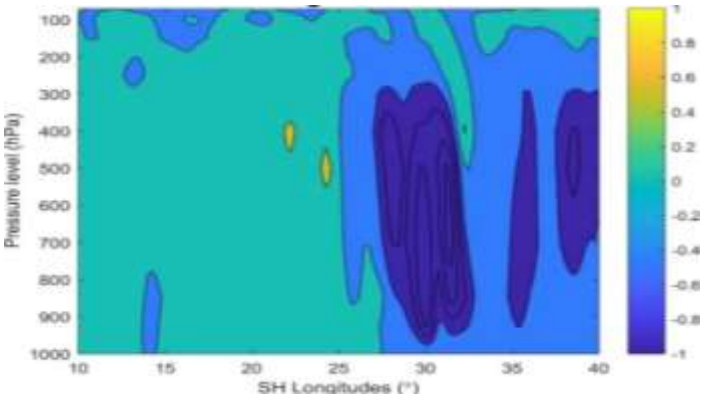

Figure 4.18: Time-lagged vertical profiles of vertical velocity evolution for **event** 2. Positive (negative) values represent vertical velocity (omega). Positive (negative) values are represented by green, yellow (blue) colours.

There was indication of upliftment at about 15°E of the study prior to the formation of the COL event three (Figure 4.19 a), although it was little/less compared to the downward motion on the far right at about 30°E (Figure 4.19 a). In conclusion, the centre of the COL in question will be located within these coordinates 15°E to 30°E. The next 12 hours showed an increase in

terms of omega over the study and a decrease in vertical motion compared to the previous time slot, whilst the shaded omega contour increased up to about 300 hPa (Figure 4.19 b).

During the day, the COL was formed, the centre of the COL event one was located at about 29°S 18°E, between the upward and downward motion location according to Figure (4.19 c). However, the vertical velocity (omega) increased (decreased) during this day compared to the previous time slots to indicate instability of COL environment which is characterised by upward (downward) motion located east (west) from the centre of the COL (Figure 4.19 c). Intense Omega (upward motion) was observed at mid-levels (at about 400hPa) during this period (Figure 4.19 c). Omega (upward motion) continued to increase 12 hours after the COL formed, indicating rising air which sorely represent convergence at the surface and is associated with clouds formation and rainfall (Figure 4.19 d).

The decay stages of the COL event in this section of the study were presented with another area of high vertical velocity development and a decrease in omega as the COL evolved over the study (Figure 4.19 e-f). Although there was still a bit of uplift as the COL is about to dissipate, it was not intense as the day the COL formed. Vertical velocity was now located closer to omega than before to indicate balance in the atmosphere representing the decay stage of the COL event one (Figure 4.19 e-f).

On the contrary, the development stage of event three is slightly different to event two but similar to event one as there was signs of upliftment prior to the day the COL event formed (Figure 4.17- 4.19 a-b). Unlike event one and two, the most intense omega was observed 12 hours prior to the formation of the COL (Figure 4.19 b). Moreover, during the day the COL was formed, event three showed a decrease in omega and an increase in vertical velocity compared to the previous timeslot, whereas events one and two had a rapid increase during this period (Figure 4.17- 4.19 c). However, the decay stage of event three is like that of event one and different compared to event two characterised by increasing vertical velocity (event one) and the other with increasing omega (event two) at this stage (Figure 4.17- 4.19 e-f).

a) t = -24 hours

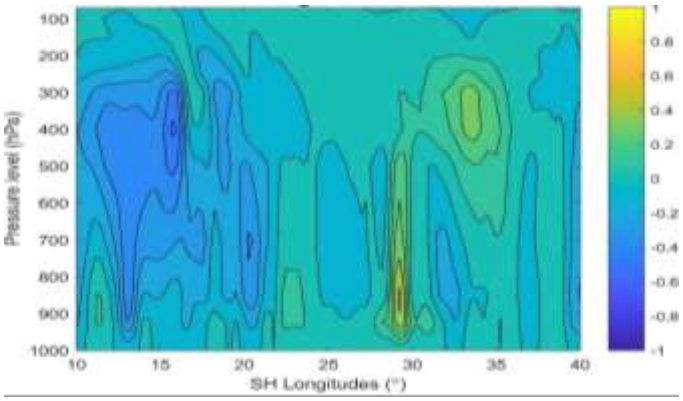

d) t = 12 hours

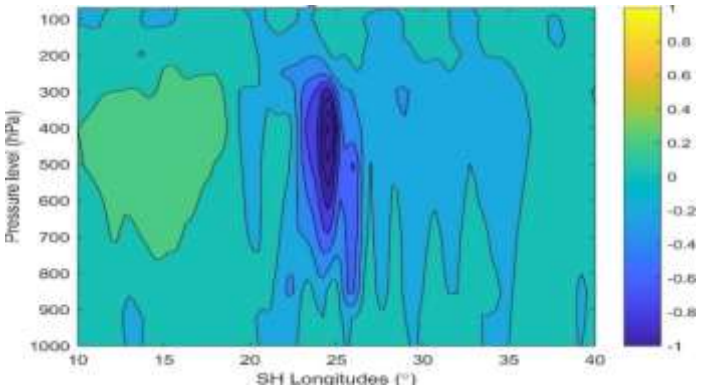

b) t = -12 hours

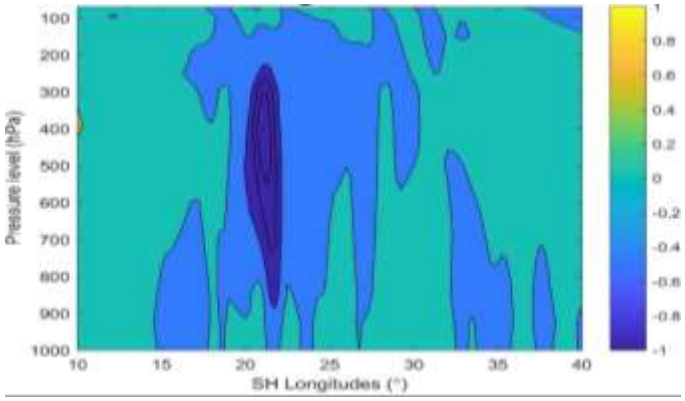

e) t = 24 hours

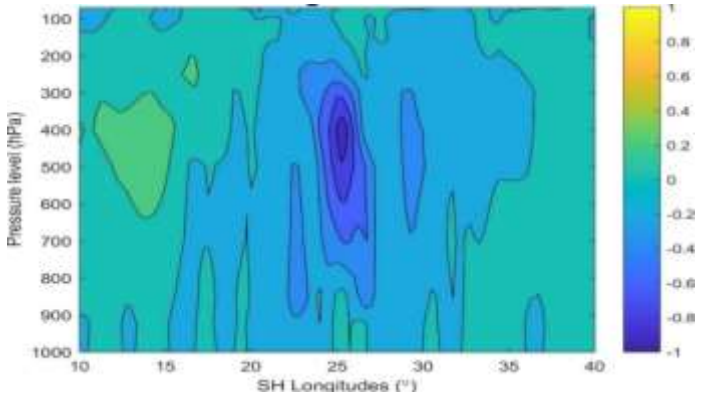

c) t = 0 hours

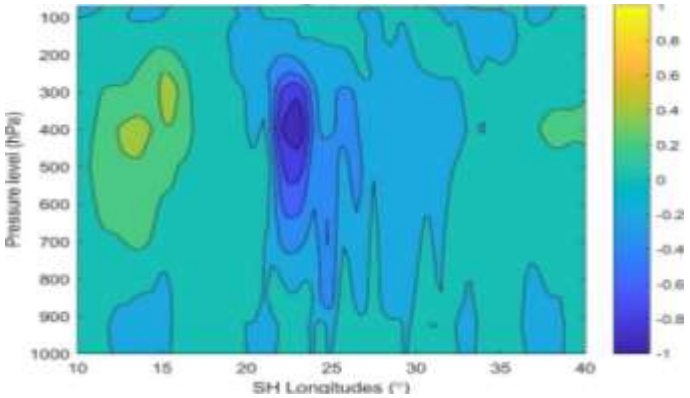

f) t = 36 hours

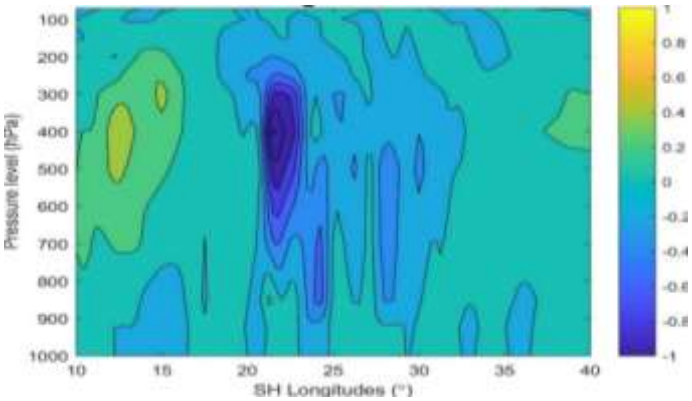

Figure 4.19: Time-lagged vertical profiles of vertical velocity evolution for **event 3**. Positive (negative) values represent vertical velocity(omega). Positive (negative) values are represented by green, yellow (blue) colours.

Indication of upliftment at about 20°E of the study was observed 24 hours prior to the formation of the COL event four (Figure 4.20 a). Although it was little/less compared to the downward motion on the far right at about 30°E (Figure 4.20 a). In conclusion, the centre of the COL in question will be located within these coordinates 20°E to 30°E. The next 12 hours showed

stability in terms of omega over the study and a decrease in vertical motion compared to the previous time slot (Figure 4.20 b).

During the day the COL was formed, the centre of the COL event four was located at about 29°S, 18°E, between the upward and downward motion location according to Figure (4.20 c). Contrastingly, the most intense vertical velocity was located at about 15°E indicating instabilities in the atmosphere during the formation of COL event three which is characterised by upward motion located far east from the centre of the (Figure 4.20 c). Omega (upward motion) was dominant at mid-levels during this stage. After the COL formed (12 hours), omega (upward motion) increased rapidly compared to the previous timeslot up to about 200 hPa indicating rising of air (Figure 4.20 d). The above mentioned sorely represent convergence at the surface and is associated with clouds formation and rainfall, although vertical velocity was also at the same level as omega on the other side (Figure 4.20 d).

The decay stages of the COL event in this section of the study were presented with decreasing vertical velocity (downward motion) and omega (upward motion) area as the COL evolved over the study (Figure 4.20 e-f). Although there was still a bit of uplift as the COL is about to dissipate, it was not intense as 12 hours after the COL formed. Vertical velocity was now located closer to omega than before to indicate balance in the atmosphere representing the decay stage of the COL event one (Figure 4.20 e-f).

In comparison to all the COL events presented above, the development stage of this COL was quite similar to that of event one and three (Figure 4.20, Figure 4.19 and Figure 4.17 a-b). Omega was observed developing 24 hours prior to the day the COL as in the two events compared above (Figure 4.20 a). Although, 12 hours prior to the day the COL formed, the study was more stable compared to COL that evolved similarly with little/no changes in terms of vertical velocity and Omega (Figure 4.20 b). During the day the COL event four formed, the study was mainly dominated by vertical velocity unlike most of previous events (Figure 4.20 c). The three events discussed above (Figure 4.17, Figure 4.18, and Figure 4.19 c) were dominated by intense Omega, although it increased rapidly 12 hours later when the COL formed (Figure 4.20 c-d). Event four decay stage was completely different compared to the presented COL events above due to decreasing vertical velocity and Omega over the study during this period (Figure 4.20 e-f).

a) t = -24 hours

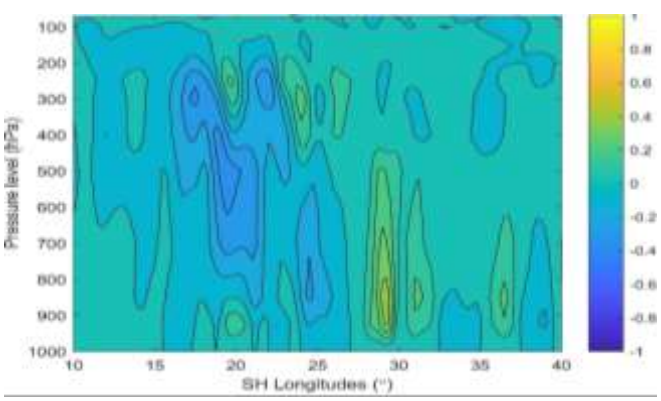

d) t = 12 hours

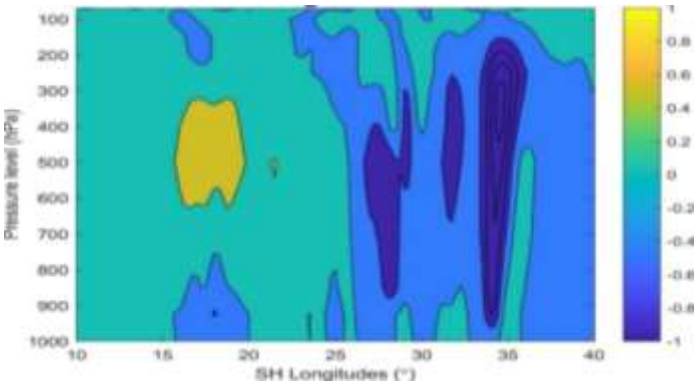

b) t = -12 hours

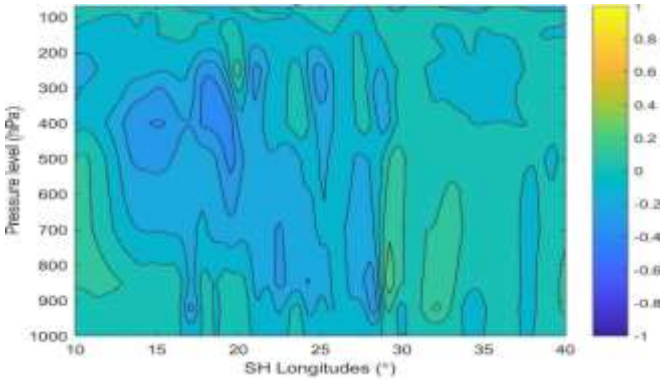

e) t = 24 hours

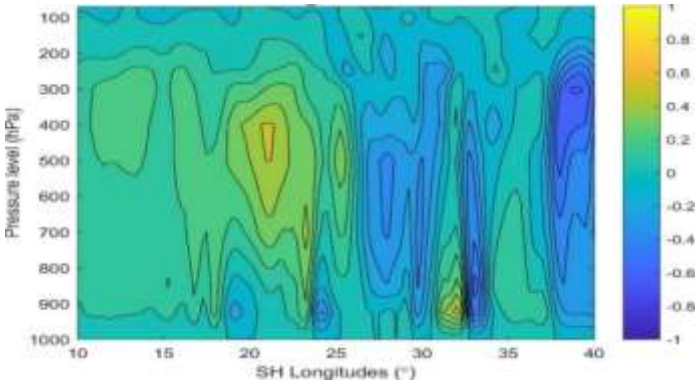

c) t = 0 hours

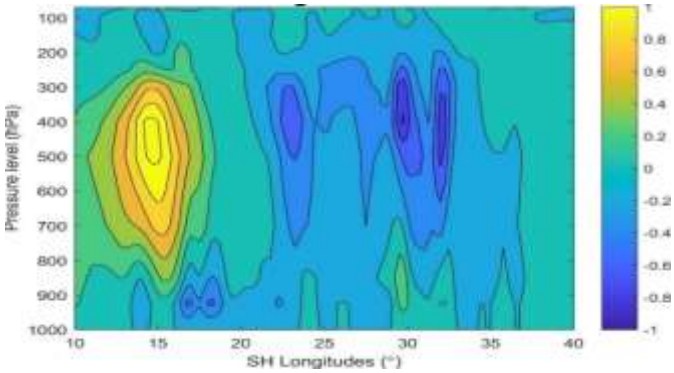

f) t = 36 hours

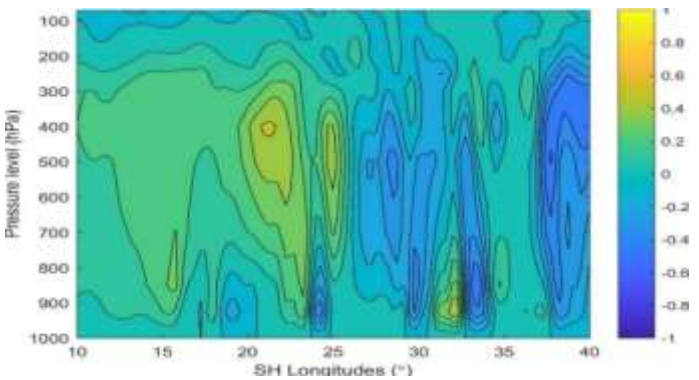

Figure 4.20: Time-lagged vertical profiles of vertical velocity evolution for **event** 4. Positive (negative) values represent vertical velocity(omega). Positive (negative)values are represented by green, yellow (blue) colours.

4.4.2 **COLs propagation to the east**

COLs are known for their propagation from west to east during their life cycles (Singleton and Reason, 2007; Muofhe *et al*, 2020). COLs propagations to the east are presented in this section of the study with geopotential heights and PV anomalies associated with their development, maturity, and decay stages (Figure 4.21- 4.24 a-f). Moreover, COLs extensions to the surface will also be observed along with another wave breaking events that occurs with/before and after COL occurred. Geopotential anomalies associated with COLs are represented by negative contours (black dotted lines) and those that are not associated with COLs are represented by positive contours (black solid lines) (Figure 4.21- 4.24 a-f). The intensity of different COLs events in terms of their PV through the propagation life cycles will also be observed in this section. Hence, the most intense PV anomaly is presented by negative values (shaded) and low PV anomaly is presented by positive values (also shaded) in the Southern Hemisphere (Figure 4.21- 4.24 a-f).

A low-pressure system was developing at about 20°E with high PV intensity (negative) located at its centre prior to the day the COL event one formed, although there was a high-pressure cell system following it with weak PV (positive) above it (Figure 4.21 a). The low-pressure system over the study represents a closed system of a COL which in this case was not fully developed, whilst the high-pressure system behind represents another wave breaking process coming in from the west. The low-pressure system remained stable (20°E) prior (12 hours) to the day the COL system fully developed (Figure 4.21 b). Although the centre became closer compared to the previous time slot with its PV increasing in strength and signs of extensions towards the surface (Figure 4.21 b). The high-pressure system also indicated little/less changes with its PV decreasing in strength compared to the previous time slot (Figure 4.21 b).

During the day the COL system fully developed, the centre of the low-pressure system was closer than before to represent the closed circulation of the COL system located at about 21°E with its pressure extending to about 750 hPa towards the surface (Figure 4.21 c). Whilst its PV also increased in strength and movement towards the surface as the system extend compared to the previous time slots (Figure 4.21 c). Furthermore, the high-pressure system following the COL system also increased in strength during this day to indicate the wave breaking process, with its PV decreasing even more during this day (Figure 4.21 c). Although the COL showed extensions to the surface during its development. PV increased in strength 12 hours after the COL system developed, with the COL extending to about 900 hPa towards the surface although it was still located at about 22°E during this day (Figure 4.21 d). Another high gph anomaly formed Infront of the COL, although the one behind started to decrease in

strength with its PV gaining strength again compared to the previous time slot, located just above it (Figure 4.21 d).

The decay stage of this system was presented with a decrease in COL strength presented by a drop in COL extensions to the surface (to about 800 hPa) and the centre shrinking once again with a decrease in PV at its centres as the COL dissipate (Figure 4.21 e-f). The COL system was now located further east at this stage compared to the previous time slots (23-30°E). Although, the high-pressure system behind the COL system represented by positive gph anomalies showed a decrease in strength with its extension now dropping to about 700 hPa(Figure 4.21 e-f). The high pressure's associated PV (positive) increased in strength as the COL system dissipates compared to the previous timeslots when the system was developing (Figure 4.21 e-f). Hence, the positive gph anomaly (high-pressure) at the front increased rapidly in strength as the COL system continue to dissipate, although it has little/less PV (positive) compared to the one on the rear (Figure 4.21 e-f).

a) t = -24 hours

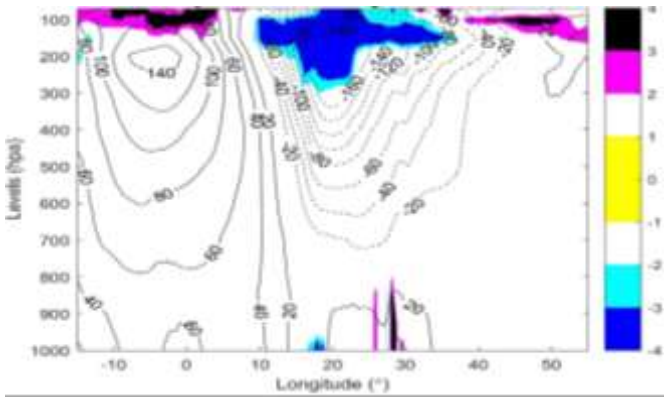

d) t = 12 hours

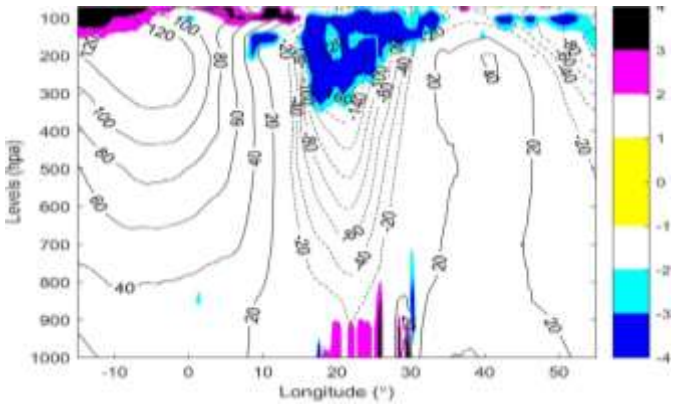

b) t = -12 hours

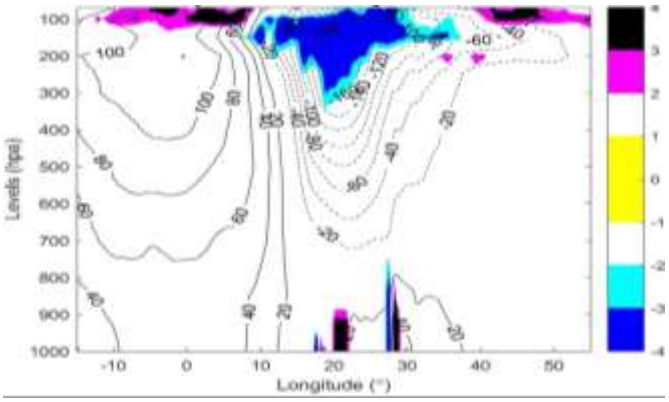

e) t = 24 hours

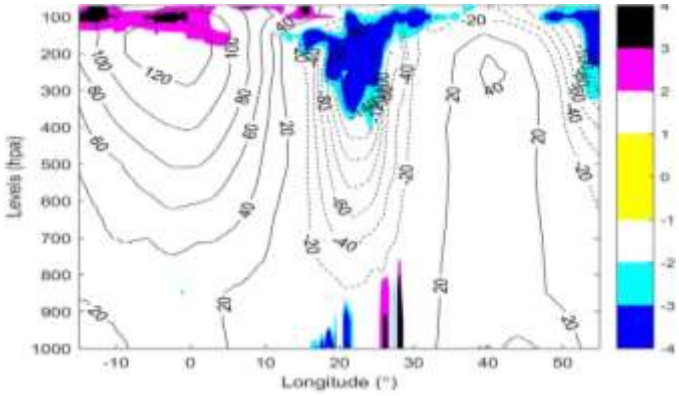

c) t = 0 hours

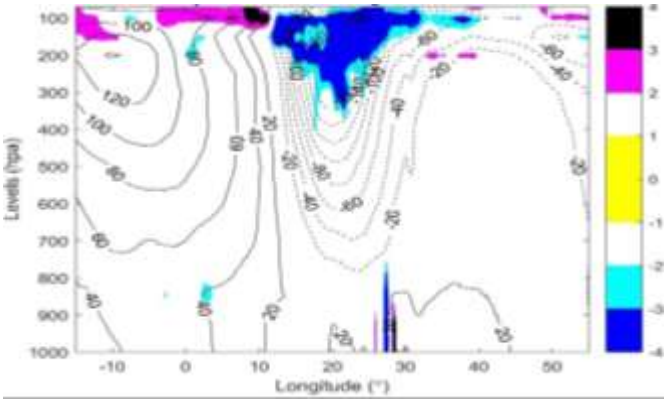

f) t = 36 hours

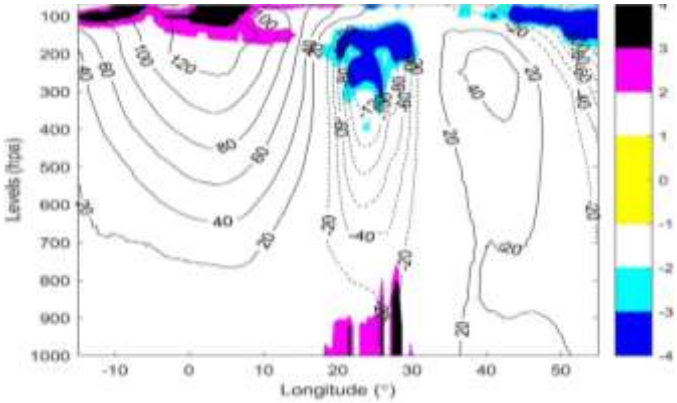

Figure 4.21: Time-lagged evolution of geopotential height anomalies at 500 hPa (contour) with potential vorticity (shaded) for **event** 1. Contour interval is at 10 m for geopotential heights. Positive (negative) geopotential contours are thin lines(dashed lines).

A low-pressure system developed at about 30°E prior to the day the COL event one formed with high PV intensity (negative) located at its centre (Figure 4.22 a). Although there was another negative gph anomaly (low pressure) following it with weak PV (positive) above it compared to the one in front, whilst the high pressure was still developing in front of the

stronger low-pressure cell (Figure 4.22 a). The low-pressure system over the study represents a closed system of a COL which in this case was not fully developed. 12 hours prior to the day the COL system fully developed, the low-pressure system displaced back to about 20°E, although its centre became close compared to the previous time slot (Figure 4.22 b). Its PV decreased in strength with signs of extensions towards the surface at this stage (Figure 4.22 b). The high-pressure system also indicated little/less changes with its PV increasing in strength compared to the previous time slot.

During the day the COL system fully developed, the centre of the low-pressure system was closer than before to represent the closed circulation of the COL system located at about 23°E (Figure 4.22 c). The COL pressure was also seen extending to about 800 hPa towards the surface during this day, whilst its PV (both the front and rear) also increased in strength and movement towards the surface compared to the previous time slots (Figure 4.22 c). Moreover, the high-pressure system in front of the COL system also increased in strength during this day to indicate the wave breaking process (Figure 4.22 c). Its PV decreased even more during this day, although it was observed with extensions to the surface during its development (Figure 4.22 c). 12 hours after the COL system developed, the system was observed with a decrease in strength and PV located above it. Hence, the other low-pressure system formed behind the COL increased in strength along with its PV above it (Figure 4.22 d) .

The decay stage of this system was presented with an increase in COL strength and a drop in COL extensions to the surface (Figure 4.22 e-f). Although the centre became closer once again with an increase in PV (both the front and rear) at its centres as the COL dissipate (Figure 4.22 e-f). The COL system was now located further east (35-40°E) at this stage compared to the previous time slots (Figure 4.22 e-f). Although, the low-pressure system located west of the COL system also indicated signs of decrease in pressure strength and PV strength following the decay stage of the COL system in front (Figure 4.22 e-f). Hence, the extension of the COL system in front was greater than the one behind (600 hPa) with a maximum of about 950 hPa (Figure 4.22 e-f). The high-pressure system was developing in between the low-pressure systems (front and rear) represented by positive gph anomalies observed with little/less associated PV as the COL system decay (Figure 4.22 e-f).

In comparison with the previous COL system presented above (Figure 4.21 a-f), the development stage of this COL system was different because its pressure (low pressure) was displaced back from initial position (Figure 4.22 a-b). A decrease in associated PV was also observed at this stage (Figure 4.22 a-b) to show its weakness compared to event one. During the day the COL formed, event two increased in PV although it was still less compared to event one with extensions towards the surface (up to about 900 hPa) which is greater than

the one during event one formation (Figure 4.21 and 4.22 c-d). 12 hours after the COLs developed, both events indicated signs of decrease in strength and PV compared to the previous timeslots (Figure 4.21 and 4.22 d). The decay stages of this COLs systems were quite similar with a decline in strength in terms of the pressures and associated PV at their centres to indicate that the COLs have now passed the study or dissipated with time (Figure 4.21 and 4.22 e-f).

a) t = -24 hours

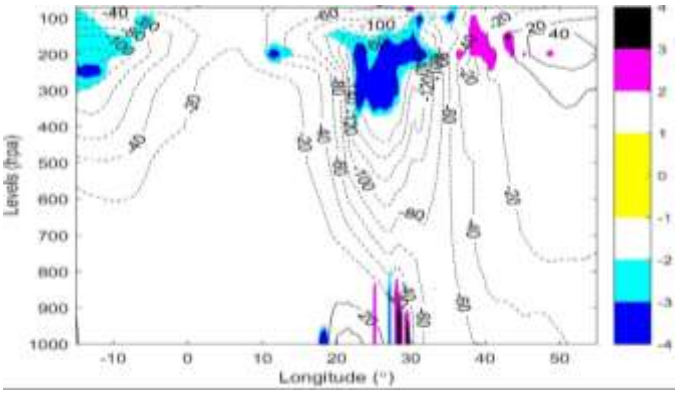

d) t = 12 hours

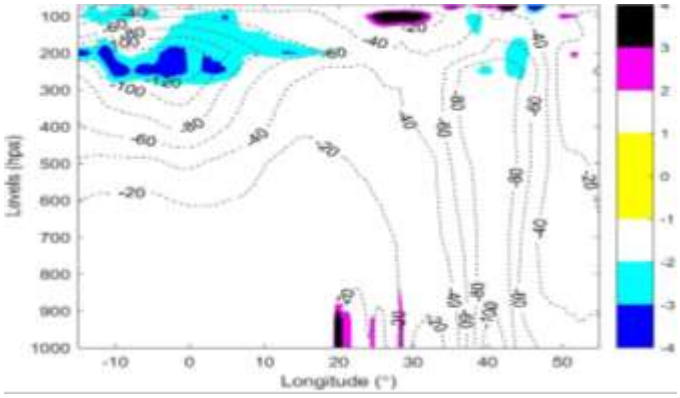

b) t = -12 hours

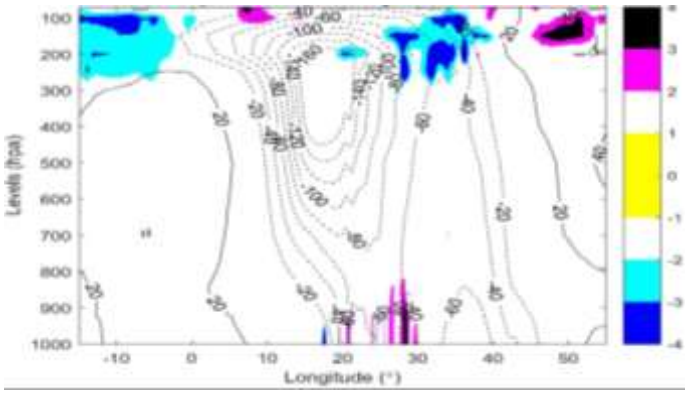

e) t = 24 hours

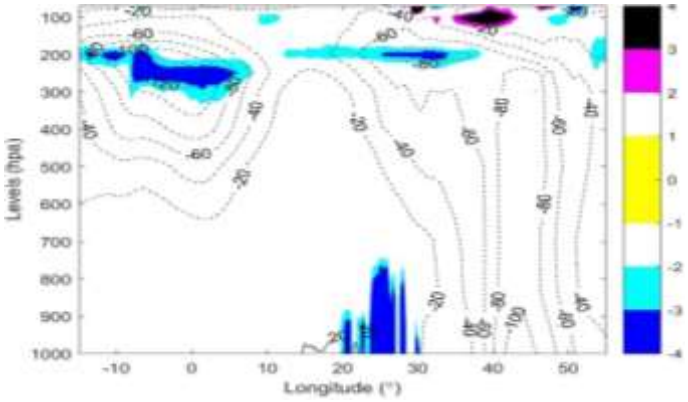

c) t = 0 hours

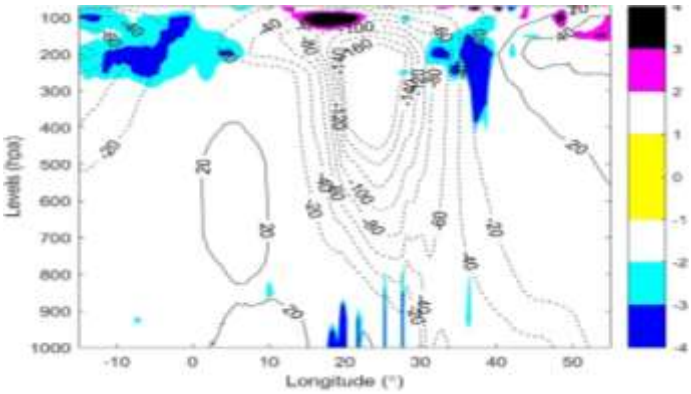

f) t = 36 hours

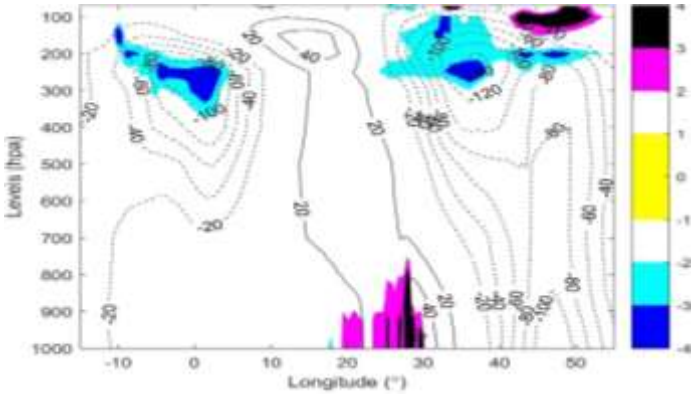

Figure 4.22: Time-lagged evolution of geopotential height anomalies at 500 hPa (contour) with potential vorticity (shaded) for **event 2**. Contour interval is at 10 m for geopotential heights. Positive (negative) geopotential contours are thin lines(dashed lines).

A low-pressure system (negative gph anomaly) developed at about 18°E prior to the day the COL event three formed (Figure 4.23 a) with high PV intensity (negative) located at its centre. Although there was a high-pressure cell system in front with associated PV (positive) above it (Figure 4.23 a). The low-pressure system over the study represents a closed system of a COL which in this case was not fully developed, whilst the high-pressure system in front represents

another wave breaking process. 12 hours prior to the day the COL system fully developed, the low-pressure system remained stable (18°E) although its centre became close compared to the previous time slot with its PV increasing in strength and signs of extensions towards the surface (Figure 4.23 b). The high-pressure system also indicated little/less changes with its PV decreasing in strength compared to the previous time slot.

During the day the COL system fully developed, the centre of the low-pressure system was closer than before to represent the closed circulation of the COL system located at about 20°E (Figure 4.23 c). Whilst its pressure extended to about 950 hPa towards the surface during this day and the associated PV decreased in strength and movement towards the surface as the system extend, compared to the previous time slots (Figure 4.23 c). Moreover, the high-pressure system in front of the COL system also increased in strength during this day to indicate the wave breaking process (Figure 4.23 c). Although it showed extensions to the surface during development, its PV decreased even more during this day (Figure 4.23 c) Conversely, there was another high-pressure (positive gph anomaly) system developing (Figure 4.23 c) far left of the COL system (at about 5°E). 12 hours after the COL system developed, the PV continued to decrease in strength with the COL now extending to about 800 hPa towards the surface to indicate that the system is now losing strength, although it was now located at about 25°E during this day (Figure 4.23 d). The high gph anomaly (pressure) formed behind (in front of) the COL increased in strength with little/no (a decrease in) PV located above it (positive), although it was now located at about 10°E (50°E) following the propagation of the COL system towards the east (Figure 4.23 d).

The decay stage of this system was presented with a decrease in COL strength and a drop in COL extensions to the surface (to about 500 hPa) (Figure 4.23 e). The centre of the closed circulation was observed shrinking once again with a decline in PV at its centre as the COL dissipate (Figure 4.23 e). The COL system was now located further east at this stage compared to the previous time slots (at about 27°E) (Figure 4.23 e-f). The high-pressure system in front of the COL system represented by positive gph anomalies showed a decrease in strength also with its associated PV (positive) decreasing in strength as the COL system dissipates compared to the previous timeslots when the system was developing (Figure 4.23 e-f). Hence, the positive gph anomaly (high-pressure) at the rear increased rapidly in strength as the COL system continue to dissipate, although it has little/less PV (positive) compared to the one in front (Figure 4.23 e-f).

In comparison to the previous COLs presented above (event one and two), the development stage of this COL system was like that of event one with an increase in low pressure system strength and associated high PV anomaly following in front of the COL till the day the COL

system formed (Figure 4.21 and 4.23 a-b). The PV of the two events decreases just after 12 hours the COL system formed to show that the COLs start to lose strength after formation, although the COLs continued to indicate signs of extensions towards the surface (Figure 4.21 and 4.23 b-c). In both events, as the COLs continued to lose strength, the high pressure (positive gph anomaly) increases in strength with its associated PV at event one only to present another wave breaking event coming after the occurrence of the COL surface (Figure 4.21 and 4.23 d-f).

a) t = -24 hours

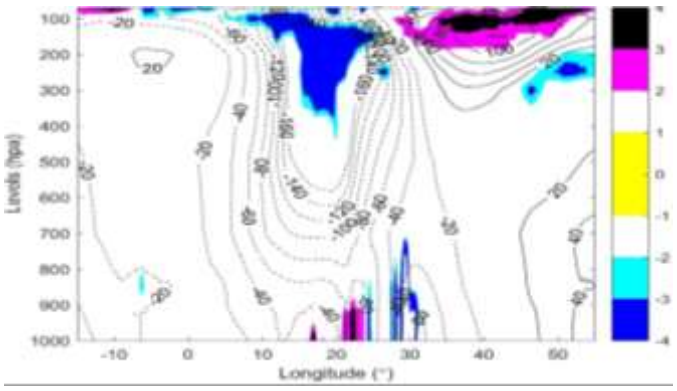

d) t = 12 hours

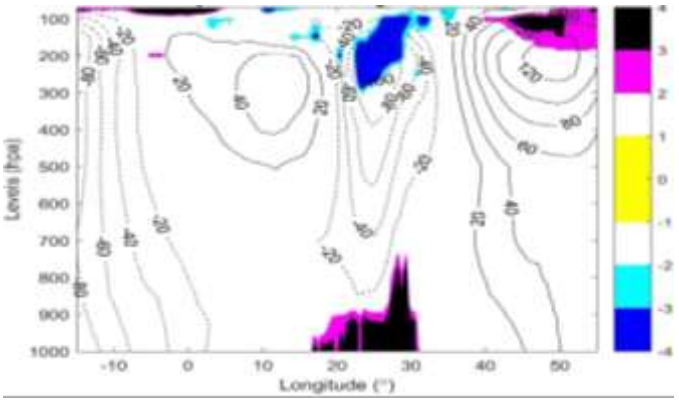

b) t = -12 hours

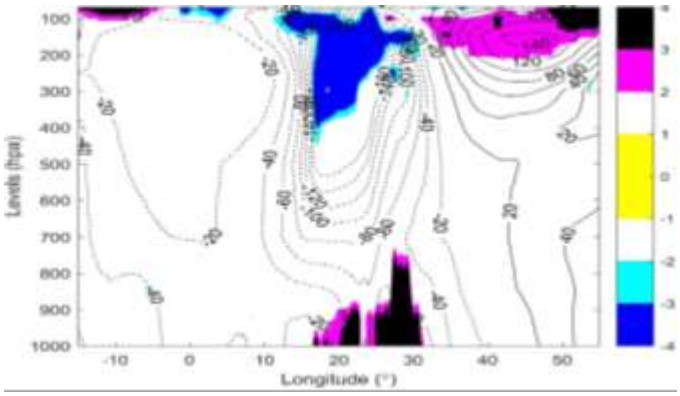

e) t = 24 hours

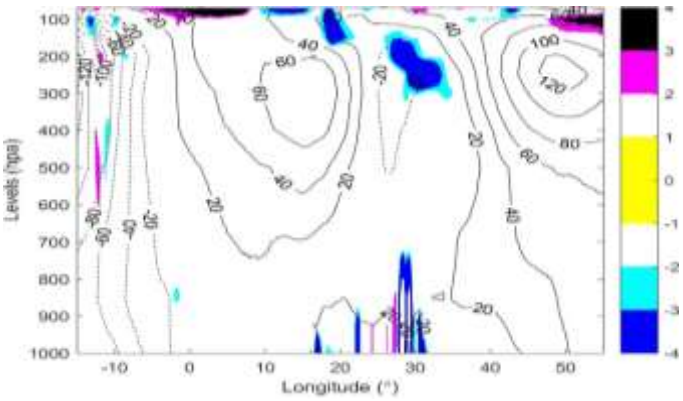

c) t = 0 hours

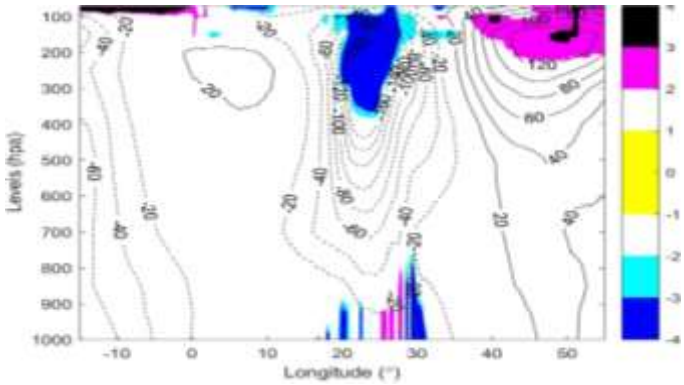

f) t = 36 hours

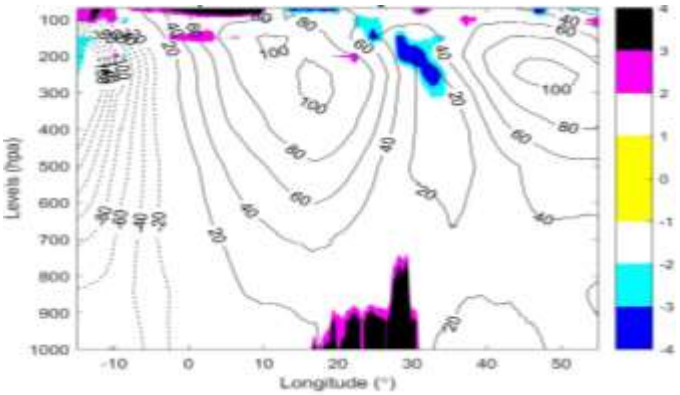

Figure 4.23: Time-lagged evolution of geopotential height anomalies at 500 hPa (contour) with potential vorticity (shaded) for **event 3**. Contour interval is at 10 m for geopotential heights. Positive (negative) geopotential contours are thin lines (dashed lines).

A day prior to the formation of the COL event four, there was a low-pressure system developed at about 18°E with high PV intensity (negative) located at its centre (Figure 4.24 a). Although there was a high-pressure cell system following it at about 5°W and another one at the front with associated PV (positive) above it (Figure 4.24 a). The low-pressure system

over the study represents a closed system of a COL which in this case was not fully developed, whilst the high-pressure system behind represents another wave breaking process coming in from the west (Figure 4.24 a). The low-pressure system was displaced eastwards 12 hours prior to the day the COL system fully developed and was now located at about (21°E) (Figure 4.24 b). Although its centre became close compared to the previous time slot with its PV increasing in strength and signs of extensions towards the surface at this stage (Figure 4.24 b). Both the high-pressure systems (positive gph anomalies) increased in strength with their PV decreasing in strength compared to the previous time slot to present the breaking process before the COL (Figure 4.24 b).

During the day the COL system fully developed, the centre of the low-pressure system was closer than before to represent the closed circulation of the COL system located between 20°E and 30°E (Figure 4.24 c). The COL pressure was seen extending to about 800 hPa towards the surface during this day, whilst its PV also increased in strength and movement towards the surface as the system extend compared to the previous time slots (Figure 4.24 c). Moreover, the front high-pressure system remained stable in terms of the strength (PV) and extension towards the surface during this day (Figure 4.24 c). The rear positive gph anomaly indicated signs of increase in strength and a decrease in associated PV representing the wave breaking process (Figure 4.24 c). 12 hours after the COL system developed, PV began to decrease in strength with the COL extending to about 700 hPa towards the surface although it was now located at about 30°E during this day (Figure 4.24 d). The rear high gph anomaly (high-pressure) began to decrease in terms of strength and associated PV to indicate that breaking already occurred , although the one in front increased in terms of strength with a decrease in associated PV located just above it compared to the previous slots (Figure 4.24 d).

The decay stage of this system was presented with a decrease in COL strength indicated by a drop in COL extensions to the surface (to about 650 hPa) and a decline in PV strength compared to the previous time slots (Figure 4.24 e-f). Although the centre was still close representing that the COL was a closed system (Figure 4.24 e-f). The COL system was now located further east at this stage compared to the previous time slots (38°E and 40°E (Figure 4.24 e-f). The rear high gph anomaly (high-pressure) demonstrated by (Figure 4.24 e-f) continued to decrease in terms of strength and associated PV after the COL system formed to indicate that breaking event already occurred. Although the one in front also continued to increase in terms of strength and associated PV compared to the previous time slots (Figure 4.24 e-f).

In comparison with the previous COL events presented above , the development stage of this COL system was quite like all the events presented above in terms of increasing strength of the Low-pressure system (negative gph anomalies) till the day the COL system forms with its closed system (Figure 4.21, 4.22, 4.23 and 4.24 a-c). However, it was different to both event two and three with associated PV decreasing throughout at those stages (Figure 4.22, 4.23 and 4.24 a-c). 12 hours after this system formed (Figure 4.24 d), the system propagated far east from its initial position (where it formed) which is like what transpired in event two, whilst both events one and three were quite slow in terms of the propagation towards the east (Figure 4.21, 4.22, 4.23 and 4.24 a-c). However, in terms of extensions towards the surface, this system was not strong enough to extend further than 900 hPa, which is higher than only event one and not the other two events (extended further) (Figure 4.21, 4.22, 4.23 and 4.24 d-f). The decay stage of this system was like both events one and three in terms of a decrease in low pressure system and decline in PV compared to the previous timeslots leading to the COL losing strength and eventual dissipate with time (Figure 4.22, 4.23 and 4.24 d-f).

a) t = -24 hours

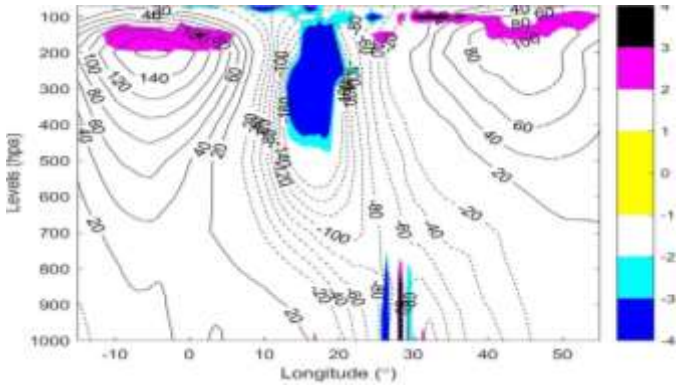

d) t = 12 hours

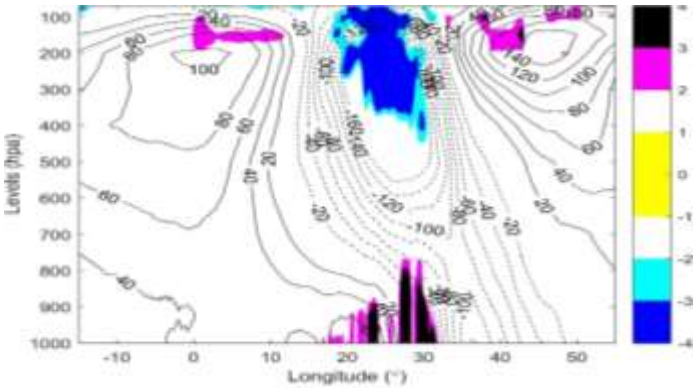

b) t = -12 hours

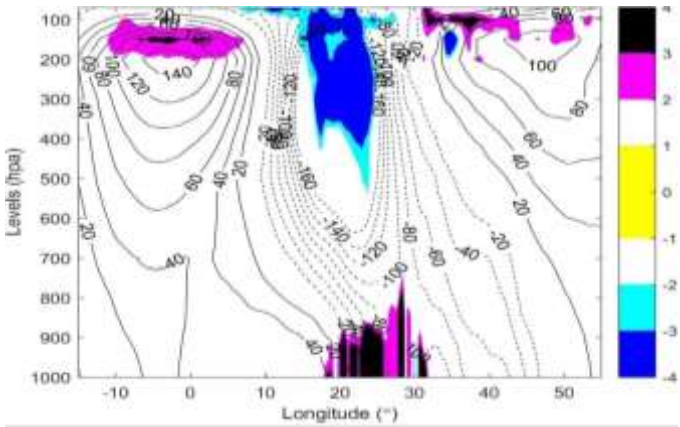

e) t = 24 hours

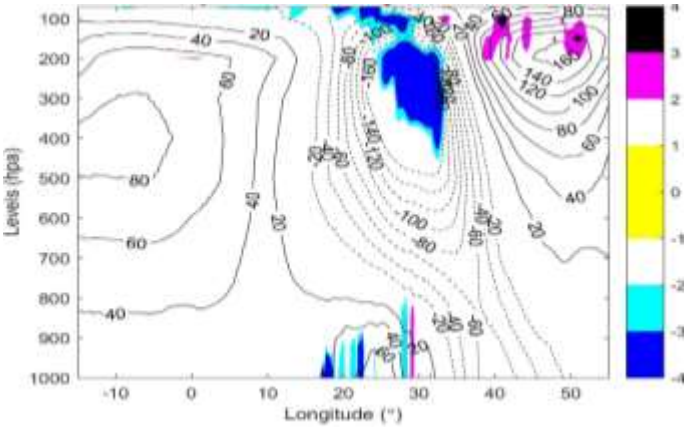

c) t = 0 hours

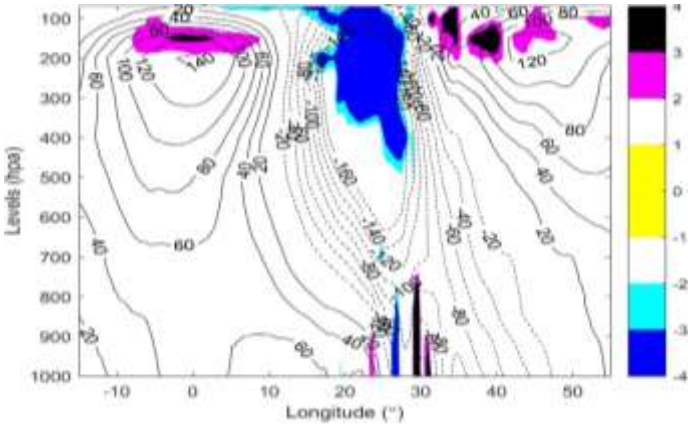

f) t = 36 hours

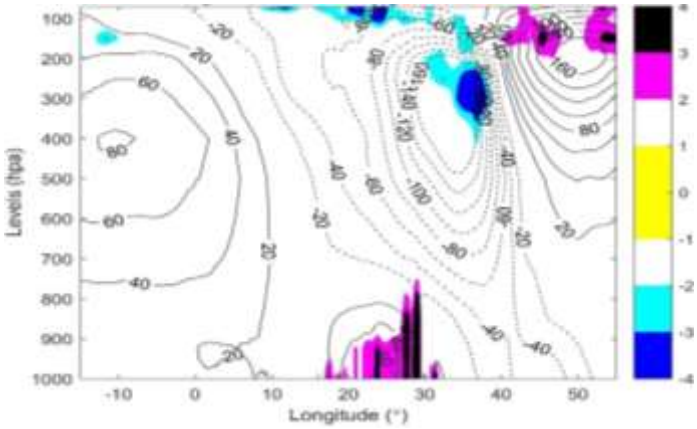

Figure 4.24 Time-lagged evolution of geopotential height anomalies at 500 hPa (contour) with potential vorticity (shaded) for **event 4**. Contour interval is at 10 m for geopotential heights. Positive (negative) geopotential contours are thin lines (dashed lines).

4.5 **Summary**

To achieve the first objective, this study used four COLs events that have occurred in the past located at four subdivided regions (A, B, C and D) according to Singleton and reason, (2007), to present the evolution of COLs case studies using PV diagnostics. The folding of the dynamical tropopause allows for the intrusion of stratospheric air into the upper troposphere to form a COL. Once there is enough transport of air into the upper troposphere, the PV deepens followed by the cut-off stage of the COL to a fully developed COL system. In other instances, the PV was used to indicate the intensity of the COL system, where an area of high PV anomaly (negative PV) implicated high intensity of the COL. This study also plotted MSLP surfaces with Gph at 250 hPa during the period of the COLs presenting the link between COLs and ridging highs. COLs that occur in the northern regions (C and D) of the subdivided regions are most likely be associated with Type-N ridging high and those that develop south of the subdivided regions (A and B) are associated with Type-S ridging high. The second objective was achieved by plotting the vertical profiles of the COLs events to showcase the location and how cold-cores occurs during COLs, which is an issue that people believe but never really seen. Vertical profiles further provided insights on the location and behaviour of the jets during COLs, as to the spilling of the jet towards the surface as COLs also do the same on some events. This study used geopotential heights to showcase the actual locations of the centres of the COLs and to present the propagations of the COLs towards the east. It was found that COLs tend to propagate east after the day that they form. Omega which is basically the uplift of air during COLs was found far east of the centre of the COLs to indicate that COLs tend to bring rain or any other precipitative form far east of the centre of the COL and not at the centre.

Chapter 5: Energetics analysis during Cut-Off Lows

5.1 **Introduction**

This chapter analyses the role of energetics in relation to the formation of Cut-Off Lows (COLs) events presented in chapter 4. This chapter presented the relationship of eddy kinetic energy (EKE) with Ageostrophic Flux Convergence (AFC), Baroclinic Convergence (BRC) and Barotropic Convergence (BRT) for each event presented in chapter 4. EKE can be defined as the kinetic energy of the time varying component of the velocity field (Danielson *et al*, 2006). AFC also known as downstream development is characterized by the development and exchange of energy between two energy centers (Ndarana *et al*, 2020). BRC can be explained as the conversion from eddy available potential energy to eddy kinetic energy (Ndarana *et al*, 2021; Pinheiro *et al*, 2022). BRT can be described as the rate of conversion from zonal to eddy kinetic energy associated with transport of momentum, although it is often linked with system dissipation (Pinheiro *et al*, 2022). The aim of this chapter is to describe which of the three processes mentioned above is associated with COL genesis, intensification (maturity) and dissipation (decay) as well as looking at their deviations and similarities from event one to event four.

5.2 **Relationship between eddy kinetic energy (EKE) and ageostrophic flux convergence (AFC)**

From the mathematical calculations illustrated above (3.3.1.6), this study presented vertical structures of downstream development where AFC increases (decreases) when it is negative (positive) in sign. EKE increases (decreases) with time when AFC is negative (positive) according to Figures 5.1 (a-f). AFC indicates an area where there is a conversion from mean potential energy to eddy available potential energy (Pinheiro *et al*, 2022). Although AFC does not increase/decrease below 500 hPa because it depends on zonal wind (u) which is higher at high levels and lower at low levels (near surface) (Ndarana *et al*,2021; Pinheiro *et al*, 2022). According to Figure 5.1 (a-b), the rear EKE centre develops and maximizes before the formation of the COL between 150 hPa and 400 hPa. EKE centre maximizes at these levels because this is the region of highest zonal wind (u). Subsequently, the front EKE centre develops and maximizes after the COL is formed (Figure 5.1 d). According to Figure 5.1 (c-d), The COL event associated with these EKE field develops and mature between the two energy centers at about 20°E to 25°E.12 hours after the COL event one formed (Figure 5.1 d), the rear (front) EKE centre decreased (increased) in strength and its extension towards the surface compared to the previous time slots indicating the transfer of energy from the rear EKE centre to the front EKE centre. The decay stages of the COL event were presented with

a decrease in both the front and rear EKE centre, although the rear EKE centre intensify again during the last day of the COL due to an increasing AFC in this day (Figure 5.1 e-f).

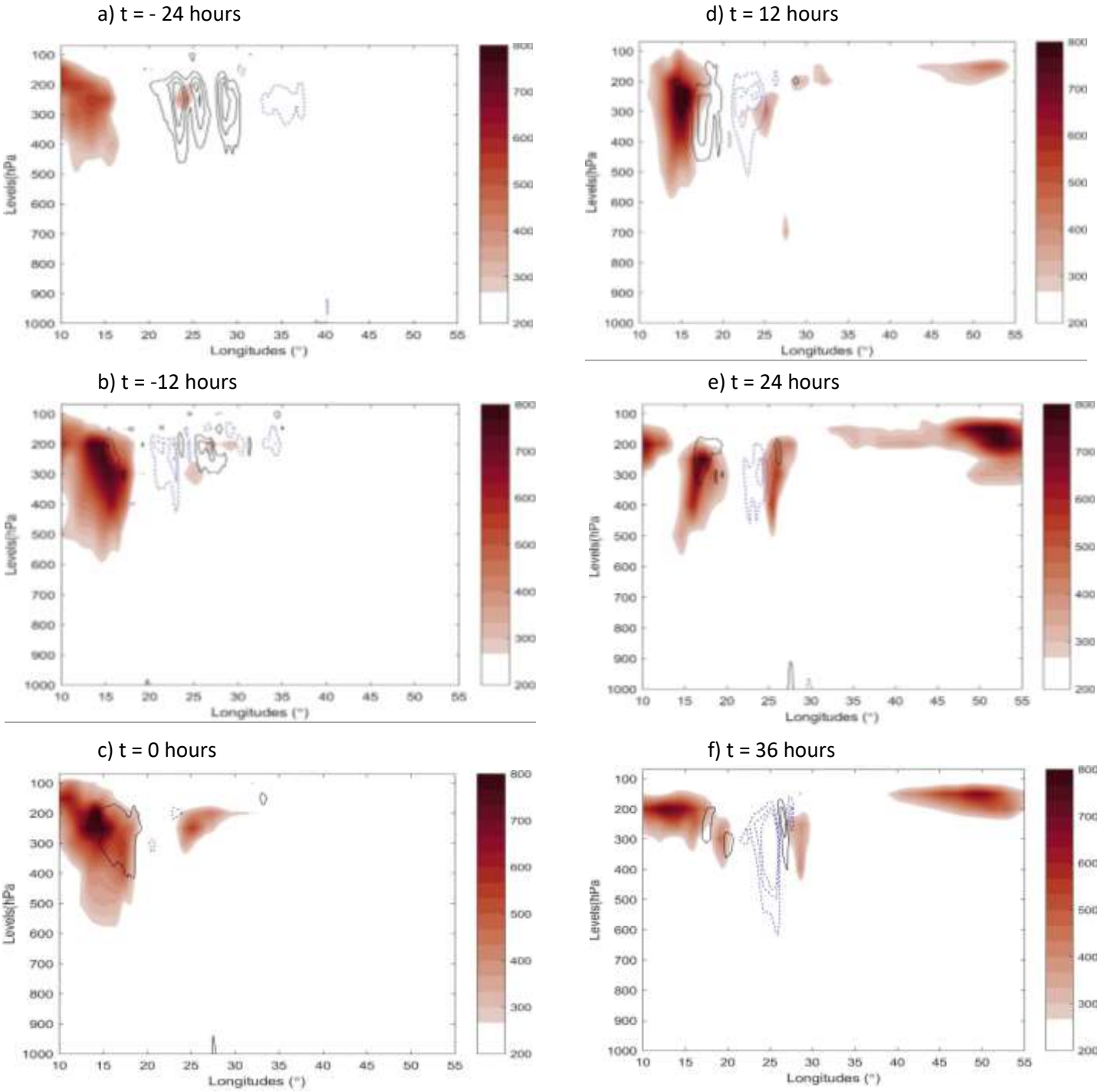

Figure 5.1: Time-lagged vertical cross-sections of the total EKE (shaded) combined with AFC (contour) for **event 1**. Intervals are $300x10^{10}$ J for total EKE with $1x10^{-3}$ $J.s^{-1}$. Positive (negative) values are indicated in black solid (blue dotted) contours.

Conversely, event two genesis showed high intensity of rear EKE and front EKE centres compared to event one because of high AFC (blue contours) which developed earlier compared to event one, according to Figure 5.2 (a-b) below. Although, this rear EKE also reached its maximum before the formation of the COL event just like the one in event one.

During the day the COL is formed, the transfer of energy from the rear EKE to the front EKE was clearly visible with a decrease in AFC on the rear and an increase situated near the front EKE to show a possible increase in front EKE during the next stages of the COL (Figure 5.2 c). According to Figure 5.2 (c-d), the COL event associated with these EKE fields develops and mature between the two energy centers at about 25°E to 35°E. 12 hours after the COL event two formed (Figure 5.2 d), the rear (front) EKE centre decreased (increased) in strength and its extension towards the surface compared to the previous time slots indicating a complete transfer of energy from the rear EKE centre to the front EKE centre. Moreover, the front EKE centre increased rapidly compared to the one in event one because of more blue AFC contours which are situated between and at the front EKE at this stage compared to the previous timeslots (Figure 5.2 d) The decay stages of the COL event were presented with a decrease in both the front and rear EKE, although the rear EKE was at its lowest level during this last stages because of high dominance of black contours situated at/near it. However, unlike during event one, the rear EKE did not show any signs of increasing again like the one at event one (Figure 5.2 e-f).

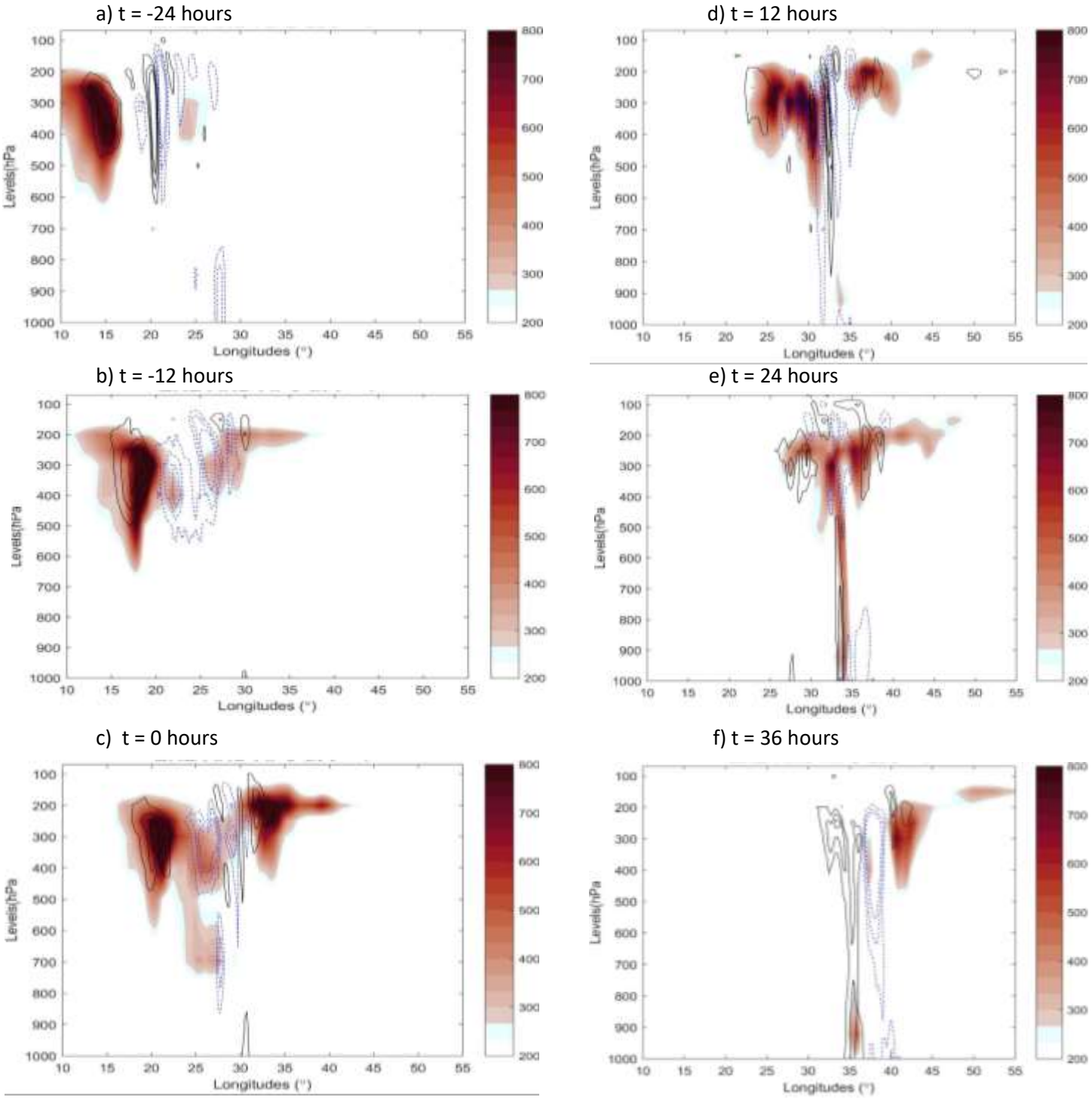

Figure 5.2: Time-lagged vertical cross-sections of the total EKE (shaded) combined with AFC (contour) for **event 2**. Intervals are 300x10^{10} J for total EKE with 1x10^{-3} J.s^{-1}. Positive (negative) values are indicated in black solid (blue dotted) contours.

COL event three genesis also showed high intensity of EKE because of blue AFC contours dominance, which developed earlier compared to event one, although there was also a high occurrence of black AFC contours present at/near the rear EKE to represent a decrease in

the rear EKE as the COL event is about to form (Figure 5.3 a-b). However, this rear EKE also reached its maximum before the formation of the COL event just like the two events discussed above. During the day the COL is formed, the transfer of energy from the rear EKE to the front EKE was showcased by a decrease in AFC (black contours) on the rear and an increase in AFC (blue contours) just like in event one, situated near the front EKE to show a possible increase in front EKE during the next stages of the COL (Figure 5.3 c). According to Figure 5.3 (c-d), the COL event associated with these EKE fields develops and mature between the two energy centers at about 20°E to 30°E. 12 hours after the COL event three formed (Figure 5.3 d), the rear (front) EKE decreased (increased) in strength and its extension towards the surface compared to the previous time slots indicating a complete transfer of energy from the rear EKE to the front EKE just like event two. Moreover, the front EKE also increased rapidly compared to the one in event one because of more blue AFC contours which are situated between and at the front EKE at this stage compared to the previous timeslots (Figure 5.3 d). The decay stages of the COL event were presented with a decrease in both the front and rear EKE, although there were no signs of AFC contours at this stage to show that the COL is dissipating (Figure 5.3 e-f).Furthermore, unlike during event two, the rear EKE was still visible during the last 12 hours with no signs of increasing again like the one at event one (Figure 5.3 e).

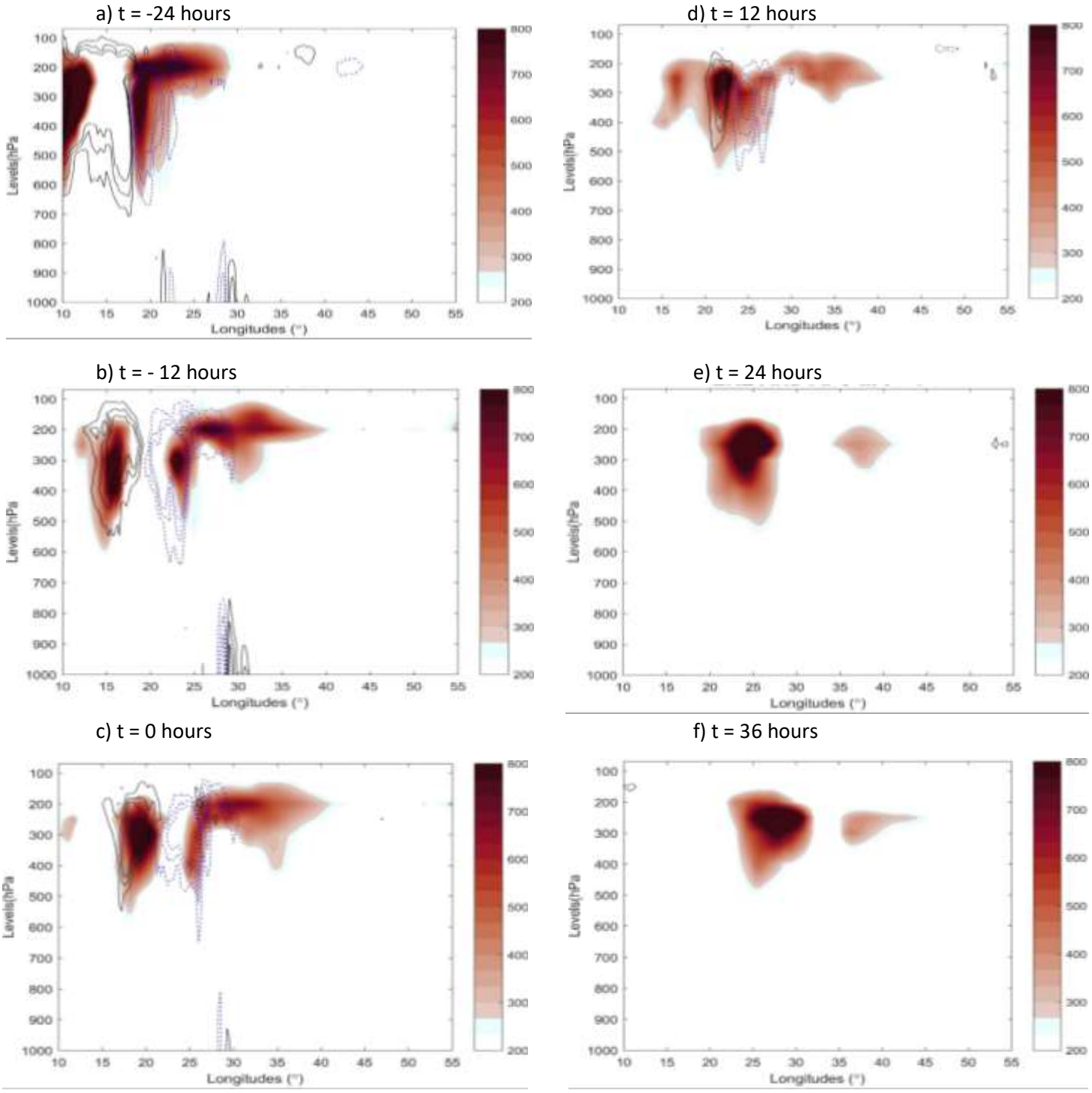

Figure 5.3: Time-lagged vertical cross-sections of the total EKE (shaded) combined with AFC (contour) for **event 3**. Intervals are 300x10^{10} J for total EKE with 1x10^{-3} J.s^{-1}. Positive (negative) values are indicated in black solid (blue dotted) contours.

Not only events two and three, but also event four showed high intensity of rear EKE and front EKE compared to event one because of high AFC dominance (blue contours) which developed earlier compared to event one, according to Figure 5.4 (a-b) below. Although, this

rear EKE also reached its maximum before the formation of the COL event just like the other events presented above. During the day the COL is formed, the transfer of energy from the rear EKE to the front EKE was showcased by a decrease in AFC (black contours) on the rear and an increase in AFC (blue contours) just like in event one and event three, situated near the front EKE to show a possible increase in front EKE during the next stages of the COL (Figure 5.4 c). According to Figure 5.4 (c-d), the COL event associated with these EKE fields develops and mature between the two energy centers at about 20°E to 35°E. 12 hours after the COL event four formed (Figure 5.4 d), the rear (front) EKE decreased (increased) in strength and its extension towards the surface compared to the previous time slots indicating a complete transfer of energy from the rear EKE to the front EKE just like the rest of the events. Moreover, the front EKE also increased rapidly compared to the one in event one because of more blue AFC contours which are situated between and at the front EKE at this stage compared to the previous timeslots (Figure 5.4 d). This resulted in the front EKE reaching its maximum just after the formation of the COL event. The decay stages of COL event four had the same characteristics as the decay stages of event two, presented with a high intensity of the front EKE compared to the rear EKE. Although they were both declining in strength and extensions towards the surface, the front EKE was still visible even during the last stages of the system with high blue AFC contours near/around it for a possible increase in the next few hours (Figure 5.4 e-f).

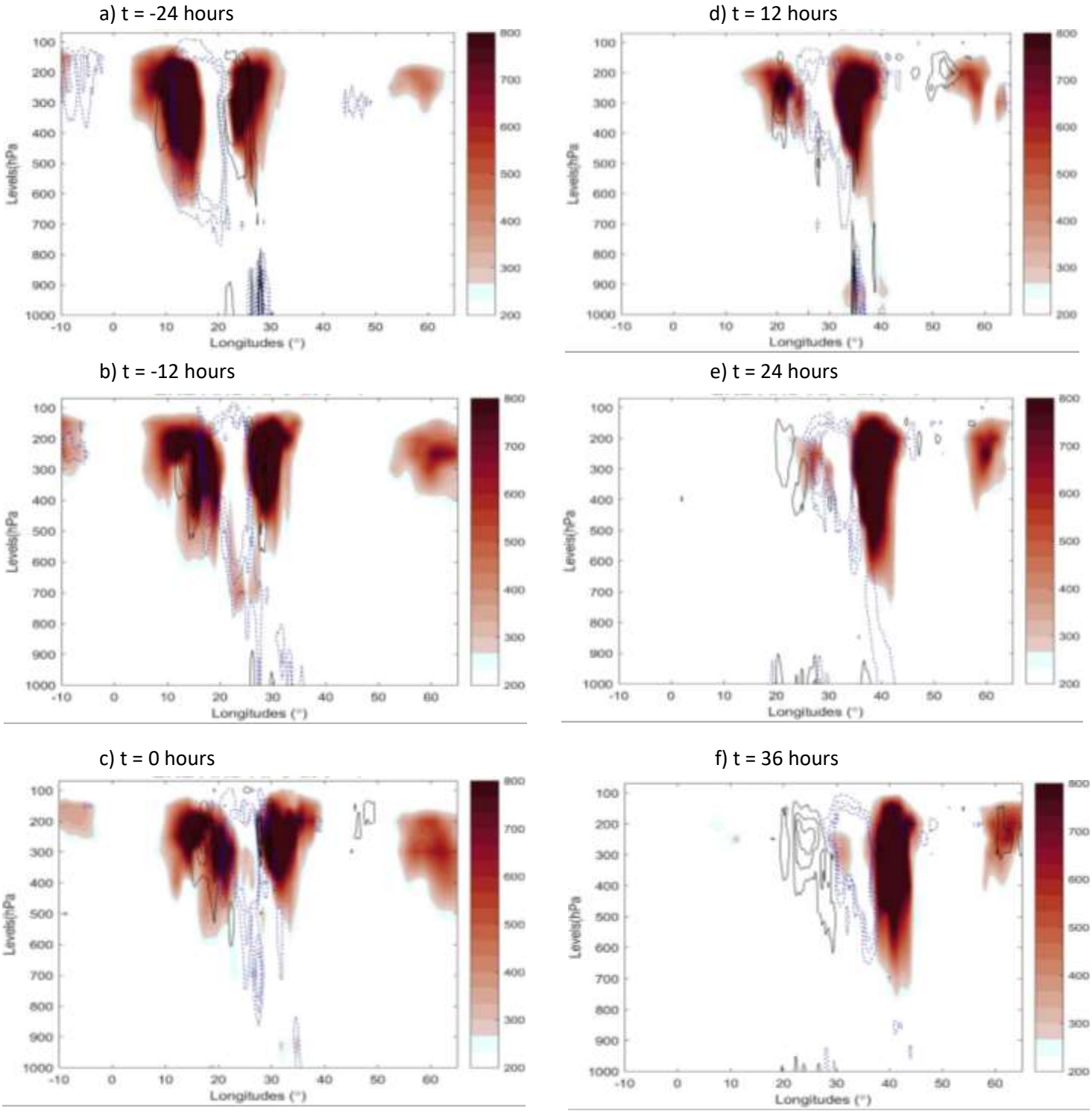

Figure 5.4: Time-lagged vertical cross-sections of the total EKE (shaded) combined with AFC (contour) for **event 4**. Intervals are $300x10^{10}$ J for total EKE with $1x10^{-3}$ $J.s^{-1}$. Positive (negative) values are indicated in black solid (blue dotted) contours.

5.3 **Relationship between eddy kinetic energy (EKE) and baroclinic convergence (BRC)**

From the mathematical calculations illustrated above (3.3.1.6), vertical profiles presented in this study show that BRC also increases (decreases) when it is negative (positive) in sign. Hence, EKE centre increases (decreases) with time when BRC is negative (positive) according to Figures 5.5 (a-f). BRC indicates an area where there is a conversion from eddy available potential energy to eddy kinetic energy (Ndarana *et al*, 2021). BRC occurs at lower levels because it depends on omega (vertical motion) which is strongest there (Pinheiro *et al*, 2022). As mentioned above, the rear EKE maximizes before the formation of the COL, but in this case with an increasing BRC trend (Figure 5.5 a-b). Consequently, this first two stages before the formation of the COL event were mostly dominated by high blue (black) BRC contours below the front (near rear) EKE to show a possible increase (decrease) in strength of the EKE in the next stages of the system. During the COL formation stages, BRC increases up to its maximum levels with high dominance in the study area to show the importance of this conversion for the maintenance of the system (Figure 5.5 c-d). Moreover, the front EKE maximizes after the formation of the COL because of this high conversion intensity. According to Figure 5.5 (c-d), The COL event associated with these EKE field develops and mature between the two energy centers at about 20°E to 25°E. The decay stages of the COL event were presented with a decrease in both the front and rear EKE centres with little/less BRC presents (Figure 5.5 e-f).

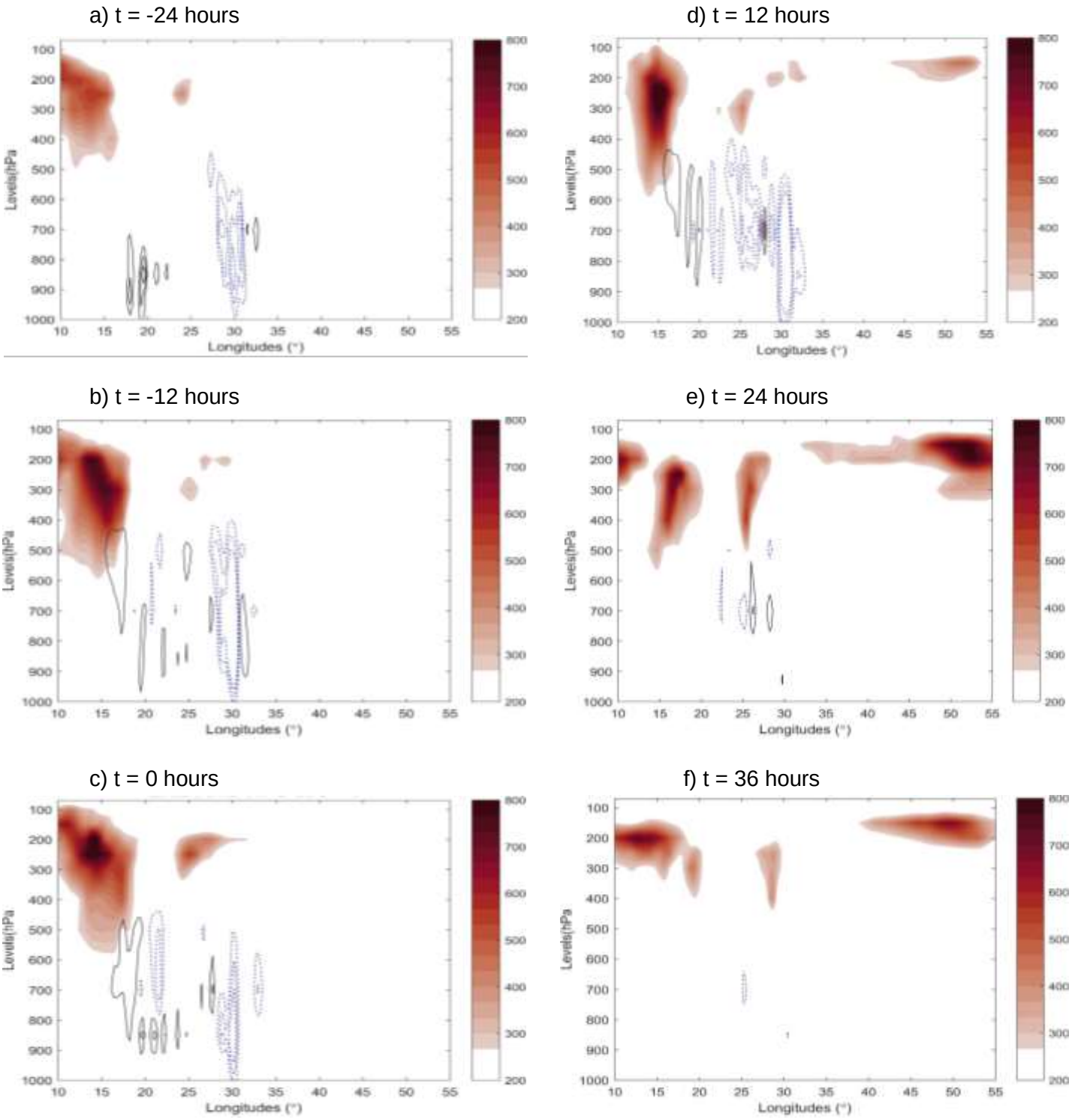

Figure 5.5: Time-lagged vertical cross-sections of the total EKE (shaded) combined with BRC (contour) for **event 1**. Intervals are $300x10^{10}$ J for total EKE with $1x10^{1}$ $J.s^{-1}$. Positive (negative) values are indicated in black solid (blue dotted) contours.

Conversely, the presents of high dominance of blue contours during the early stages of the system were lower compared to event one, although it was also denoting an increasing trend at these stages (Figure 5.6 a-b). unlike event one, this first two stages before the formation of

the COL event two were mostly dominated by high positive (negative) BRC contours below the front (near rear) EKE to show a possible increase in strength of the EKE in the next stages of the system. During the COL formation stages, BRC increases up to its maximum levels with high dominance in the study area to show the importance of this conversion for the maintenance of the system (Figure 5.6 c-d). Furthermore, the front EKE maximizes after the formation of the COL because of this high conversion intensity shown at these stages. The COL event associated with these EKE fields develops and matures between the two energy centers at about 25°E to 35°E (Figure 5.6 c-d). The decay stages of this COL system were presented with decreasing positive BRC contours and stable negative BRC contours indicating a high maintained COL system (Figure 5.6 e-f).

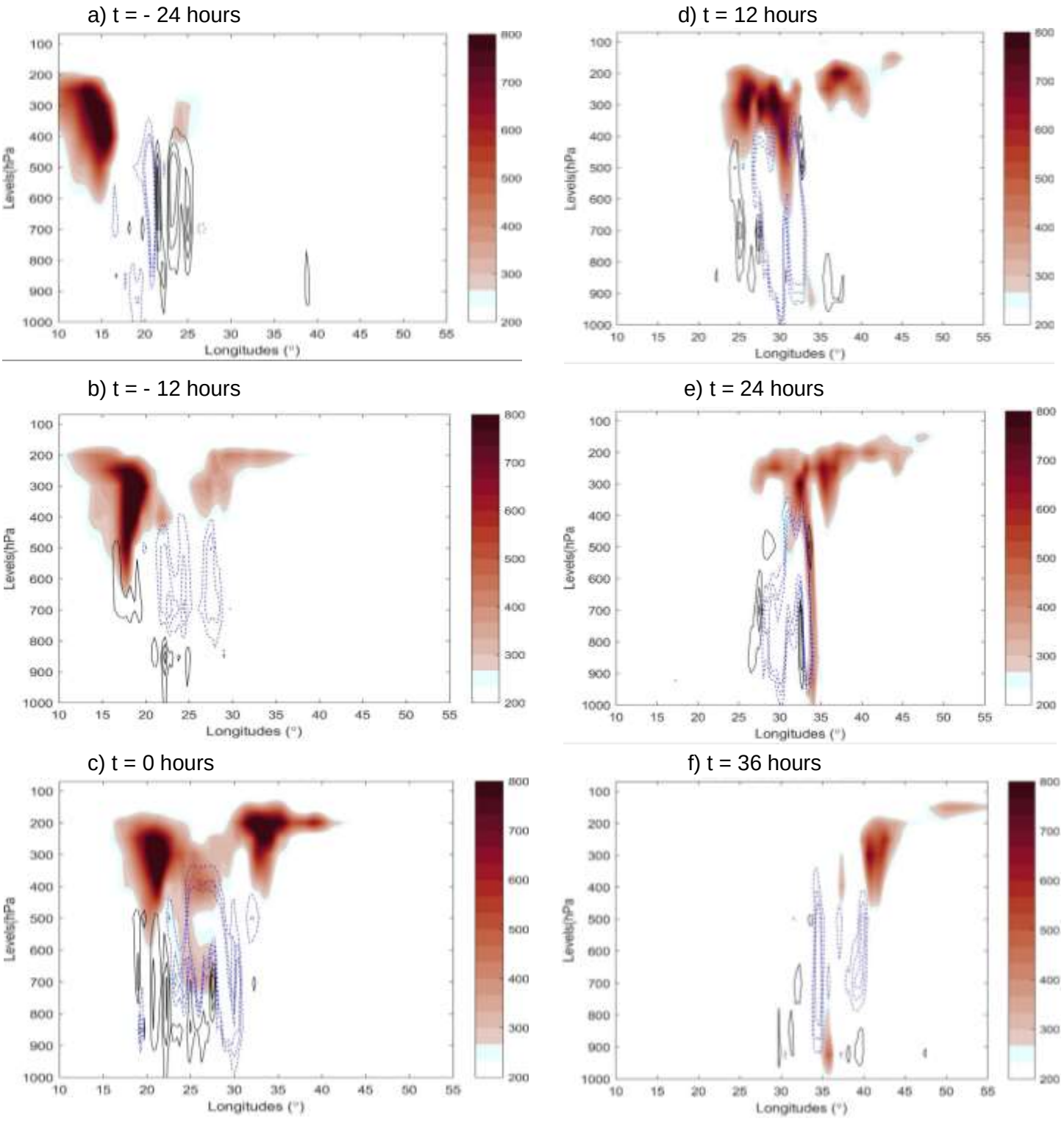

Figure 5.6: Time-lagged vertical cross-sections of the total EKE (shaded) combined with BRC (contour) for **event 2**. Intervals are $300x10^{10}$ J for total EKE with $1x10^{1}$ $J.s^{-1}$. Positive (negative) values are indicated in black solid (blue dotted) contours.

COL event three had similar characteristics during the first two stages of development of the COL with event one, although 12 hours earlier, the rear EKE is dominated by high black contours of BRC which may have been implying a decrease in strength of the EKE in the next

stages of the COL development (Figure 5.7 a-b). Moreover, the front EKE was dominated with high areas of negative BRC contours near/around the EKE indicating a rapid increase in strength of the front EKE (Figure 5.7 a-b). Unlike the previous two events, BRC showed a decreasing trend during the formation of the COL and its intensification stage compared to the previous timeslots indicating a low maintenance of the COL system (Figure 5.7 c-d). Furthermore, the front EKE maximized just after the formation of the COL unlike the other events which reached their maximum 12 hours after the formation of the COL because of this little/less negative BRC contours presents in the study area which eventually led to the decay stages of the COL system, characterized by little/no BRC contours (Figure 5.7 e-f).

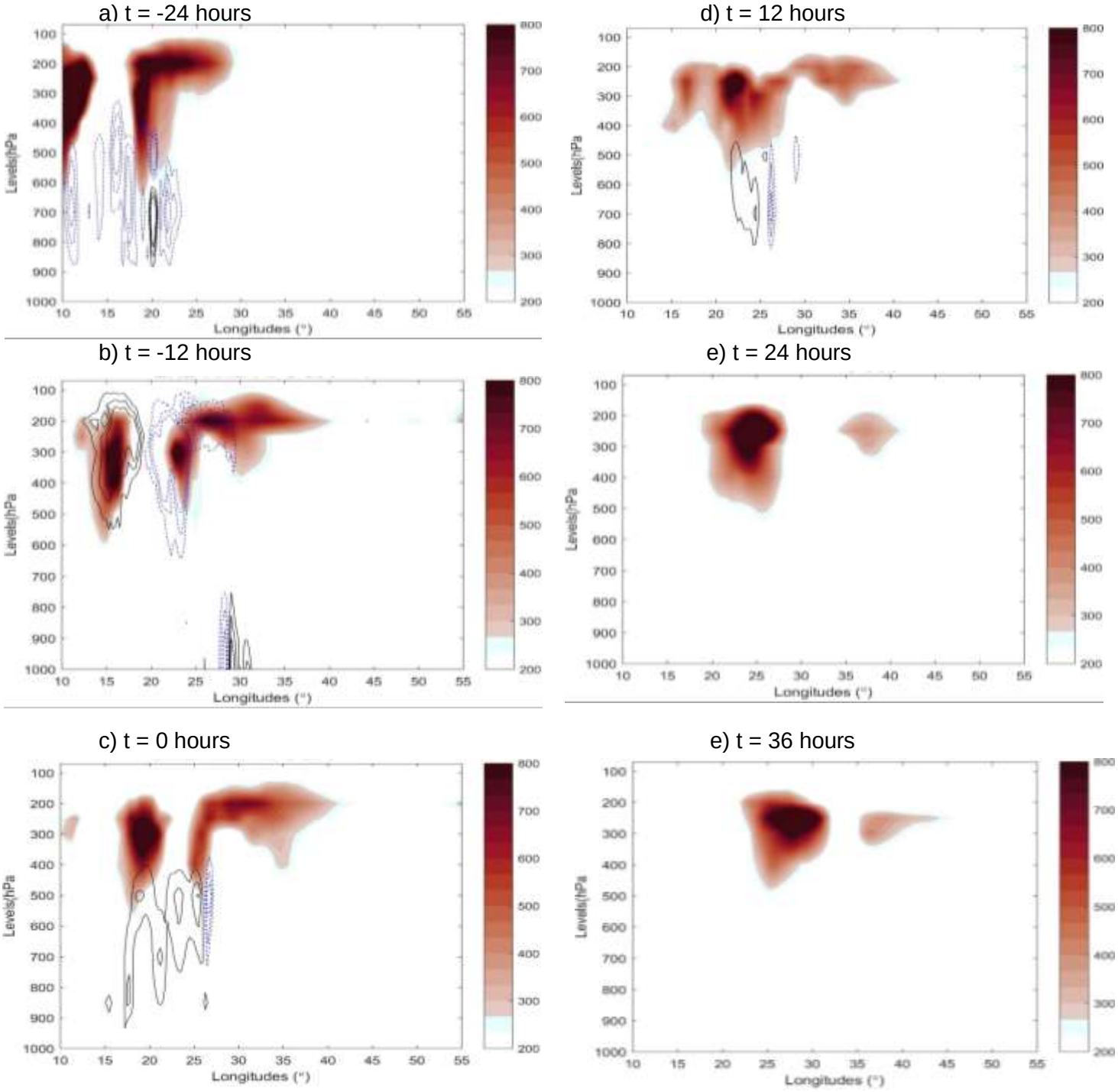

Figure 5.7: Time-lagged vertical cross-sections of the total EKE (shaded) combined with BRC (contour) for **event 3**. Intervals are 300x10^{10} J for total EKE with 1x10^{1} J.s^{-1}. Positive (negative) values are indicated in black solid (blue dotted) contours.

The presents of blue contours during the early stages of COL event four was lower compared to events one and three, although it was also denoting an increasing trend at these stages just like during event two (Figure 5.8 a-b). Moreover, these first two stages before the formation of the COL event were mostly dominated by black BRC contours below/near the energy centers

denoting a possible decrease in strength of the energy fields in the next stages. The dominance of blue BRC contours was clearly visible between the two energy centers illustrating the transfer of energy from the rear EKE to the front (Figure 5.8 a-b). During the COL formation stages, BRC increases up to its maximum levels with high dominance in the study area to show the importance of this conversion for the maintenance of the system (Figure 5.8 c-d). Furthermore, the front EKE maximizes after the formation of the COL because of this high conversion intensity shown at these stages. The COL event associated with these EKE fields develops and matures between the two energy centers at about 20°E to 35°E (Figure 5.8). The decay stages of this COL system were presented with both decreasing positive BRC contours and negative BRC contours indicating little/less impact of BRC at this stage of the system (Figure 5.8 e-f).

.

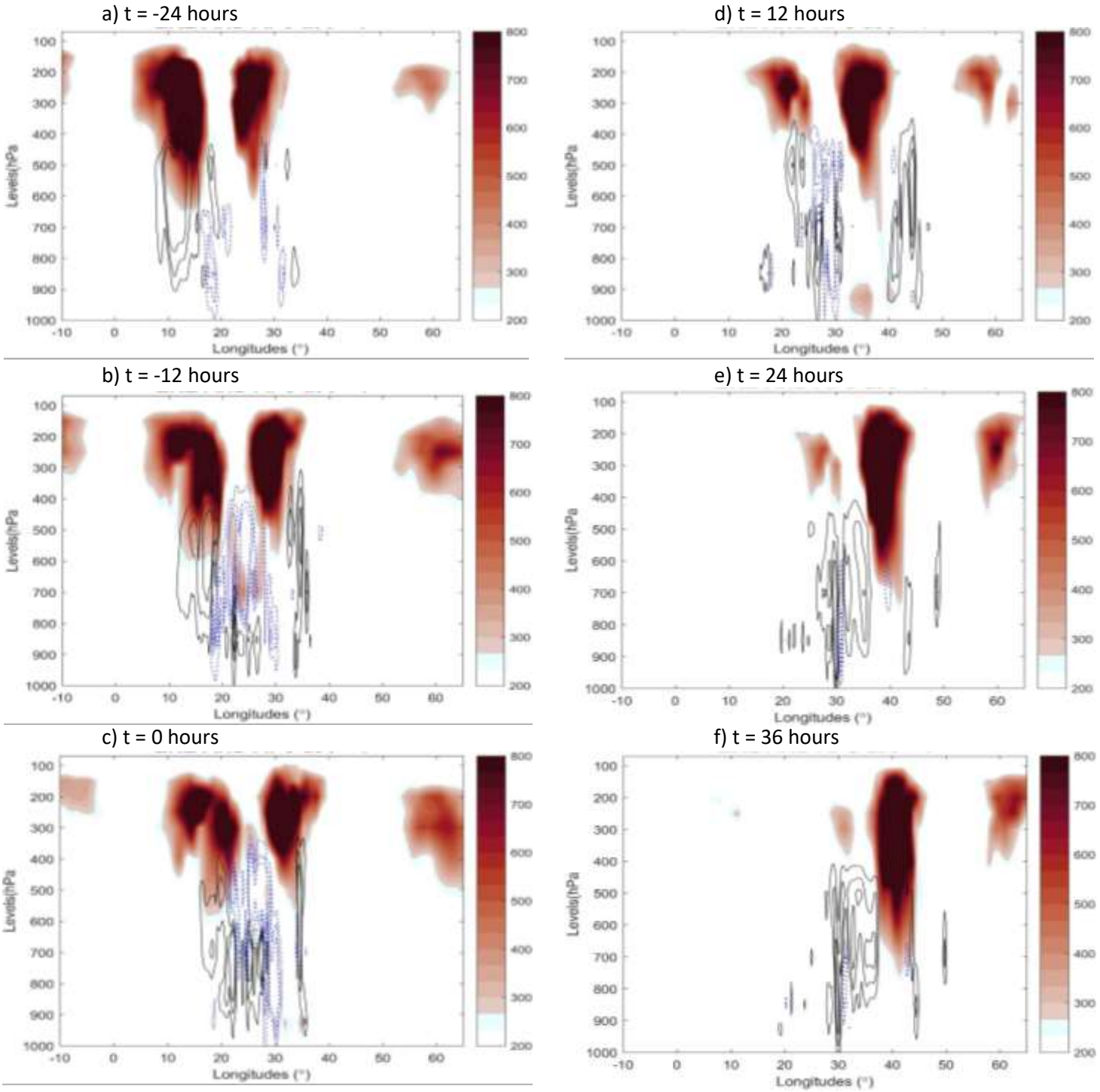

Figure 5.8: Time-lagged vertical cross-sections of the total EKE (shaded) combined with BRC (contour) for **event 4**. Intervals are $300x10^{10}$ J for total EKE with $1x10^{1}$ $J.s^{-1}$. Positive (negative) values are indicated in black solid (blue dotted) contours.

5.4 **Relationship between eddy kinetic energy (EKE) and barotropic convergence (BRT)**

From the mathematical calculations illustrated above (3.3.1.6). BRT decreases (increases) when it is negative (positive) in sign. Hence, EKE increases (decreases) with time when BRT is negative (positive) according to Figures 5.9 (a-f). BRT shows an area where there is a conversion of eddy kinetic energy (EKE) to mean kinetic energy (MKE). Hence, intense BRT decreases the strength of the EKE according to Figures 5.9 (a-f). The rear EKE centre develops and maximizes before the formation of the COL between 150 hPa and 400 hPa (Figure 5.9 a-b). There is high dominance of blue BRT contours over the study during the development stages of the COL indicating less impact of the conversion during these stages of the system (Figure 5.9 a-b). During the formation of the COL, the study area was mostly dominated by both negative and black BRT contours indicating less impact of the BRT during these stages of the system (Figure 5.9 c-d). Moreover, the front EKE develops and maximizes after the COL is formed. According to Figure 5.9 (c-d), The COL event associated with these EKE field develops and mature between the two energy centers at about 20°E to 25°E. COLs are baroclinic and when BRT dominates the field then the COL is decaying/dissipating. The decay stages of the COL event were presented with a decrease in both the front and rear EKE, although there was high dominance of black BRT contours during these stages indicating high impact of BRT at these timeslots compared to the previous ones (Figure 5.9 e-f).

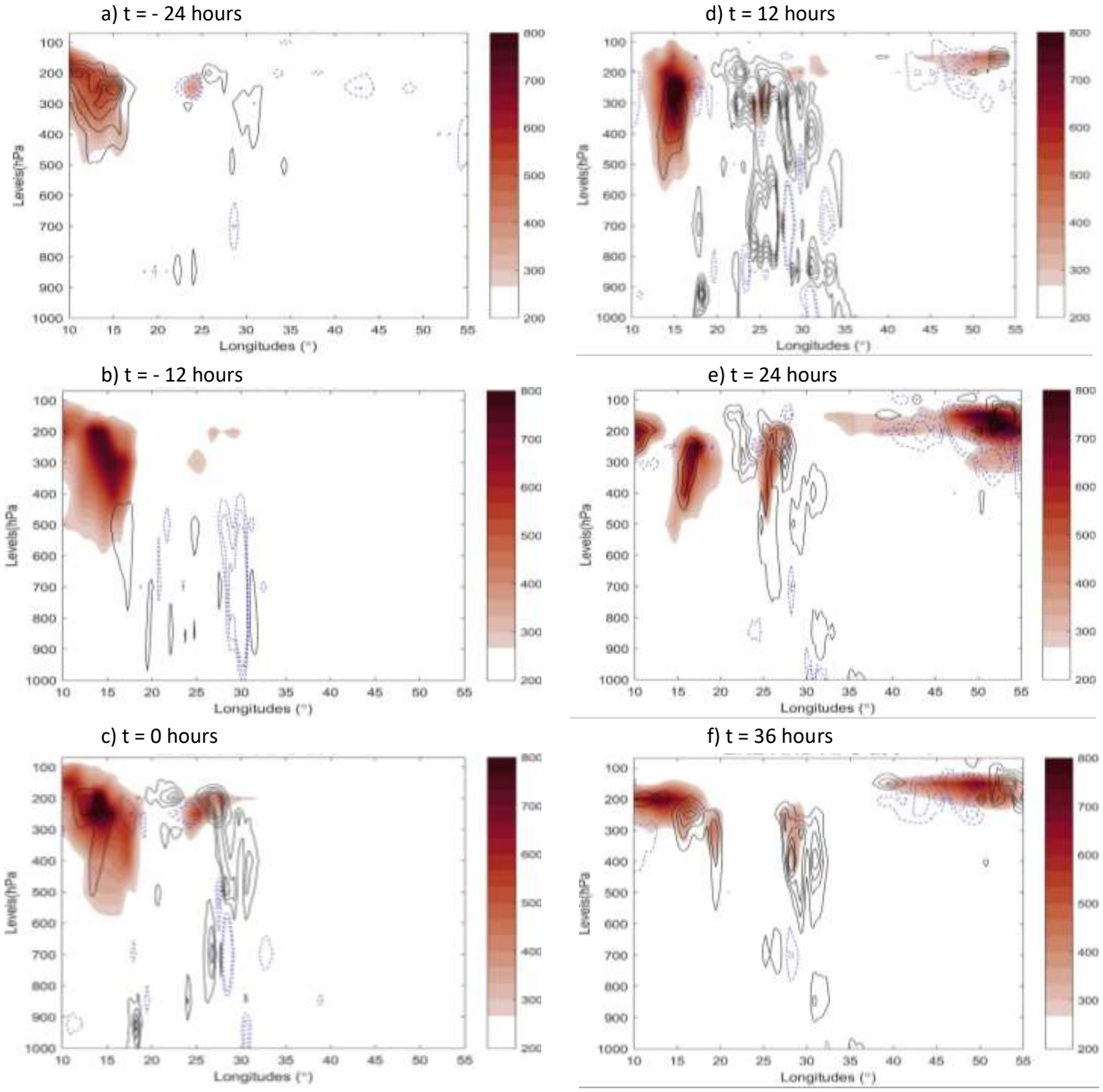

Figure 5.9 Time-lagged vertical cross-sections of the total EKE (shaded) combined with BRT (contour) for **event 1**. Intervals are $300x10^{10}$ J for total EKE with $1x10^{4}$ $J.s^{-1}$. Positive (negative) values are indicated in black solid (blue dotted) contours.

There is high dominance of blue BRT contours over the study during the development stages of the COL event two indicating less impact of the conversion during these stages of the system, although an increasing trend of black BRT contours were also spotted developing at

this stage (Figure 5.10 a-b). During the formation of the COL, the study area was mostly dominated by both blue and black BRT contours indicating less impact of the BRT during these stages of the system (Figure 5.10 c-d). The front (rear) EKE centre which develops and maximizes after (before) the COL is formed was dominated by positive (negative) contours of BRT indicating a possible decrease (increase) in strength of the EKE centre during these stages of the COL (Figure 5.10 c-d). The COL event associated with these EKE fields develops and matures between the two energy centers at about 25°E to 35°E. COLs are baroclinic and when BRT dominates the field then the COL is decaying/dissipating. The decay stages of the COL event were presented with a decrease in both the front and rear EKE, although there was high dominance of black BRT contours during these stages indicating high impact of BRT at these timeslots compared to the previous ones (Figure 5.10 e-f).

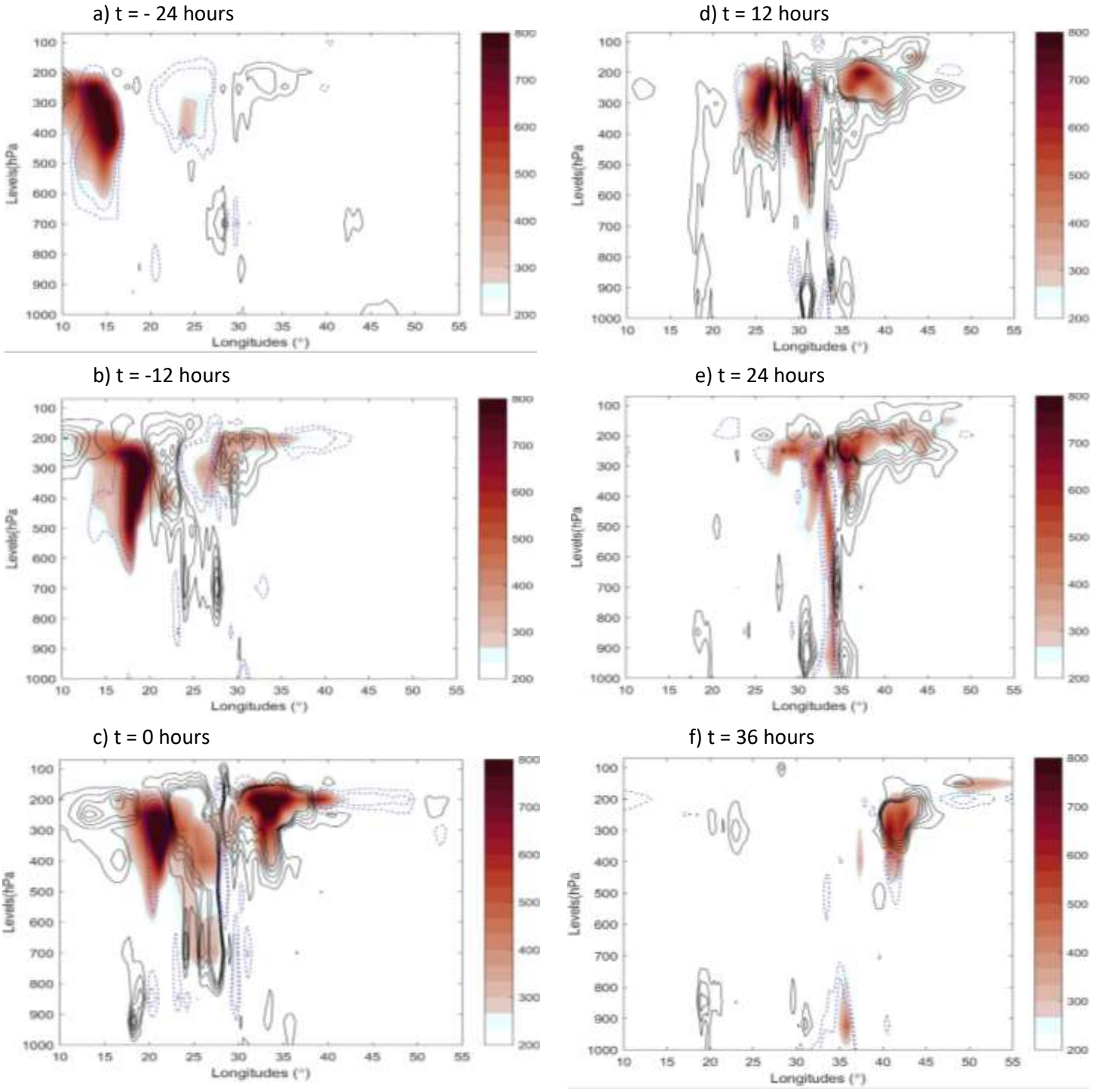

Figure 5.10 Time-lagged vertical cross-sections of the total EKE (shaded) combined with BRT (contour) for **event 2**. Intervals are $300x10^{10}$ J for total EKE with $1x10^{4}$ $J.s^{-1}$. Positive (negative) values are indicated in black solid (blue dotted) contours.

Event three further showed similar characteristics of development stages like events one and two in terms of the BRT with high dominance of blue BRT contours over the study indicating little/less impact during these stages of the system (Figure 5.11 a-b). Unlike event two (Figure

5.11 a-b), blue BRT contours were situated near/closer to both the front and rear EKE centres, indicating a possible increase in strength of the EKE during the next stages of the COL system (Figure 5.11 a-b). During the formation of the COL, the study area was mostly dominated by black BRT contours indicating the loss of energy from both the rear and front EKE centres (Figure 5.11 c-d). Furthermore, the front EKE had some visible blue contours of BRT at/around its center indicating a possible increase of strength during the next stages of the COL system (Figure 5.11 c-d). The COL event associated with these EKE field develops and mature between the two energy centers at about 20°E to 30°E. COLs are known for being baroclinic and when BRT dominates the field then the COL loses its strength and energy (dissipates) (Ndarana *et al*, 2021; Pinheiro *et al*, 2022). Just like the two events provided above, the decay stages of the COL event were presented with a decrease in both the front and rear EKE centres (Figure 5.11 e-f). There was also a high dominance of black BRT contours during these stages indicating high impact of BRT at these timeslots compared to the previous ones (Figure 5.11 e-f).

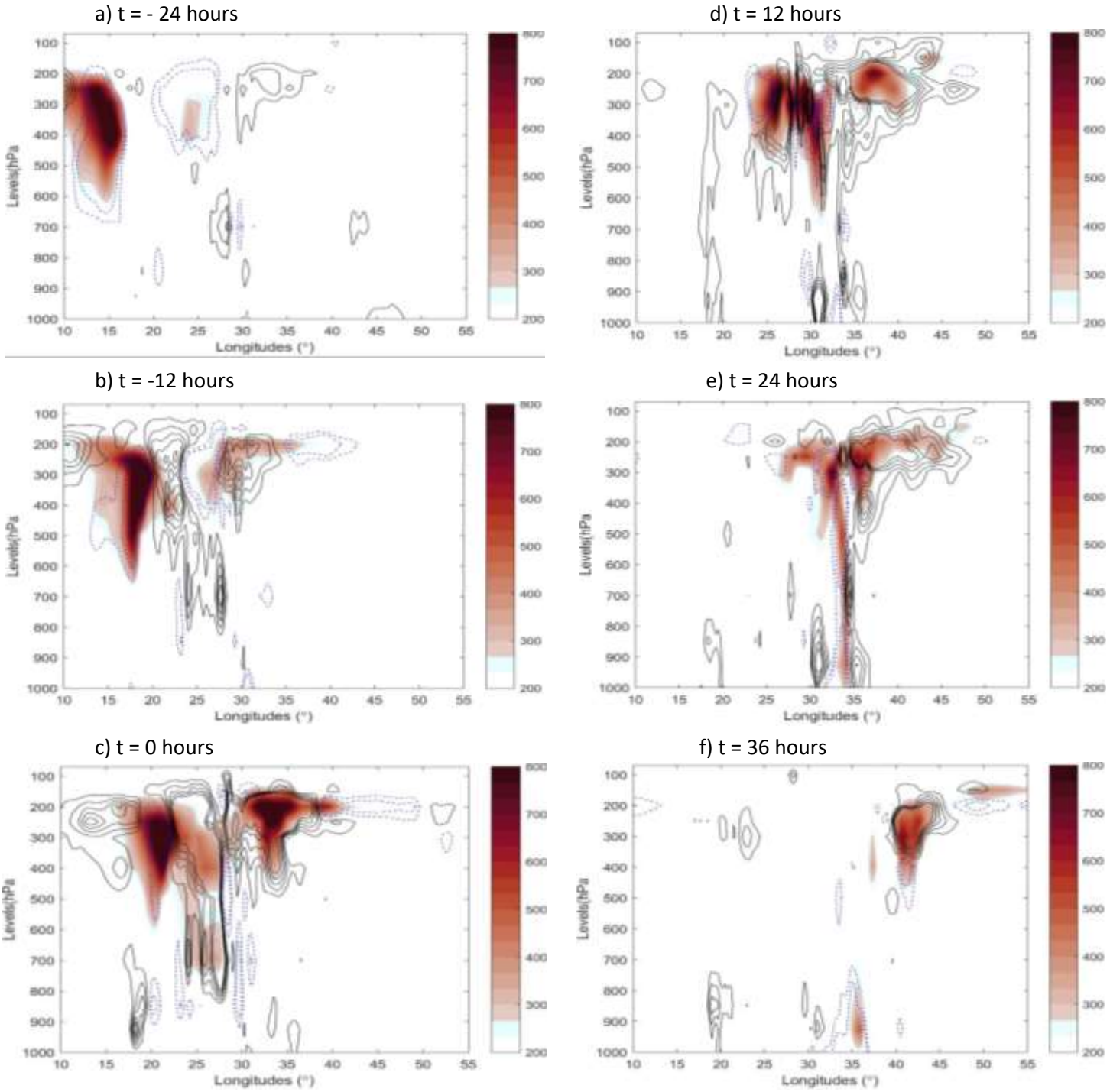

Figure 5.11 Time-lagged vertical cross-sections of the total EKE (shaded) combined with BRT (contour) for **event 3**. Intervals are $300x10^{10}$ J for total EKE with $1x10^{4}$ J.s^{-1}. Positive (negative) values are indicated in black solid (blue dotted) contours.

Event four also showed high dominance of black BRT contours over the study during the development stages of the COL (Figure 5.12 a-b). The dominance of BRT (blue contours) at this stage indicated less impact of the conversion during these stages of the system, although

an increasing trend of blue BRT contours (black contours) were also spotted developing at this stage (Figure 5.12 a-b). Moreover, the presence of both the blue and black BRT contours around the two energy centers indicates a balance that results in little/less impact of the BRT during these early stages of the COL system (Figure 5.12 a-b). During the formation of the COL, the study area was mostly dominated by blue BRT contours indicating the loss of energy from both the rear and front EKE centres (Figure 5.12 c-d). The front EKE centre had some visible blue contours of BRT at/around its center indicating a possible increase of strength during the next stages of the COL system (Figure 5.12 c-d). The COL event associated with these EKE fields develops and mature between the two energy centers at about 20°E to 35°E. COLs are known for being baroclinic and when BRT dominates the field then the COL loses its strength and energy (dissipates). Just like the three events provided above, the decay stages of the COL event were presented with a decrease in both the front and rear EKE centre strength, although the impact was higher on the rear EKE due to the presence of high positive BRT values near/around its center during the previous timeslots. Furthermore, this high dominance of black BRT contours during these stages indicates high impact of BRT at these timeslots compared to the previous ones (Figure 5.12 e-f).

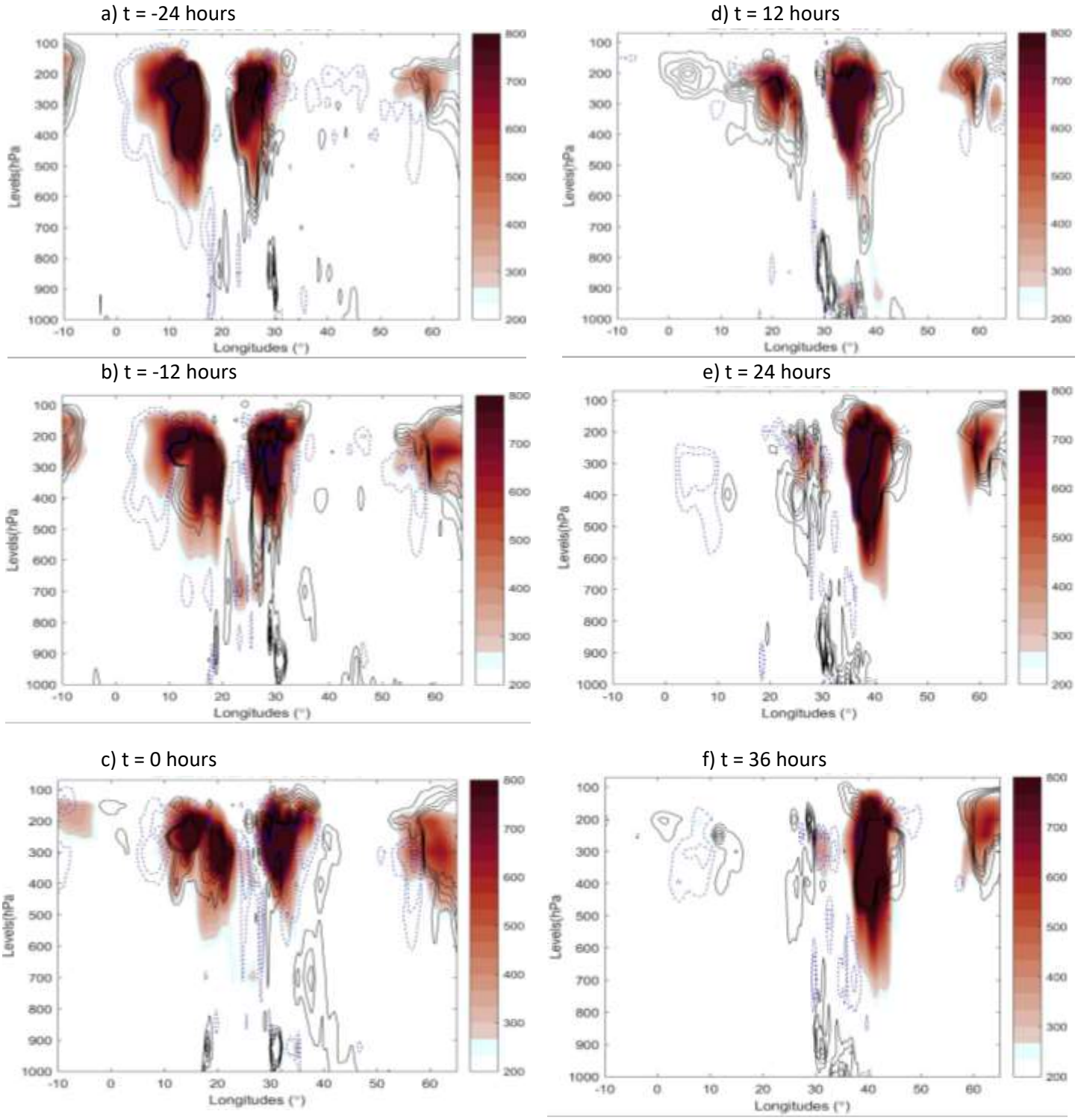

Figure 5.12 Time-lagged vertical cross-sections of the total EKE (shaded) combined with BRT (contour) for **event 4**. Intervals are $300x10^{10}$ J for total EKE with $1x10^{4}$ $J.s^{-1}$. Positive (negative) values are indicated in black solid (blue dotted) contours.

5.5 **Summary**

In this chapter, the third objective was achieved by computing the EKE budget to explain the role of energetic on COLs along with the dynamical processes involved in their formation such as the Ageostrophic flux convergence (AFC), Baroclinic convergence (BRC) and the Barotropic convergence (BRT). The vertical structures provided in this section ensure that we need vertical cross sections to understand these issues (i.e., downstream development) from a case study point of view. The rear EKE develops and intensifies before the formation of the COL due to the impact of high blue contours of AFC (high intensity) during these stages of the COL. The front EKE develops and intensifies after the formation of the COL due to the presence of high blue BRC contours (high intensity) for the maintenance of the COL systems. AFC is higher before the COL was formed and lower after the COL was formed, which implies that AFC is important for COL genesis stage. BRC is higher during the formation and maturity stage of the COL to indicate its importance for the maintenance of the COL. BRT black contours (high intensity) is higher during the decay stages of the COL indicating that the BRT conversion is important for the decay stages of the COLs.

Chapter 6: Conclusions and Recommendations

6.1 **Introduction**

The study focused on providing a developed understanding of dynamical processes during COLs over the South African domain. COLs are one of the most severe weather systems associated with extreme weather conditions over the country (South Africa). The study analysed four previous case studies of COL events which have been associated with heavy rainfalls from 2016 to 2019 to find deviations within them in terms of their development, maturity, propagation, and decay stages.

The important findings of the current study are discussed in this chapter, together with their contribution to the body of knowledge. There is also a comparison of the findings between this study and other studies on the COL systems in South Africa. There is also explored recommendations and consequences in respect to the traits of the extreme COL events and the effects of dynamical processes on them.

6.2 **Discussion and synthesis of key findings**

6.2.1 **Recent Cut-off Lows in South Africa : characteristics**

COLS are linked to the existence of ridging highs over the study using 250 hPa geopotential height contour and the mean sea level pressure (MSLP) to indicate which type of ridging high the COL is associated with. COLS that develop and mature north of the study are associated with Type-N ridging high and those that develop south of the study, are associated with Type-S ridging high (Ndarana *et al*, 2022). Moreover, the existence of the COLs was also maintained by identifying the COL system on the 500 hPa pressure level using a closed geopotential contour lasting for then 24 hours and the associated pool of negative potential vorticity (PV) at 330 K.

During the initial stages (development) of the systems, COLs are characterized by a deep trough with a closed circulation and associated pool of negative PV at the centre (Muofhe *et al*, 2020). The mature stages of the COLs (event one to four) from this point of view are characterised by increased closed-circulation and cyclonic pools of negative PVs at their centres. Furthermore, the cyclonic pool of negative PV decreases as the closed-circulation decreases representing the decay stages of the COLs.

In other instances, the zonal and the meridional view of the COLs was provided using PV, potential temperature, and the zonal wind (jet streak). The development stages are characterised by the folding of the PV and the presence of the jet located just above it. Moreover, the mature stages of the COLs are presented by the cut-off stages, increased jets

and the presence of the cold cores at about 500 hPa. The jet streaks decrease as the COLs dissipates over time. COLs tend to extend towards the surface as they reach the maturity stage, some COLs reach the surface, and some may not. Furthermore, the extension towards the surface is presented by the PV contour extension beyond 850 hPa and the spilling of the jet towards the surface.

COLs propagations to the east are presented using the geopotential height anomalies and the PV anomalies. All the COL case studies presented above shows signs of propagation towards the east as soon as the COL is fully developed. The high negative pool of PV anomaly increases with increasing closed circulation of negative geopotential height anomaly indicating the development and maturity stages of the COL. Furthermore, it decreases with decreasing geopotential height anomaly highlighting the decay stages of the COLs. However, this study also presented the role of vertical velocity on COLs. Negative vertical velocity (omega) indicated areas where there was uplift of air. Although from all the cases presented above, the uplift is found far east from the centre of the COL, and it is expected to increase up to about 600 hPa and not beyond.

The study findings in terms of ridging highs detection and characteristics correlate with the findings of Ndarana *et al,* (2022) who also found that Type-N ridging highs tend to move zonally across the country whereas the Type-S extend further south as it moves. Furthermore, the study findings in relation to the characteristics of COLs over South Africa correlate with Ndarana *et al*, (2021); Singleton and Reason (2007) who also found that 500 hPa geopotential height and PV plays a critical role in identification of the COL events. Muofhe *et al*, (2020) also found that cold cores of the COLs are clearly visible at about 500 hPa. The location of the jet above the COL and the COL extension towards the surface findings of this study correlated with the findings of Barnes *et al*, (2021b) who also found that deep COLs are associated with deeper intrusions which are sorely driven by high PV. This study highlighted that COLs tends to propagate east after their formation with vertical motion (uplift) also found far east from the centre of the COL which correlate with Muofhe *et al*, (2020); Pinheiro *et al*, 2020 and Reboita *et al,* (2010).

6.2.2 **Dynamical processes influence on COLs over South Africa**

For this study to achieve its objectives in relation with energy balances that are previous linked to COLs, Eddy kinetic energy (EKE) budget illustrated at 3.2.1.6 above was computed using MATLAB to showcase the relationships of EKE with ageostrophic fluxes convergence (AFC) (downstream development), Baroclinic convergence (BRC) and Barotropic convergence (BRT) which influences the development, intensification, maturity, and the decay stages of the COLs. During COLs, the current study compromises of two energy centres which are

differentiated as the rear EKE and front EKE for the purpose of this study. Moreover, in some instances they may be referred to as the upstream and downstream EKE centres (Ndarana *et al*, 2021). The rear EKE develops and maximizes before the formation of the COL by means of AFC that is observed to be higher than the other processes during these stages of development of the COL. Hence, AFC is higher during the development stage of the COL because it is responsible for the genesis of the COL system. The front EKE grows and reach its maximum intensity after the formation of the COL. The front EKE growth is dependent on the BRC which is often higher during the formation and maturity stages of the COL. Furthermore, the BRC is higher during these stages of the COL because it is responsible for the intensification and the maintenance of the system. BRT is observed to be higher than the other dynamical processes during the last stages of the COL because it is responsible for the decay stages of the COL.

The findings of this study in terms of the relationships of EKE with AFC, BRC and BRT including their influence on the development, intensification, maturity, and the decay stages of the system correlate with Ndarana *et al*, (2021) and Pinheiro *et al*, (2021) who found that the AFC is essential for the development of the COL (genesis), BRC is important for the maintenance of the COL system and the presence of high BRT threatens the life of the COL (decay stages).

6.3 **Implications and future work**

Climate change has negative impacts on both environmental and economic activities, as well as the life of people in Southern Africa. Nonetheless, there are already climate models at work anticipating changes in the region's weather, particularly in terms of temperature and rainfall distribution. It is particularly crucial to have a better grasp of the peculiarities of meteorological systems that affect how rain falls over South Africa. As a result, forecasts of the characteristics of severe weather conditions linked to the emergence of COL weather systems will be more accurate.

Even though the characteristics of COL events, which are coupled with different surface pressure circulation and Potential Vorticity (PV) were analysed, the influence of surface and stratospheric processes on deep convection during COL systems were not considered and need further investigation. Following key findings about the COL extensions along with the spilling of the jet towards the surface over the South African interior (Barnes *et al*, 2021b), the role of small-scale jets and the cause of the spilling during COLs still needs to be studied. While characteristics associated with the occurrence of COL systems have been analysed, the intrusion of stratospheric ozone during the development of COL events still requires further research.

Furthermore, the present study provided a 3-dimensional view (3D) of the COLs which the characteristics of COLs were thoroughly presented according to different locations of their origin over the South African interior. The South African Weather service (SAWS) and any other interested party can use these findings to improve the understanding of COLs over the South African interior. The vertical cross-section of energetics on COLs provided on this study will also help other researchers understand energy conversions better.

6.4 **Conclusion**

The current study identified four COL weather systems, by closed geopotential height at 500 hPa from 2016 to 2019 according to where they developed over the study. Identified COL systems were associated with pools of cyclonic potential vorticity (PV) and cold air in the centre. COLs that develop north of this study are linked to Type-N ridging high whereas COLs that develop south of the study are linked with Type-S ridging high. During the formation stage, high PV folds were observed indicating the intrusion of air from the stratosphere to the upper troposphere to form the COL. During their mature stages, COL systems were observed with high PV intensity and cold cores. By analysing the geopotential and PV anomalies, the speed of movement towards the east is different from one COL to the next. The study further found that during COLs extension, the jet also spills towards the surface on some events. The role of dynamical processes during COLs was examined with the Ageostrophic fluxes convergence responsible for the development of the COL, Baroclinic conversion for system maintenance and the Barotropic conversion for the decay stages of the system. Following these findings, forecasters and researchers can be aware about the energy conversion that occurs during COLs.

References

Abba Omar, S. and Abiodun, B.J. 2020. Characteristics of cut-off lows during the 2015–2017 drought in the Western Cape, South Africa. Atmospheric Research. 235 DOI:10.1016/j.atmosres.2019.104772.

Abba Omar, S. and Abiodun, B.J. 2021. Simulating the influence of topography on cut-off lows over Southern Africa. International Journal of Climatology. 41:E2231-E2243. DOI:10.1002/joc.6842.

Barnes, E.A., Hartmann, D.L., 2012. Detection of Rossby wave breaking and its response to shifts of the midlatitude jet with climate change. Journal of Geophysics. Res. 117, D09117

Barnes, M.A., Ndarana, T. and Landman, W.A., 2021a. Cut-off lows in the southern Hemisphere and their extension to the surface. Climate Dynamics, 56(11), pp.3709-3732.

Barnes, M.A., Turner, K., Ndarana, T. and Landman, W.A., 2021b. Cape storm: A dynamical study of a cut-off low and its impacts on South Africa. Atmospheric Research, 249, p.105290

Bazarov, D.R., Vokhidov, O.F., Lutsenko, L.A. and Sultanov, S., 2019, November. Restrictions applied when solving one-dimensional hydrodynamic equations. In *International Scientific Conference on Energy, Environmental and Construction Engineering* (pp. 299-305). Cham: Springer International Publishing.

Cambaza, E., Mongo, E., Anapakala, E., NhahPaire, R., Singo, J and Machava, E., 2019. Outbreak of cholera due to cyclone Kenneth in northern Mozambique ,2019. International journal of environmental research and public health 16.16 (2019): 2925.

Chameides, W.L., Yu, H., Liu, S.C., Bergin, M., Zhou, X., Mearns, L., Wang, G., Kiang, C.S., Saylor, R.D., Luo, C. and Huang, Y., 1999. Case study of the effects of atmospheric aerosols and regional haze on agriculture: an opportunity to enhance crop yields in China through emission controls? *Proceedings of the National Academy of Sciences*, *96*(24), pp.13626-13633.

Change, A.D.C., Blair, T., Pachauri, R.K. and Pachauri, R., 2006. Avoiding dangerous climate change. Cambridge University Press

Chapman, L., Bell, C. and Bell, S., 2017. Can the crowdsourcing data paradigm take atmospheric science to a new level? A case study of the urban heat island of London quantified using Netatmo weather stations. *International Journal of Climatology*, *37*(9), pp.3597-3605.

Crowe, S., Cresswell, K., Robertson, A, Huby, G., Avery, A. and Sheikh, A., 2011. The case study approach. *BMC medical research methodology*, 11(1), p.100

Danielson, R.E., Gyakum, J.R., Straub, D., 2006. A case study of downstream baroclinic development over the North Pacific Ocean. Part II: diagnoses of eddy energy and wave activity. Mon. Wea. Rev. 134, 1549–1567. https://doi.org/10.1175/ MWR3173.1.

Edouard, S., Vautard, R. and Brunet, G., 1997. On the maintenance of potential vorticity in isentropic coordinates. *Quarterly Journal of the Royal Meteorological Society*, *123*(543), pp.2069-2094.

Eisenberg, D., and Warner, K.E., 2005. Effects of snowfalls on motor vehicle collisions, injuries, and fatalities. American journal of public health, 95(1), pp.120-124.

Elliot, R., 2008. *Faking nature: the ethics of environmental restoration*. Routledge.

Fauchereau, N., Pohl, B., Reason, C.J.C., Rouault, M., Richard, Y., 2009. Recurrent daily OLR patterns in the southern Africa/Southwest Indian Ocean region, implications for south African rainfall and teleconnections. Climate Dynamics. 32, 575–591. https://doi.org/ 10.1007/s00382-008-0426-2.

Favre, A., Hewitson, B., Lennard, C., Cerezo-Mota, R. and Tadross, M., 2012. Cut-off Lows in the South Africa region and their contribution to precipitation. Climate Dynamics., 41, 2331–2351, doi 10.1007/s00382-012-1579-6

Feldstein, S. and Lee, S., 1998. Is the atmospheric zonal index driven by an eddy feedback? *Journal of the atmospheric sciences*, *55*(19), pp.3077-3086.

Felicísimo, Á.M., Muñoz, J. and González-Solis, J., 2008. Ocean surface winds drive dynamics of transoceanic aerial movements. Public Library of Science one, 3(8).

Fink, A., 2014.Conducting Research Literature Reviews: From the internet to paper. Thousand Oaks, 4th Edition.

Hart, N.C.G., Reason, C.J.C and Fauchereau, N., 2013. Cloud bands over southern Africa: Seasonality, contribution to rainfall variability and modulation by the MJO. *Climate dynamics*, 41(5), pp.1199-1212

Hopsch, S., Cohen, J. and Dethloff, K., 2012. Analysis of a link between fall Arctic Sea ice concentration and atmospheric patterns in the following winter. *Tellus A: Dynamic Meteorology and Oceanography*, *64*(1), p.18624.

Huijun, W., Guangqing, Z. and Yan, Z., 2000. An effective method for correcting the seasonal—interannual prediction of summer climate anomaly. *Advances in Atmospheric Sciences*, *17*(2), pp.234-240.

Independent Online (IOL News), Gauteng hail horror., 2012. https://www.iol.co.za/news/southAfrica/Gauteng/gauteng-hail-horror-1407784 Accessed online on 17/08/2021

Iyakaremye, V., Zeng, G., Yang, X., Zhang, G., Ullah, I., Gahigi, A., Vuguziga, F., Asfaw, T.G. and Ayugi, B., 2021. Increased high-temperature extremes and associated population exposure in Africa by the mid-21st century. *Science of The Total Environment*, *790*, p.148162.

Jury, M.R., 2018. Modulation of currents near Durban. Reg. Stud. Mar. Sci. 18, 208–218. https://doi.org/10.1016/j.rsma.2017.10.009.

Kaminski, T., Knorr, W., Rayner, P.J. and Heimann, M., 2002. Assimilating atmospheric data into a terrestrial biosphere model: A case study of the seasonal cycle. *Global Biogeochemical Cycles*, *16*(4), pp.14-1.

Kenyon, L., Schwarz, C., and Hug, B., 2008. The benefits of scientific modelling. National science teaching association

Kenyon, S., Pike, K., Jones, D.R., Brocklehurst, P., Marlow, N., Salt, A., and Taylor, D.J., 2008. Childhood outcomes after prescription of antibiotics to pregnant women with spontaneous preterm labour: 7-year follow-up of the ORACLE II trial. *The Lancet*, *372*(9646), pp.1319-1327.

Kunz, T., Fraedrich, K. and Lunkeit, F., 2009. Response of idealized baroclinic wave life cycles to stratospheric flow conditions. *Journal of the atmospheric sciences*, *66*(8), pp.2288-2302.

Lackmann, G.M., Keyser, D., Bosart, L.F., 1999. Energetics of an intensifying jet streak during the Experiment on Rapidly Intensifying Cyclones over the Atlantic (ERICA). Mon. Weather Rev. 127, 2777–2795.

Liu, C., Liao, X., Qiu, J., Yang, Y., Feng, X., Allan, R.P., Cao, N., Long, J. and Xu, J., 2020. Observed variability of intertropical convergence zone over 1998—2018. *Environmental Research Letters*, *15*(10), p.104011.

Louis-Jean, J. and Cenat, K., 2020. Beyond the Face-to-Face Learning: A Contextual Analysis. *Pedagogical Research*, *5*(4).

Malherbe, J., Engelbrecht, F.A., Landman, W.A. and Engelbrecht, C.J., 2012. Tropical systems from the southwest Indian Ocean making landfall over the Limpopo River Basin, southern Africa: a historical perspective. *International Journal of Climatology*, *32*(7), pp.1018-1032.

Martínez-Moreno, J., Hogg, A.M., Kiss, A.E., Constantinou, N.C. and Morrison, A.K., 2019. Kinetic Energy of Eddy-Like Features from Sea Surface Altimetry. *Journal of Advances in Modelling Earth Systems*, *11*(10), pp.3090-3105.

Mcleod, J.C., Stokes, T. and Phillips, S.M., 2019. Resistance exercise training as a primary countermeasure to age-related chronic disease. *Frontiers in Physiology*, *10*, p.645.

Milly, P.C.D., Wetherald, R.T., Dunne, K.A. and Delworth, T.L., 2002. Increasing risk of great floods in a changing climate. Nature, 415(6871), pp.514-517.

Modarres, R. and da Silva, V.D.P.R., 2007. Rainfall trends in arid and semi-arid regions of Iran. Journal of arid environments, 70(2), pp.344-355.

Muofhe, T.P., Chikoore, H., Bopape, M.J.M., Nethengwe, N.S., Ndarana, T. and Rambuwani, G.T., 2020. Forecasting intense Cut-Off Lows in South Africa Using 4.4 km Unified Model. Climate, 8(11), p.129.

Mwafulirwa, N.D., 1999. *Climate variability and predictability in tropical southern Africa with a focus on dry spells over Malawi* (Doctoral dissertation).

Nakajima, J., Matsuzawa, T., Hasegawa, A. and Zhao, D., 2001. Three-dimensional structure of Vp, Vs, and Vp/Vs beneath north-eastern Japan: Implications for arc magmatism and fluids. *Journal of Geophysical Research: Solid Earth*, *106*(B10), pp.21843-21857.

Ndarana, T. and Waugh, D.W., 2010. The link between cut-off lows and Rossby wave breaking in the Southern Hemisphere. Quarterly Journal of the Royal Meteorological Society, 136(649), pp. 869-885.

Ndarana, T. and Waugh, D.W., 2011. A climatology of Rossby wave breaking on the Southern Hemisphere tropopause. *Journal of the Atmospheric Sciences*, *68*(4), pp.798-811.

Ndarana, T., Rammopo, T.S., Bopape, M.J., Reason, C.J. and Chikoore, H., 2021. Downstream development during South African cut-off low pressure systems. *Atmospheric Research*, *249*, p.105315.

Ndarana, T., Rammopo, T.S., Chikoore, H., Barnes, M.A. and Bopape, M.J., 2020. A quasi-geostrophic diagnosis of the zonal flow associated with cut-off lows over South Africa and surrounding oceans. Climate Dynamics, 55(9), pp.2631-2644.

Ndarana, T., Rammopo, T.S., Reason, C.J., Bopape, M.J., Engelbrecht, F. and Chikoore, H., 2022. Two types of ridging South Atlantic Ocean anticyclones over South Africa and the associated dynamical processes. *Atmospheric Research*, *265*, p.105897.

Nieto, R., Sprenger, M., Wernli, H., Trigo, R.M. and Gimeno, L., 2008. Identification and Climatology of Cut-off Lows near the Tropopause. Ann. N. Y. Acad. Sci., 1146, 256-290

O'Brien, J.J., 1970. Alternative solutions to the classical vertical velocity problem. *Journal of Applied Meteorology (1962-1982)*, pp.197-203.

Pinheiro, H., Gan, M. and Hodges, K., 2021. Structure and evolution of intense austral cut-off lows. *Quarterly Journal of the Royal Meteorological Society*, *147*(734), pp.1-20.

Pinheiro, H.R., Hodges, K.I. and Gan, M.A., 2019. Sensitivity of identifying cut-off lows in the Southern Hemisphere using multiple criteria: implications for numbers, seasonality, and intensity. Climate Dynamics, 53(11), pp.6699-6713

Pinheiro, H.R., Hodges, K.I. and Gan, M.A., 2020. An intercomparison of subtropical cut-off lows in the Southern Hemisphere using recent reanalyses: ERA-Interim, NCEP-CFRS, MERRA-2, JRA-55, and JRA-25. *Climate Dynamics*, *54*(1), pp.777-792.

Pinheiro, H.R., Hodges, K.I., Gan, M.A. and Ferreira, N.J., 2017. A new perspective of the climatological features of upper-level cut-off lows in the Southern Hemisphere. *Climate Dynamics*, *48*(1), pp.541-559.

Pinheiro, H.R., Hodges, K.I., Gan, M.A., and Ferreira, N.J., 2017. A new perspective of the climatological features of upper-level cut-off lows in the Southern Hemisphere. Climate Dynamics, 48(1-2), pp.541-559.

Pinheiro, H.R., Hodges, K.I., Gan, M.A., Ferreira, S.H. and Andrade, K.M., 2022. Contributions of downstream baroclinic development to strong Southern Hemisphere cut-off lows. *Quarterly Journal of the Royal Meteorological Society*, *148*(742), pp.214-232.

Reason, C.J.C. and Rouault, M., 2002. ENSO-like decadal variability and South African rainfall. *Geophysical Research Letters*, *29*(13), pp.16-1.

Reboita, M.S., Nieto, R., Gimeno, L., Da Rocha, R.P., Ambrizzi, T., Garreaud, R. and Krüger, L.F., 2010. Climatological features of cut-off low systems in the Southern Hemisphere. *Journal of Geophysical Research: Atmospheres*, *115*(D17).

Remsberg, E., Lingenfelser, G., Harvey, V.L., Grose, W., Russell III, J., Mlynczak, M., Gordley, L. and Marshall, B.T., 2003. On the verification of the quality of SABER temperature, geopotential height, and wind fields by comparison with Met Office assimilated analyses. *Journal of Geophysical Research: Atmospheres*, *108*(D20).

Ren, Y., Zhang, J.A., Vigh, J.L., Zhu, P., Liu, H., Wang, X. and Wadler, J.B., 2020. An observational study of the symmetric boundary layer structure and tropical cyclone intensity. *Atmosphere*, *11*(2), p.158.

Singleton, A.T. and Reason, C.J., 2006. A numerical model study of an intense cut-off low-pressure system over South Africa. Mon. Wea. Rev., 135, 1128–1150

Singleton, A.T. and Reason, C.J.C., 2007. Variability in the characteristics of cut-off low pressure systems over subtropical southern Africa. International Journal of Climatology: A Journal of the Royal Meteorological Society, 27(3), pp.295-310.

Stella, J.C., Rodríguez-González, P.M., Dufour, S. and Bendix, J., 2013. Riparian vegetation research in Mediterranean-climate regions: common patterns, ecological processes, and considerations for management. *Hydrobiologia*, *719*(1), pp.291-315.

Stull, R., 2016. Practical Meteorology: an algebra-based survey of atmospheric science. BC Campus.

Tennant, W.J., Reason, C.J.C., 2005. Associations between the Global Energy Cycle and Regional Rainfall in South Africa and Southwest Australia. Journal of Climate. 18, 2032–3047

Tinsley, B.A. and Heelis, R.A., 1993. Correlations of atmospheric dynamics with solar activity evidence for a connection via the solar wind, atmospheric electricity, and cloud microphysics. *Journal of Geophysical Research: Atmospheres*, *98*(D6), pp.10375-10384.

Uhlík, F., Slanina, Z. and Hinchliffe, A., 1993. Gas-phase association of O2: a computational thermodynamic study. *Thermochemical acta*, *228*, pp.9-14.

Ummmenhofer, C.C., Gupta, A.S., England, M.H. and Reason, C.J., 2009. Contributions of Indian Ocean Sea surface temperatures to enhanced East African rainfall. *Journal of climate*, *22*(4), pp.993-1013.

Van der Walt, A.J. and Fitchett, J.M., 2020. Statistical classification of South African seasonal divisions on the basis of daily temperature data. *South African Journal of Science*, *116*(9-10), pp.1-15.

Vigh, J.L., 2017. What is composite analysis in meteorology and what is its importance. Natural centre for atmospheric research. Research gate available online

Wang S, Polvani LM (2011) Double tropopause formation in idealized baroclinic life cycles: the key role of an initial tropopause inversion layer. J Geophysics Res 116:D05108

Wang, C.-H., Lin, K.-Y., Davis, C.A., Huang, S.-U., Liu, C.-S., Tsuboki, K., Jou, B.J.-D., 2020. A Modelling Study on the Impacts of Typhoon Morakot (2009)'s Vortex Structure on Rainfall in Taiwan using Piecewise Potential Vorticity Inversion. Journal of Meteorology Society Japan. 136, 869–885. https://doi.org/10.2151/ jmsj.2020-036.

Wang, H., Long, L., Kumar, A., Wang, W., Schemm, J.K.E., Zhao, M., Vecchi, G.A., Larow, T.E., Lim, Y.K., Schubert, S.D. and Shaevitz, D.A., 2014. How well do global climate models simulate the variability of Atlantic tropical cyclones associated with ENSO?. *Journal of Climate*, *27*(15), pp.5673-5692.

Washington, R., and Preston, A., 2006. Extreme wet years over southern African: Role of Indian Ocean Sea surface temperatures. Journal of Geophysics. Res., 24, 555-568